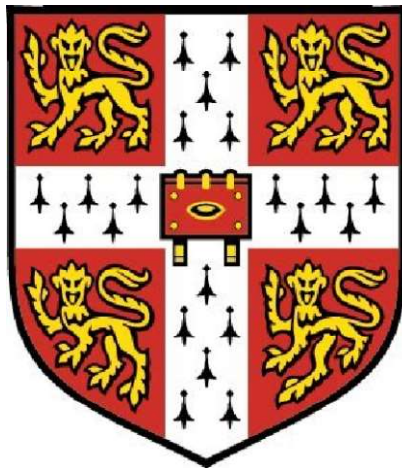


# Flexo electro-optic Liquid Crystals for Phase Modulation

---



**Shabeena Nosheen**

Department of Engineering  
University of Cambridge

*This dissertation is submitted for the degree of*  
***Doctor of Philosophy***

(Jesus College)

September 2018







## Abstract

### Flexo electro-optic Liquid Crystals for Phase Modulation

Shabeena Nosheen

Soft matter, self-assembled 3D photonic structures such as blue phase liquid crystals have of great interest to the displays industry and are highly desirable as spatial light modulators because of their polarisation independence and fast switching. However, these types of devices suffer from multistep fabrication conditions and require high threshold voltages.

To overcome these limitations, two key points were considered: High flexoelectric liquid crystals are capable of uniform 3D self-assembly, with a wide temperature range but have high threshold voltages, whereas, other classes of high dielectric liquid crystals have fast electro-optic response times with low threshold voltages but show poor 3D self-assembly. In this work, new mixture formulations have been devised having both properties in moderation in order to achieve simple yet stable 3D self-assembled blue phases with fast response times at as low as possible applied fields. Dielectric materials were considered from a commercial source whereas, miscible flexoelectric soft materials were synthesised in-house.

These synthesised materials were fully characterised. Then mixtures were formulated in commercial high dielectric hosts to study their miscibility, new mesogenic transitions and electro-optic responses in terms of flexoelectric and dielectric properties. The selected mixtures were further investigated for the rapid growth of blue phases and their compatibility with reactive mesogens to form stable blue phases at room temperature. This new formulation of materials has given rise to mixtures and devices which are inherently easy to fabricate allowing the robust and resilient growth of blue phases under an hour in standard laboratory conditions. Furthermore, polarisation independent electro-optic switching has been characterised at fields  $<1\text{V}\mu\text{m}^{-1}$ .

For phase modulation studies of these stabilised blue phase devices, phase shift was measured using a modified Young's slit interferometer. The observed results were very promising, with a full  $2.5\pi$  phase shift observed at a field of  $9.25\text{V}\mu\text{m}^{-1}$  when compared to earlier reported devices (which required complicated multistep fabrication processes) giving values of full  $1.8\pi$  phase shifts at  $20\text{V}\mu\text{m}^{-1}$ .



## **Declaration**

This dissertation is the result of my personal work as a PhD candidate at the University of Cambridge and contains nothing which is the outcome of work done in any collaboration. I hereby declare that except where specific reference is made to the work of others, the contents of this thesis are original. No part of this dissertation has been submitted for full or partial accomplishment of the requirements for any other degree or certificate at this or any other institution of higher education or organisation of learning. This dissertation contains 37124 words including appendices, bibliography, footnotes, tables and equations and has 89 figures.

Shabeena Nosheen

September 2018

## Acknowledgement

This dissertation would be quite impossible without the help of my colleagues in the department and a consistent feedback provided from the Merck.

First of all, my sincere gratitude to my supervisor Prof. Tim Wilkinson for funding, research support and last but not the least, proof reading of this manuscript. He has provided me enormous support and encouragement throughout my PhD work.

Thanks to EPSRC and Merck for providing the financial support during this period. I would like to extend my special thanks to Merck advisors Dr. Tuffin and Dr. Vaughan-Spickers for support and Merck's case-conference each year which is a best learning platform in this field of advance technology.

All members of research group CMMPE have provided me very welcoming, friendly and supportive environment which is very appreciative, especially thanks to Dr. Calum Williams and Dr. Richard Barthlomew for clean room and SEM support. I am thankful to our workshop technician Steve for making meticulous optical parts which were very crucial during my research work.

I am obliged to family friend for looking after my son during this study period. I am really grateful to my parents for their endless prayers and support throughout my whole life. I am thankful to my brother and sisters being compassionate during all years of my formal education.

I am in debt to my loving and inspiring husband Dr. Malik Qasim. Without his endless support, it would not be possible to complete my higher education. He is always there even in hard times of my life and cannot repay what he has done for me, making everything more valuable. Finally, to my son who has completed me, gives a new life every time with his affection smiles and hugs. I cannot think of a life without them so thank you for being a part of my life making its every moment joyful and precious.



## Acronyms

5CB	4-Cyano-4'-pentylbiphenyl
6CB	p-n-Hexyl-p'-cyanobiphenyl
AP	Anti-parallel planar alignment
BL006	Merck commercial nematic liquid crystal
BP	Blue phase
BPLCoS	Blue phase liquid crystal on silicon
CBE11ECB	bis(4'-cyano-[1-1'-biphenyl]-4-yl)tridecanedioate
CCD	Charge couple device
CGH	Computer generated holography
DC	Direct current
DCC	N,N'-dicyclohexylcarbodiimide
DCM	Dichloromethane
DMAP	4-Dimethylaminopyridine
DSC	Differential scanning calorimetry
EBBA	N-(4-ethoxybenzylidene)-4-butylaniline
EHA	Ethyl hexyl acrylate
FFE9ECB	1-(4'-cyano[1,1'-biphenyl]-4-yl)11-(2,4'-difluoro-[1,1'-biphenyl]-4-yl) undecanedioate
FSCLCDs	Frame sequential colour liquid crystal displays
HTP	Helical twisting power
HUD	Head up display
IPS	In plane switching
ITO	Indium tin oxide
LC	liquid crystal
LC SLMs	Liquid crystal spatial light modulators
LCDs	Liquid crystal displays

LCoS	Liquid crystal on silicon
LED	Light emitting diode
MBBA	N-(4-Methoxybenzylidene)-4-butylaniline
MEMS	Micro electro mechanical systems
Mix-1	10% FFE9ECB in BL006
Mix-2	20% FFE9ECB in BL006
Mix-3	40% FFE9ECB in BL006
Mix-4	60% FFE9ECB in BL006
Mix-5	80% FFE9ECB in BL006
Mix-6	10% CBE11ECB in BL006
Mix-7	20% CBE11ECB in BL006
NMR	Nuclear magnetic resonance
NOA68	Norland Optical Adhesive 68
PDLC	Polymer dispersed liquid crystals
POM	Polarised optical microscope
PSBP	Polymer stabilised blue phase
SEM	Scanning electron microscope
SLMs	Spatial light modulators
TLC	Thin layer chromatography
TMPTA	Trimethylolpropane triacrylate
ULH	Uniform lying helix
USH	Uniform standing helix
UV	Ultra violet

## Symbols

$\Delta n$	Refractive index
$C$	Speed of light
$E_f$	External electric field
$J$	Coupling constant
$K$	Elastic constant
$K_{11}$	Splay constant
$K_{22}$	Twist constant
$K_{33}$	Bend constant
$n_e$	Extraordinary index of refraction
$nm$	Nano meter
$n_o$	Ordinary index of refraction
$p$	Pitch
$S$	Order parameter
$V_{\parallel}$	Parallel velocity
$V_{\perp}$	Perpendicular velocity
$\Delta\epsilon$	Dielectric anisotropy
$\epsilon_{\parallel}$	Dielectric permittivity parallel to the director
$\epsilon_{\perp}$	Dielectric permittivity perpendicular to the director
$\gamma$	Viscosity
$\lambda_o$	Incident light
$\lambda_v$	Wavelength in vacuum
$\mu m$	Micro meter
$\mu s$	Micro second
$\tau$	Response time



# Table of Contents

.....	<b>CHAPTER 1: MOTIVATION AND RESEARCH WORK SCOPE</b>	
.....		<b>1</b>
1.1	MOTIVATION AND OBJECTIVES FOR RESEARCH WORK:.....	2
1.2	THESIS OUTLINE: .....	4
.....	<b>CHAPTER 2: INTRODUCTION AND BACKGROUND</b>	
.....		<b>6</b>
2.1	LIQUID CRYSTAL:.....	7
2.1.1	<i>Historical Background and Discovery:</i> .....	8
2.1.2	<i>Classifications:</i> .....	9
2.1.3	<i>Phases:</i> .....	11
2.1.4	<i>Characterisation of Liquid Crystals:</i> .....	16
2.1.5	<i>Thermal characterisation:</i> .....	18
2.1.6	<i>Polarised optical microscopic characterisation:</i> .....	19
2.2	ELECTRO-OPTIC PROPERTIES (ULH &USH):.....	20
2.2.1	<i>Dielectric properties:</i> .....	21
2.2.2	<i>Polar effects and flexoelectric coupling:</i> .....	22
2.2.3	<i>Response time:</i> .....	26
2.3	CHEMICAL STRUCTURE OF LIQUID CRYSTALS:.....	27
2.4	OPTICAL PROPERTIES: .....	28
2.4.1	<i>Bragg scattering:</i> .....	28
2.4.2	<i>Circular dichroism:</i> .....	29
2.4.3	<i>Waveguide properties:</i> .....	29
2.4.4	<i>Birefringence:</i> .....	30
2.5	EUTECTIC MIXTURES:.....	31
2.6	PHASE MODULATION:.....	32
2.6.1	<i>Spatial light modulators and Holograms:</i> .....	33
2.7	PHASE MEASUREMENT: .....	34
2.7.1	<i>Young's double slit experiment:</i> .....	35
.....	<b>CHAPTER 3: INSTRUMENTATION AND DEVICES</b>	
.....		<b>37</b>
3.1	INSTRUMENTATION: .....	38
3.1.1	<i>Optical setup for electro-optic measurements:</i> .....	38
3.1.2	<i>Young's slit Interferometer Setup:</i> .....	40
3.1.3	<i>Kossel diagram Setup:</i> .....	43
3.2	DEVICE FABRICATION:.....	44
3.2.1	<i>Glass cells:</i> .....	44
3.2.2	<i>Silicon Backplane devices:</i> .....	45
.....	<b>CHAPTER 4: SYNTHESIS AND CHARACTERISATION OF MATERIALS</b>	
.....		<b>48</b>
4.1	SYNTHESIS OF MESOGENIC DIMERS:.....	49
4.1.1	<i>Mesogenic dimers with ester linkage:</i> .....	49
4.1.2	<i>Ester bridged-ether linked mesogenic dimers:</i> .....	51
4.1.3	<i>Synthesis of Mesogenic monomers:</i> .....	53

4.2	MIXTURE FORMULATION:.....	55
4.3	CHARACTERISATION OF MIXTURES: .....	56
4.3.1	<i>Thermal characterisation:</i> .....	57
	CONCLUSION: .....	58
<b>..... CHAPTER 5: ELECTRO-OPTIC PROPERTIES OF FORMULATED MIXTURES</b>		
<b>.....</b>		<b>59</b>
5.1	DIELECTRIC ANISOTROPY: .....	60
5.1.1	<i>Result and Discussion:</i> .....	61
5.2	FLEXOELECTRO-OPTIC MEASUREMENTS:.....	64
5.2.1	<i>ULH mode for flexoelectro-optic switching:</i> .....	65
5.2.2	<i>Pitch measurements:</i> .....	69
5.3	RESPONSE TIME: .....	72
5.4	SUMMARY: .....	73
<b>..... CHAPTER 6: BLUE PHASE, ELECTRO-OPTIC STUDY, POLYMER STABILISATION AND PHASE MODULATION</b>		
<b>.....</b>		<b>74</b>
6.1	BLUE PHASE; ADVANTAGES AND SHORT COMINGS IN DISPLAY TECHNOLOGY:.....	75
6.2	BLUE PHASE MIXTURE: .....	75
6.3	STABILITY AND POLYMER FREE SWITCHING OF BLUE PHASE: .....	77
6.4	THERMAL SCANNING AND BAND GAP OPTIMISATION:.....	78
6.5	FORMULATION OF STABILISED BLUE PHASE:.....	79
6.5.1	<i>Nematic liquid crystal:</i> .....	80
6.5.2	<i>Chiral dopants:</i> .....	80
6.5.3	<i>Reactive mesogens:</i> .....	81
6.5.4	<i>RM257 and EHA [Set 1]:</i> .....	83
6.5.5	<i>UCL-011-K1 [Set 2 (a) and (b)]:</i> .....	83
6.5.6	<i>RM257 and QM02-01 [Set 3]:</i> .....	84
6.5.7	<i>RM257 and TMPTA [Set 4 (a), (b) and (c)]:</i> .....	84
6.6	ELECTRO-OPTIC PROPERTIES OF POLYMER STABILISED BLUE PHASE:.....	86
6.7	OPTICAL CHARACTERISATION OF POLYMER STABILISED BLUE PHASE: .....	89
6.8	BIGGER DOMAINS:.....	90
6.9	ELECTRO-OPTIC PROPERTIES OF POLYMER STABILISED BLUE PHASE: .....	92
6.10	EFFECT OF POLYMER CONCENTRATION ON RESPONSE TIME OF PSBP:.....	94
6.11	SEM MICROGRAPHS FOR POLYMER STABILISED BLUE PHASE: .....	95
6.12	PHASE MODULATION OF LIGHT USING PSBP: .....	96
6.12.1	<i>Polymer stabilised blue phase:</i> .....	96
	CONCLUSION: .....	101
<b>..... CHAPTER 7: DOPING EFFECTS OF NOVEL MESOGENS</b>		
<b>.....</b>		<b>102</b>
7.1	DOPING OF Mix-2 WITH SYNTHESISED COMPOUNDS: .....	104
7.2	ELECTRO-OPTIC PROPERTIES:.....	105
7.2.1	<i>Mix-2 doped with dimers:</i> .....	106
7.2.2	<i>Mix-2 doped with monomers:</i> .....	107
7.2.3	<i>Flexoelectro-optic measurements:</i> .....	109
7.2.4	<i>Response time of doped Mix-2:</i> .....	112
7.3	BLUE PHASE APPEARANCE IN THE DOPED MIX-2: .....	115
	CONCLUSIONS: .....	115

.....	<b>CHAPTER 8: CONCLUSIONS AND FUTURE PLANS</b>	
.....		<b>117</b>
8.1	OUTCOME OF THIS DISSERTATION:.....	118
8.2	FUTURE PLANS:.....	120
<b>BIBLIOGRAPHY:</b> .....		<b>I</b>
.....	<b>ADDENDUM</b>	
.....		<b>A</b>
9.1	SELECTED RESPONSE TIMES: .....	A
9.2	RESPONSE TIMES FOR MIX-2 DOPED WITH SYNTHESISED MESOGENS: .....	E

## List of Figures:

FIGURE 2.1: ILLUSTRATION OF THE RELATIVE DEGREE OF ORDER IN MOLECULES.....	7
FIGURE 2.2: CHOLESTERYL BENZOATE.....	8
FIGURE 2.3: TRANSITIONS OBSERVED IN HEATING AND COOLING OF CHOLESTERYL BENZOATE. ....	8
FIGURE 2.4: MOLECULAR ARRANGEMENTS IN NEMATIC PHASE.....	11
FIGURE 2.5: A FEW EXAMPLES OF CHIRAL OBJECTS. ....	12
FIGURE 2.6: MOLECULAR ARRANGEMENTS IN CHOLESTERIC OR CHIRAL NEMATIC PHASE AND TEXTURES UNDER POLARISED OPTICAL MICROSCOPE. IMAGE (B) REPRODUCED WITH PERMISSION FROM DR. MALIK QASIM .....	13
FIGURE 2.7: PHASE DIAGRAM FOR THREE TYPES OF BLUE PHASE THAT APPEAR IN CHIRAL NEMATIC LIQUID CRYSTALS. ADAPTED FROM [28].....	14
FIGURE 2.8: BLUE PHASE SELF ORGANISATION, ARRAY OF DISCLINATION LINES [35] AND THE ACTUAL POLARISED OPTICAL MICROGRAPH. ....	15
FIGURE 2.9: MOLECULAR ARRANGEMENT AND PHASE DESCRIPTION WITH RESPECT TO TEMPERATURE CHANGE. REPRODUCED FROM [28].....	16
FIGURE 2.10: PICTORIAL REPRESENTATION OF THE MOLECULAR DIRECTOR.....	17
FIGURE 2.11: ORDER PARAMETER VERSUS TEMPERATURE. [43].....	17
FIGURE 2.12: DSC THERMAL SCAN FOR 20% CBE11ECB IN BLO06.....	19
FIGURE 2.13: REPRESENTATION OF (A) HOMEOTROPIC AND (B) PLANAR ALIGNMENT.....	20
FIGURE 2.14: CHIRAL NEMATIC LIQUID CRYSTAL IN A SANDWICH CELL GEOMETRY, (A) UNIFORM LYING HELIX, ULH, .....	20
FIGURE 2.15: FREDERICKSZ TRANSITION FOR LIQUID CRYSTALLINE MATERIAL WITH POSITIVE DIELECTRIC ANISOTROPY. ....	22
FIGURE 2.16: THREE POSSIBLE DEFORMATIONS IN THE MOLECULES. ....	23
FIGURE 2.17: MEYER'S MODEL OF CURVATURE ELECTRICITY, (A) UN-DEFORMED AND (B) WITH DEFORMATIONS [46]. ....	23
FIGURE 2.18: AN ILLUSTRATION OF QUADRUPOLAR FLEXOELECTRICITY; A) SHOWS THE UN-DEFORMED SYSTEM, WHILE B) SHOWS A SPLAY CURVATURE. ....	24
FIGURE 2.19: AN ILLUSTRATION OF THE FLEXOELECTRO-OPTIC EFFECT.....	25
FIGURE 2.20: A GRAPHIC REPRESENTATION OF TEXTURE CHANGES DEMONSTRATED BY THE SHORT PITCH CHIRAL NEMATIC WITH RESPECT TO AN EXTERNAL APPLIED ELECTRIC FIELD.....	25
FIGURE 2.21: AN ILLUSTRATION OF UNWINDING OF HELIX BY INCREASING ELECTRIC FIELD AMPLITUDE.....	26
FIGURE 2.22: GENERIC STRUCTURE OF LIQUID CRYSTAL P-N-HEXYL-P'-CYANOBIIPHENYL (6CB). ....	28
FIGURE 2.23: GENERIC MOLECULAR STRUCTURE OF A MESOGENIC DIMER 4',4'''-(HEXANE-1,6-DIYL)BIS([1,1'-BIPHENYL]-4-CARBONITRILE)). ....	28
FIGURE 2.24: RIGHT-HAND CIRCULARLY POLARISED LIGHT (BOTTOM) BEING ABSORBED BY A MATERIAL MORE STRONGLY THAN LEFT-HAND CIRCULARLY POLARISED LIGHT (TOP). (IMAGE BY WIKIPEDIA COMMONS).....	29
FIGURE 2.25: A SCHEMATICS OF BIREFRINGENCE, (A) AN ORDINARY LIGHT TRAVELLING THROUGH A NEMATIC LIQUID CRYSTAL AND (B) LIGHT ENTERING A BIREFRINGENT MATERIAL. ....	31
FIGURE 2.26: PHASE DIAGRAM OF THE BINARY MIXTURE OF LIQUID CRYSTALS. [58].....	32
FIGURE 2.27: THE OCCURRENCE OF CONSTRUCTIVE AND DESTRUCTIVE INTERFERENCE.....	35
FIGURE 2.28: THE PHENOMENON OF DIFFRACTION OF LIGHT THROUGH A DOUBLE SLIT. (A) EXPLAINS THE DIFFRACTION TREND THROUGH A DOUBLE SLIT. (B) SHOWS THE DETAILED CONSTRUCTIVE AND DESTRUCTIVE INTERFERENCE PATTERN. (C) THE GRAPHICAL REPRESENTATION OF THE DIFFRACTION PATTERN OBSERVED THROUGH A DOUBLE SLIT INDICATING ORDER OF BRIGHTNESS OBSERVED. (D) ELUCIDATE THE RELATIONSHIP AMONG THE ANGLE AND THE DISTANCE BETWEEN THE SLITS. IMAGE (A) IS TAKEN FROM <a href="http://www.daviddarling.info/encyclopedia/L/LIGHT.HTML">HTTP://WWW.DAVIDDARLING.INFO/ENCYCLOPEDIA/L/LIGHT.HTML</a> (E) ACTUAL DIFFRACTION IMAGE OBSERVED DURING EXPERIMENT. ....	36
FIGURE 3.1: GENERAL EXPERIMENTAL SET-UP FOR ELECTRO-OPTIC STUDIES. ....	39
FIGURE 3.2: THE OLYMPUS POLARISING MICROSCOPE. (FIGURE FROM SUPPLIER WEBSITE).....	39
FIGURE 3.3:(A) SCHEMATICS OF YOUNG'S SLIT INTERFEROMETER. (B) YOUNG'S SLIT EXPERIMENTAL SETUP. [70].....	41



FIGURE 3.4: METAL GRATING USED TO CONCEAL THE DEVICE. (A) NOVEL REFLECTIVE METAL SURFACE SLIT MASK. (B) SAME MASK COLOURED IN BLACK TO REDUCE REFLECTIONS. [70]	43
FIGURE 3.5: OPTICAL SETUP TO OBSERVE KOSSEL DIAGRAM.	44
FIGURE 3.6: LATERAL VIEW AND TOP VIEW OF AP (ANTI PARALLEL PLANAR) CELL USED IN THE LC MATERIAL CHARACTERISATION.	44
FIGURE 3.7: A SCHEMATICS OF WEDGES CELL (A) LATERAL VIEW (B) TOP VIEW OF A WEDGE CELL (C) OPTICAL POLARISING MICROGRAPH FOR 20% FFE9ECB IN BL006 SHOWING TYPICAL PATTERN OF DOMAIN SEPARATION BY THE DEFECT LINES.	45
FIGURE 3.8: THE LCoS DEVICE ASSEMBLY AND MASK DIMENSIONS FOR THE PIXEL PATTERN.	46
FIGURE 3.9: (A) SUBSTRATE WITH PHOTORESIST SPIN COATED ON THE SURFACE. (B) UV CURED WITH PIXEL MASK AND DEVELOPED SILICON SUBSTRATE. (C) FINALISED BACKPLANE WITH ALUMINIUM PIXELS AFTER ETCHING PROCESS. (D) MULTI-PIXEL SUBSTRATE. (E) COMPLETED TWO PIXEL AND MULTI PIXEL DEVICES.	46
<b>FIGURE 4.1: SYNTHESIS OF ESTER LINKED MESOGENIC DIMERS.</b>	50
FIGURE 4.2: SYNTHESIS OF ESTER BRIDGED ETHER LINKED MESOGENIC DIMERS.	52
FIGURE 4.3: SYNTHESIS OF MESOGENIC MONOMERS.	55
FIGURE 5.1: (A) THE CAPACITANCE CURVE AS A FUNCTION OF APPLIED VOLTAGE. [79] (B) SCHEMATIC OF THE DEVICE USED TO MEASURE DIELECTRIC PROPERTIES. (SUPPLIED BY MERCK)	61
FIGURE 5.2: DIELECTRIC ANISOTROPY FOR FFE9ECB MIXTURES IN BL006.	62
FIGURE 5.3: DIELECTRIC PERMITTIVITY COMPARISON FOR MIXTURES (MIX-2 TO MIX-5).	63
FIGURE 5.4: DIELECTRIC MEASUREMENTS FOR 10 AND 20 % MIXTURES OF CBE11ECB.	64
FIGURE 5.5: CHEMICAL STRUCTURE OF BDH1281.	65
FIGURE 5.6: ULH ALIGNMENT ACHIEVED BY COOLING A CHIRAL NEMATIC LIQUID CRYSTAL FROM ISOTROPIC PHASE WITH THE APPLICATION OF ELECTRIC FIELD WITH ORIENTATION OF OPTIC AXIS AT 45° AND 0° WITH RESPECT TO POLARISER. [82]	65
FIGURE 5.7: THE TEXTURE OBSERVED FOR THE UNIFORMLY LYING HELIX GEOMETRY IN MIX-2 BOTH BRIGHT AND DARK STATES.	66
FIGURE 5.8: AN EXAMPLE OF THE ROTATION OF THE OPTIC AXIS IN A CHIRAL NEMATIC LIQUID CRYSTAL WITH AN APPLIED ELECTRIC FIELD PERPENDICULAR TO THE HELICAL AXIS.	66
FIGURE 5.9: A DIAGRAMMATIC REPRESENTATION OF THE PHOTODIODE RESPONSE, FOR A BIPOLAR SQUARE WAVE APPLIED FIELD, WHEN THE ZERO POSITION OF THE OPTIC AXIS IS A) PARALLEL AND B) AT 22.5° TO THE TRANSMISSION AXIS OF ONE OF THE POLARISERS.	67
FIGURE 5.10: AN ILLUSTRATION APPLIED VOLTAGE AS A FUNCTION OF TIME, OPTICAL RESPONSE IN ULH MODE TO MEASURE INDUCED TILT AS EXPLAINED IN TEXT. [79]	68
FIGURE 5.11: PHOTODIODE RESPONSE OF MIX-2 AND APPLIED SQUARE WAVE ELECTRIC FIELD (2.5V $\mu\text{m}^{-1}$ ) AT 90°C.	71
FIGURE 5.12: FLEXO-ELASTIC RATIOS ( $E/k$ ) FOR MIX-1 TO MIX-7.	72
FIGURE 6.1: APPEARANCE OF A STABLE BLUE IN MIX-2. (5.5% CHIRAL DOPANT)	76
FIGURE 6.2: GROWTH OF BLUE PHASE WITHIN ONE HOUR. (SCALE BAR: 200 $\mu\text{m}$ AND 7.5% CHIRAL DOPANT)	77
FIGURE 6.3: THE SWITCHING OF THE POLYMER FREE BLUE PHASE USING MIX-2 AT 114 °C. SCALE BAR: 400 $\mu\text{m}$	78
FIGURE 6.4: THE REFLECTION BANDS OF (A) NEMATIC LIQUID CRYSTALS (B) BLUE PHASE RESPECTIVELY*. (C) DSC TRACED SHOWING AN EXTRA ENDOTHERM THAT BELONGS TO BLUE PHASE AND (D) THE REFLECTION BAND OF THE TIGHT PITCH MIX-2.]	79
FIGURE 6.5: CHEMICAL STRUCTURE OF COMPONENTS USED IN STABILISATION OF BLUE PHASE.	82
FIGURE 6.6: (A) BLUE PHASE IN AN IN-PLANE DEVICE (B) DEGRADATION OF POLYMER MATRIX ON HIGH VOLTAGE. SCALE BAR: 200 $\mu\text{m}$ .	83
FIGURE 6.7: PHASE SEPARATION AND DROPLET FORMATION IN BLUE PHASE MIXTURE WITH UCL-011-K1 UNDER UV FILTER. SCALE BAR: 200 $\mu\text{m}$	84
FIGURE 6.8: CHEMICAL STRUCTURE OF QM02-01	84
FIGURE 6.9: BLUE PHASE DEVICE LEFT OVERNIGHT TO OPTIMISE POLYMERISATION PROCESS. (SCALE BAR: 200 $\mu\text{m}$ )	85
FIGURE 6.10: IN-PLANE DEVICE ASSEMBLY FOR POLYMER STABILISED BLUE PHASE. (IMAGE HAS BEEN ADAPTED FROM INSTEC SUPPLIER WEBSITE.)	87
FIGURE 6.11: IN-PLANE SWITCHING OF POLYMER STABILISED BLUE PHASE AT 20X (SCALE: 200 $\mu\text{m}$ ) AND 10X (SCALE: 400 $\mu\text{m}$ ) MAGNIFICATION	88
FIGURE 6.12: IN-PLANE SWITCHING OF THE POLYMER STABILISED BLUE PHASE WITH RESPECT TO THREE DIFFERENT POLARISATION STATES.	89

FIGURE 6.13: SCHEMATIC DIAGRAM ILLUSTRATES KOSSEL DIAGRAM WHEN PARALLEL COHERENT LIGHT IS REFLECTED FROM SAMPLE.	90
FIGURE 6.14: OPTICAL MICROGRAPHS OF BIGGER PLATELETS AT 20X (SCALE BAR: 200 $\mu$ M) AND 40X (SCALE BAR: 100 $\mu$ M) MAGNIFICATIONS. ....	90
FIGURE 6.15: VOLTAGE TRANSMISSION DATA FOR THE PSBP IN AN IN-PLANE DEVICE AT THREE POLARISATION STATES. VT CURVE (A), AT 90° POLARISERS, GREY LINE (—) IS THE FIRST RUN, WHEREAS, THE DARKER LINE (—) IS THE TENTH AND ONWARD RUNS OF THE SAMPLE. VT CURVE (B), AT 45° POLARISERS AND VT CURVE (C), IS AT PARALLEL POLARISATION STATE. ....	93
FIGURE 6.16: SWITCHING TIMES IN MICRO SECONDS WITH RESPECT TO THE FIELD A 1 KHZ SIGNAL APPLIED AT ROOM TEMPERATURE. ....	94
FIGURE 6.17: SEM MICROGRAPHS OF POLYMER STABILISED BLUE PHASE REVEALING INSIDE TEXTURE OF THE DEVICE.....	95
FIGURE 6.18: HAND HELD UV CURER AND ITS MOUNT. IMAGE COPIED FROM THE SUPPLIER’S WEB SITE (MIGHTEX). ....	96
FIGURE 6.19 (A): ACTUAL IMAGES OF PHASE MODULATION IN THE REPLAY FIELD SHOWING THE MAXIMA SHIFT ON INCREASING THE VOLTAGE WHEREAS, IMAGE (B) IS THE ILLUSTRATION FOR CALCULATING THE PHASE SHIFT. ....	99
FIGURE 6.20: PHASE MODULATION WITH RESPECT TO APPLIED FIELD. ....	100
FIGURE 7.1: DIELECTRIC MEASUREMENTS FOR MIX-2 DOPED WITH SYNTHESISED MESOGENIC DIMERS. ....	106
FIGURE 7.2: DIELECTRIC MEASUREMENTS FOR MIX-2 DOPED WITH SYNTHESISED MESOGENIC MONOMERS WITH RESPECT TO TEMPERATURE. ....	108
FIGURE 7.3: FLEXOELASTIC RATIO OF MIX-2 DOPED WITH SYNTHESISED MESOGENIC DIMERS WITH RESPECT TO TEMPERATURE. ....	110
FIGURE 7.4: FLEXO MEASUREMENTS FOR MIX-2 DOPED WITH SYNTHESISED MESOGENIC MONOMERS WITH RESPECT TO TEMPERATURE. ....	112

## List of Tables:

TABLE 2.1: TYPES, PHASES, NAMES, FORMULAS AND TRANSITION RANGES OF SOME LIQUID CRYSTAL MOLECULES. ....	10
TABLE 2.2: FACTORS AFFECTING THE RESPONSE TIME OF LIQUID CRYSTAL. ....	27
TABLE 2.3: DUAL NATURE PHENOMENON OF LIGHT.....	32
TABLE 4.1: <sup>A</sup> (FFE9ECB) AND <sup>B</sup> (CBE11ECB) IN LC HOST BL006.....	56
TABLE 5.1: PITCH FOR THE FFE9ECB AND CBE11ECB MIXTURES.....	70
TABLE 6.1: REACTIVE MESOGENS AND THEIR COMPOSITION IN A 100 MG MIXTURE.....	82
TABLE 6.2: CURING CONDITIONS OF REACTIVE MESOGENS. ....	86
TABLE 6.3: OBSERVED KOSSEL DIFFRACTION PATTERN AND SCHEMATIC ILLUSTRATION. ....	91
TABLE 6.4: CHANGE IN PHASE SHIFT WITH RESPECT TO THE APPLIED FIELD PER MICROMETER. ....	101
TABLE 7.1: THERMAL TRANSITION TEMPERATURES OF NEWLY SYNTHESISED DIMERS AND MONOMERS.....	103
TABLE 7.2: TRANSITION TEMPERATURES AND BLUE PHASE TRANSITIONS OF Mix-2 ON 10% DOPING WITH NEWLY SYNTHESISED MATERIALS. ....	105

## List of Appendix Figures:

APPENDIX FIGURE: 1 RISE AND DECAY TIME OF Mix-2 WITH RESPECT TO THE APPLIED VOLTAGE AT DIFFERENT TEMPERATURES. ....	A
APPENDIX FIGURE: 2 RISE AND DECAY TIME OF Mix-3 WITH RESPECT TO THE APPLIED VOLTAGE AT DIFFERENT TEMPERATURES. ....	B
APPENDIX FIGURE: 3 RISE AND DECAY TIME OF Mix-4 WITH RESPECT TO THE APPLIED VOLTAGE AT DIFFERENT TEMPERATURES. ....	C
APPENDIX FIGURE: 4 RISE AND DECAY TIME OF Mix-5 WITH RESPECT TO THE APPLIED VOLTAGE AT DIFFERENT TEMPERATURES. ....	D
APPENDIX FIGURE: 5 RISE AND DECAY TIME OF Mix-2+3 WITH RESPECT TO THE APPLIED VOLTAGE AT DIFFERENT TEMPERATURES. ....	E
APPENDIX FIGURE: 6 RISE AND DECAY TIME OF Mix-2+17 WITH RESPECT TO THE APPLIED VOLTAGE AT DIFFERENT TEMPERATURES. ...	F
APPENDIX FIGURE: 7 RISE AND DECAY TIME OF Mix-2+18 WITH RESPECT TO THE APPLIED VOLTAGE AT DIFFERENT TEMPERATURES. ...	G
APPENDIX FIGURE: 8 RISE AND DECAY TIME OF Mix-2+27 WITH RESPECT TO THE APPLIED VOLTAGE AT DIFFERENT TEMPERATURES. ...	H
APPENDIX FIGURE: 9 RISE AND DECAY TIME OF Mix-2+28 WITH RESPECT TO THE APPLIED VOLTAGE AT DIFFERENT TEMPERATURES. ....	I
APPENDIX FIGURE: 10 RISE AND DECAY TIME OF Mix-2+29 WITH RESPECT TO THE APPLIED VOLTAGE AT DIFFERENT TEMPERATURES. ...	J
APPENDIX FIGURE: 11 RISE AND DECAY TIME OF Mix-2+30 WITH RESPECT TO THE APPLIED VOLTAGE AT DIFFERENT TEMPERATURES. .	K
APPENDIX FIGURE: 12 RISE AND DECAY TIME OF Mix-2+31 WITH RESPECT TO THE APPLIED VOLTAGE AT DIFFERENT TEMPERATURES. .	L



## **Chapter 1: Motivation and research work scope**

## **1.1 Motivation and objectives for research work:**

Liquid crystals have been around in modern society for decades, since their discovery in 1888. These materials have been widely researched in different fields due to their peculiar properties. These materials are optically anisotropic and hence they are birefringent due to the orientation of molecules. Their dielectric properties can be coupled with external applied electric field to manipulate the properties of light that passes through the liquid crystal. Liquid crystals possess different optical textures and entirely depend on the packing and orientation of molecules. Further this packing and molecular orientation is temperature dependent and at higher temperature these materials are less ordered when compared to those at room temperature. These materials can be polymer stabilised to enhance the stability of a particular texture required in a certain application. This process involves the UV curing of a polymer matrix caging the desired molecular orientation.

Among other classes of LCs, thermotropic liquid crystals have been widely utilised in various technical applications due to their unusual and versatile thermo-electro-optical properties. In laboratory applications, nematic liquid crystals have been used in a range of characterisation techniques. For example, in gas liquid chromatography these materials are used as a stationary phase to obtain a good separation in the impure samples. In the case of NMR spectroscopy, nematic liquid crystal can act as a solvent to yield more information about molecular parameters and spatial arrangement of atoms in a molecule. Further to this, these are used in thermal, mechanical, electrical, optical devices, radiation sensors, cosmetics and medical applications.[1]–[9] However, the most common application of thermotropic liquid crystals is in display technology due to their light modulating ability. It is a multi-billion dollar industry having achieved \$141 billion in 2010. [10], [11]

One of the main focuses in the development of display devices is to enhance their response time. Faster response time is a key to improving the quality of motion in video which can be further developed to create frame sequential colour liquid crystal displays (FSCLCDs) which exhibit a much larger optical efficiency due to the removal of colour filters. In this type of liquid crystal displays (LCDs) the back light emits red, green and blue light in successions, so there is no need for individual colour filters. This in turn reduces power consumption and creates a substantial cost reduction. Further to this, FSCLCDs can

provide enhanced resolution.[12] 3D displays and spatial light modulators for real time holography will also greatly be benefited from fast switching liquid crystals.

As demonstrated in this thesis, an interesting property of chiral nematic liquid crystals is flexoelectric coupling which exhibits a high-speed switching electro-optic effect. This faster switching response presents an outstanding opportunity over nematic liquid crystal displays which usually exhibit switching response of several milliseconds.[13] In standard off the shelf liquid crystals, flexo-electric coupling creates a minimal rotation of the optic axis hence limiting their use. However, recent research shows that newly developed mesogenic dimers show significantly higher tilt angles with much faster response time.[14]–[16] Although, there has been significant advances in developing new materials and mixture formulations for the flexoelectro-optic effect, there is still a need for a progress to reduce down the threshold driving voltage with a higher tilt angle for use in commercial displays. An in-plane switching (IPS) display device uses a driving voltage with a magnitude of 6V. Mixture optimisation to obtain lower driving voltages will allow the use of current driver circuitry for a thriving commercial development of this next generation of display technology.

The 3-D arrangement in highly ordered chiral nematic phase of liquid crystals is well known in the form of blue phases and as a result is optically isotropic in its nature. Electro-optic properties exhibited by these optically isotropic materials can result in fast response times and wider viewing angles in optical devices such as optical shutters, holograms and displays. Traditional blue phases usually possess very narrow phase transition of only a few degrees Kelvin which makes these phases much harder to study for stable display applications. Polymer stabilisation localises the blue phase and hence broadens the temperature range but with the expense of high driving voltage. [17]

It is evident that stable blue phases can be obtained from high flexo-electric bimesogens. [18] Furthermore, for a switchable blue phase under an applied electric field (as used for a phase modulation), two crucial and time consuming steps have been previously reported involving polymer templating or casting methods.[19] In the step a- blue phase 3D template is made by polymer stabilisation of a blue phase obtained from a high flexo mesogenic dimer followed by solvent washing out of the dimer. Then, in a second step, a high dielectric liquid crystalline material is introduced, replacing the mesogenic dimers after the wash-in-out process. There are a few limitations associated with this complicated and time

consuming method; it is hard to obtain the initial stabilisation as this step needs a precise temperature control upon cooling ( $0.01^{\circ}\text{C}/\text{minute}$ ). Furthermore, some of the polymer may leach out into the solvent during the washing-in-out process. In addition, the template of non-mesogenic polymer in the cell increases the threshold of the applied voltage ( $\sim 20\text{V}\mu\text{m}^{-1}$ ).

To address these issues, a range of mixtures of mesogenic dimers in high dielectric nematic host with different compositions have been formulated. Optimised flexo and dielectric characteristics in a single mixture have been utilised to polymer stabilise the blue phase and to study its electro-optic switching in a single step. As a result, only 10% wt of reactive meogens is used in polymer stabilisation of blue phase lowering down the threshold of the applied voltage to a quarter of those reported in the templating method.

Currently, continuous full ( $>2\pi$ ) phase modulation is only possible using nematic liquid crystals. However, these are slow-switching usually in milliseconds, and are also usually polarisation dependent which makes them complicated to use. These devices are hard to use in the optical communication where speed is essential. So this research covers another aspect to investigate the mixture which provides high speed full phase, polarisation independent modulation in an optically isotropic system.

## **1.2 Thesis outline:**

In chapter 2 liquid crystal states are introduced including types and phases of liquid crystals, physical properties and their generic chemical structure. This chapter also focuses on chiral nematics, their flexoelectro-optical properties and states in which these properties can be studied. It also deals with the applications, requirements and their limitations in latest technology. Optical properties, their utility in SLMs and measurement of phase modulation introduction using Young's slits theory is also explained in this chapter.

All the experimental techniques and setups employed in this research work are explained in chapter 3. Starting from thermal characterisation to the electro-optic studies to find out their flexoelastic properties and finally the Young's slits experimental setup is discussed in detail. Here, device fabrication and cell types are also explained thoroughly starting from a simple ITO glass test cell to specific LCoS cell design and fabrication.

New desired materials required for this research work have been synthesised in house and their structural characterisation has been carried out through NMR data analysis.



Synthetic routes and their structural NMR data are presented in chapter 4. Mixture formulation has been carried out in different commercial nematic hosts and the detailed mixture formation has been studied in a highly dielectric nematic host- BL006 by doping of dimers from 10-80% by weight. This chapter also explains the details of mixture formulation, their transition temperatures and phase diagram based on DSC thermograms.

The most important aspect of this research is to optimise a mixture with an ample nematic transition, along with sufficient dielectric anisotropy and a moderate flexoelastic ratio which in turn can be utilised to devise a truly switchable blue phase. All of the formulated mixtures have been scrutinised through their flexoelectro-optic data to get the desired composition. All of the findings related to their electro-optic properties are discussed in chapter 5. The desired mixture is confirmed through its transition temperature, dielectric anisotropy and flexo-elastic coefficient.

Short pitch chiral nematic liquid crystals with high flexo coefficients have the ability to self assemble in 3D platelets which can impart a blue colour by selective reflection of blue wavelengths. The pitch of the desired mixture has been optimised by adding sufficient amount of an appropriate chiral dopant without any separation or precipitates to obtain a “black blue phase” in UV region. This is thoroughly discussed in chapter 6. To lock in the blue phase platelets, polymerisation technique has been employed to get more stability in the blue phase system. Reactive mesogens of different compositions are used to optimise the polymerisation process in such a way that it has a low impact on threshold voltage for switching and exhibits minimal hysteresis. Details of this investigation are part of this chapter as well as the electro-optic properties of the polymer stabilised blue phase.

Once the mixture has been optimised for blue phase, the effect of newly synthesised compounds on the blue phase mixture is explored. Doping of new materials has been done by up to 10% wt of the mixture and their thermal and electro-optic properties are studied to give an insight regarding the doping effect. The possibilities of initial blue phase appearance are also studied. All of the mentioned results about new materials are presented in chapter 7 including the transition temperatures of the pure materials.

Last but not the least, conclusions, findings of this research work and future plans are then presented in chapter 8.

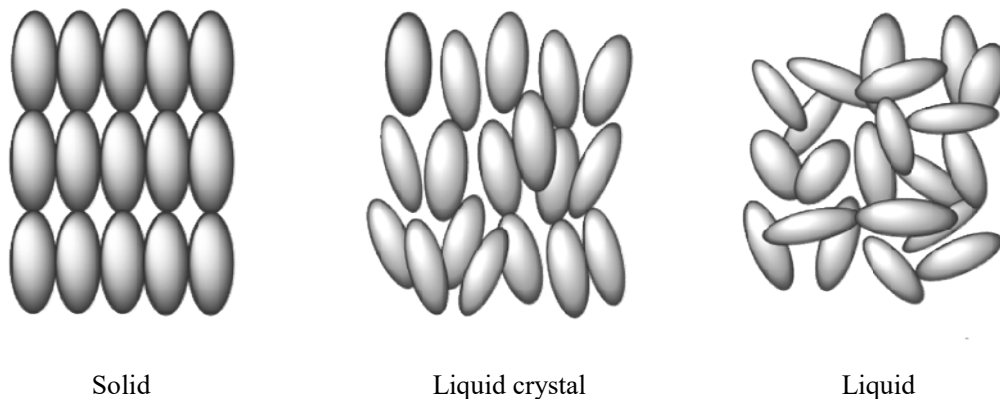
## **Chapter 2: Introduction and Background**

This chapter places emphasis on the liquid crystal's (LCs) physical and chemical properties in a general, classification of LCs, their physical characterisation, electro-optic properties and the principles of phase modulation. In chiral nematics helical pitch is an important factor and can be manipulated to obtain the blue phase which is an important aspect of this research work. Optical properties of LCs will be discussed with relevant details. The requirement to optimise a liquid crystalline mixture which can be utilised in a display technology will also be introduced in this chapter.

Solids and liquids are two universal types of condensed matter and are differentiated by the molecular order. In the case of solids, molecules are well packed and normally possess positional and orientational order to constrain the molecules in a lattice. On the other hand, liquid molecules show a freedom of molecular movement in the sample container and hence they are the least ordered. Liquids are isotropic in nature with the same properties at any angle they are viewed. However, there are certain materials which share both solid and liquid properties and these are known as liquid crystals. These materials have been a main focus in technology over the last few decades due to their unique optical properties

## 2.1 Liquid Crystal:

The molecules in the liquid crystal phase of matter diffuse more readily as would be seen in liquids but also hold some degree of orientational and occasionally positional order as well however; the degree of order is quite small compared with full crystals. An illustration of order in solids, liquid crystals and liquids is shown in figure 2.1. Since liquid crystal phases are transitional between crystalline solids and isotropic liquids they are often referred to as “mesogens” or “mesogenics”[20]

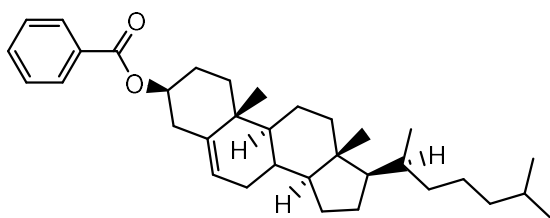


**Figure 2.1:** Illustration of the relative degree of order in molecules.

### 2.1.1 Historical Background and Discovery:

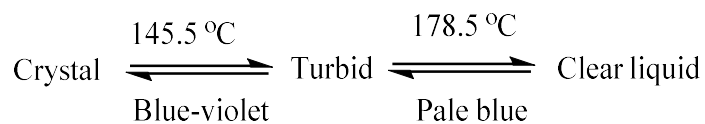
In the 1860s, Otto Lehmann, a German physicist, was observing the crystallisation properties in various substances. He constructed a light-polarising microscope with a temperature controlled heat-stage for the accurate melting and crystallisation of sample materials. He observed a strange behaviour of some substances which upon cooling underwent a transition from clear liquid to a cloudy liquid before crystallisation and considered this as imperfect phase transition[21].

In 1888 Friedrich Reinitzer an Austrian botanist and chemist was interested to know the biological function of cholesterol and its derivatives. Reinitzer was looking at the melting behaviour of cholesterol related substances and observed two melting points in cholesteryl benzoate (figure 2.2) and cholesteryl acetate[22].



**Figure 2.2:** Cholesteryl benzoate

Reinitzer observed that cholesteryl benzoate melted at 145.5 °C to an opaque liquid before turning into a clear liquid at 178.5 °C. Not only was a strange melting pattern observed, but also an unusual colour pattern was noticed: at first pale blue when clear liquid turned to a muddy liquid and finally a bright blue-violet upon crystallization of material as follows in figure 2.3.



**Figure 2.3:** Transitions observed in heating and cooling of cholesteryl benzoate.

Reinitzer then forwarded his samples to Otto Lehmann for further observations under his microscope who found similarity to some of his own samples. At first he named them *soft*

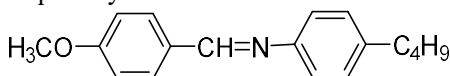
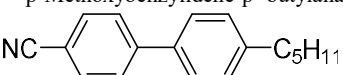
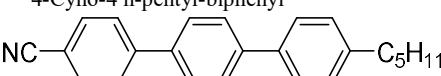
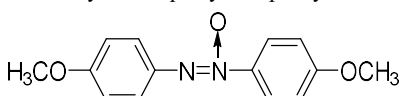
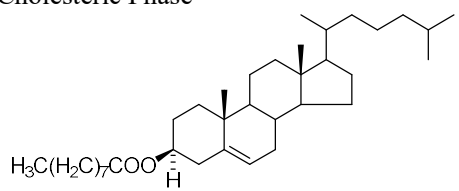
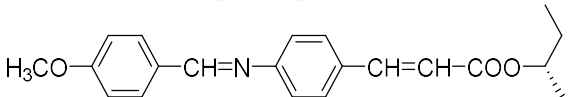
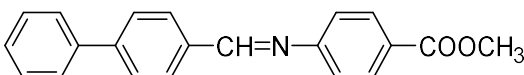
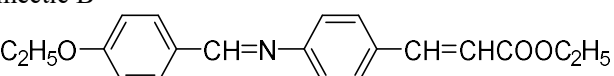
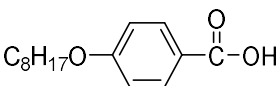
*crystals*; later he used the term *crystalline fluids*. He was more convinced that the opaque phase was a uniform phase of matter possessing properties of both liquid and solids and after one year he termed this phase as “*Flüssiger Kristall*”(Liquid Crystal)[23]. Lehmann was quite influential in getting a group of French workers interested in liquid crystals. The conclusion of this effort was a classification scheme introduced by George Friedel in 1922[21]. It comprised of three main phases (nematic, smectic and cholesteric phases), with the smectic phase having a layered structure. There were some further experiments on this topic during the 1930s and 1940s mainly focusing on their elastic properties, X-ray studies, and the effect of electric and magnetic fields.

So far, more than 90,000 different compounds showing liquid crystal behaviour have been reported covering low molecular mass to polymeric materials. Most of these can be found in the database LiqCryst and can be accessed online[24].

### 2.1.2 Classifications:

Liquid crystals can be classified into two main types based on the appearance of a transition. If a transition occurs with respect to temperature change then these are known as “thermotropic liquid crystals” whereas if influenced by the changes in solvent or concentration they are generally referred to as “lyotropic liquid crystals”. There are also a few materials which exhibit liquid crystal behaviour under the influence of temperature and solvent and are known as “amphotropic liquid crystals” [25]–[27] . This present research work is focused on thermotropic liquid crystals.

In thermotropic liquid crystals, transitions to a liquid crystal state are thermally induced as raising the temperature of a solid and / or lowering the temperature of a liquid. These are further categorised into two sub-classes: enantiotropic liquid crystals (which can be changed into the liquid crystal state by either lowering the temperature of a liquid or raising of the temperature of a solid) and monotropic liquid crystals (which can only be changed into the liquid crystal state by either an increase in the temperature of a solid or a decrease in the temperature of a liquid, but not both). Thermotropic liquid crystals are of interest in optical systems and display technology, whereas lyotropic liquid crystals are mainly used in the shampoo and detergent industry. Some examples of thermotropic and lyotropic liquid crystals are shown in table 2.1. [28]

1- Thermotropic liquid crystal		Liquid Crystalline Range
a- Nematic liquid crystals		
 <p>H<sub>3</sub>CO-C<sub>6</sub>H<sub>4</sub>-CH=N-C<sub>6</sub>H<sub>4</sub>-C<sub>4</sub>H<sub>9</sub></p> <p>p-Methoxybenzylidene-p'-butylaniline MBBA</p>	21-47 °C	
 <p>NC-C<sub>6</sub>H<sub>4</sub>-C<sub>6</sub>H<sub>4</sub>-C<sub>5</sub>H<sub>11</sub></p> <p>4-Cyano-4'-n-pentyl-biphenyl</p>	24-35 °C	
 <p>NC-C<sub>6</sub>H<sub>4</sub>-C<sub>6</sub>H<sub>4</sub>-C<sub>6</sub>H<sub>4</sub>-C<sub>5</sub>H<sub>11</sub></p> <p>4-Cyano-4''-n-pentyl-nterphenyl</p>	131-240 °C	
 <p>H<sub>3</sub>CO-C<sub>6</sub>H<sub>4</sub>-N=N(O)-C<sub>6</sub>H<sub>4</sub>-OCH<sub>3</sub></p> <p>p-Azoxyanisole PPA</p>	117-137 °C	
b-Cholesteric Phase		
 <p>H<sub>3</sub>C(H<sub>2</sub>C)<sub>7</sub>COO-</p> <p>Cholesteryl nonanoate</p>	145-179 °C	
c-Noncholesteryl, chiral-type compound		
 <p>H<sub>3</sub>CO-C<sub>6</sub>H<sub>4</sub>-CH=N-C<sub>6</sub>H<sub>4</sub>-CH=CH-COO-</p> <p>(-)-2-Methylbutyl p(p'-methoxy-benzylideneamino)cinnamate</p>	76-125 °C	
d-Smectic A		
 <p>C<sub>6</sub>H<sub>5</sub>-C<sub>6</sub>H<sub>4</sub>-CH=N-C<sub>6</sub>H<sub>4</sub>-COOCH<sub>3</sub></p> <p>Ethyl p-(p'-phenylbezalamino)benzoate</p>	121-131 °C	
e-Smectic B		
 <p>C<sub>2</sub>H<sub>5</sub>O-C<sub>6</sub>H<sub>4</sub>-CH=N-C<sub>6</sub>H<sub>4</sub>-CH=CHCOOC<sub>2</sub>H<sub>5</sub></p> <p>Ethyl p-ethoxybenzal-p'-aminocinnamate</p>	77-116 °C	
f-Smectic C		
 <p>C<sub>8</sub>H<sub>17</sub>O-C<sub>6</sub>H<sub>4</sub>-C(=O)-OH</p> <p>p-n-Octyloxybenzoic acid</p>	226-297 °C	
2- Lyotropic Liquid Crystal		
a-Sodium stearate		
$\text{CH}_3(\text{CH}_2)_{16}\text{COO}^- \text{Na}^+$		
b- α-Lecithin		
$\begin{array}{l} \text{H}_2\text{C}-\text{O}-\text{CO}-(\text{CH}_2)_{16}-\text{CH}_3 \\   \\ \text{HC}-\text{O}-\text{CO}-(\text{CH}_2)_{16}-\text{CH}_3 \\   \\ \text{H}_2\text{C}-\text{O}-\text{P}(=\text{O})(\text{O}^-)-\text{O}-\text{CH}_2-\text{CH}_2-\text{N}^+(\text{CH}_3)_3 \end{array}$		

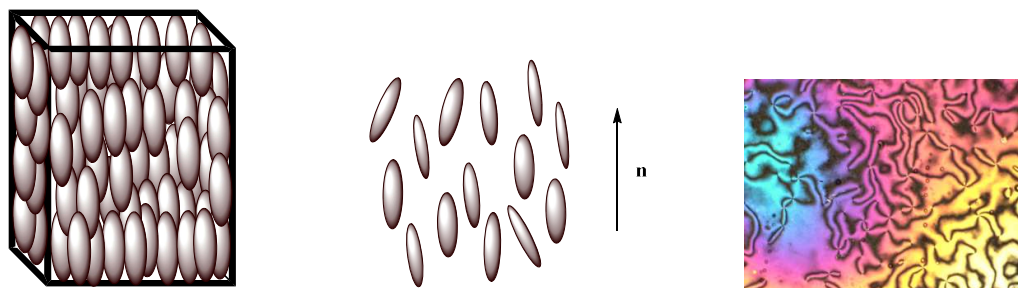
**Table 2.1:** Types, Phases, Names, formulas and transition ranges of some liquid crystal molecules.

### 2.1.3 Phases:

Liquid crystal phases often referred to as mesophases, are usually characterised by the positional and orientational order of the molecules. Positional order refers to the molecular arrangement in any form of an ordered lattice whereas; orientational order refers to the average direction of the liquid crystal molecules. On the basis of this order liquid crystalline molecules can be sub classed in to two kinds of mesophases: the nematic and smectic phases.

#### 2.1.3.1 Nematic phase:

The term “nematic” which originates from the Greek word ‘νήμα’ meaning thread-like was first used by Friedel to describe their optical texture.[29] The nematic phase denoted by the letter N has the lowest degree of order but more symmetry, as in this phase molecules do not have any translation or long-range positional order but only a short range orientational order. The molecules in the nematic phase are oriented on average along a particular direction known as the director. As a result, there is a macroscopic anisotropy in many material properties, such as dielectric constants and refractive indices. These properties are then coupled with high fluidity, which is used in many liquid crystal devices because the average orientation may be controlled by an applied electric field. The polarisation of light will follow the molecular orientation as it changes through a cell. Nematic molecular orientation is shown in figure 2.4.

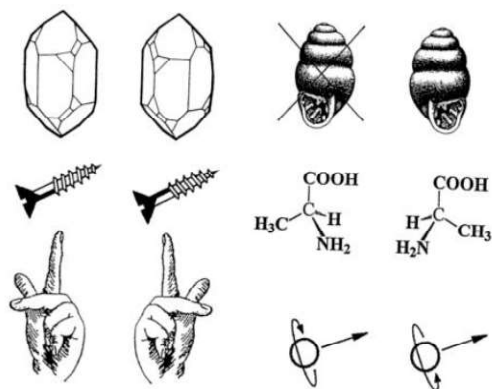


**Figure 2.4:** Molecular arrangements in nematic phase

#### 2.1.3.2 Chiral nematics:

Chirality is an intrinsic property that subsists in various naturally existing asymmetric systems like snails, shells and most commonly plants. A chiral system is distinct structure from its mirror image or in other words defines itself by the lack of mirror symmetry. Similar concepts can be employed in chemical structures; if a molecule is identical to its mirror image

then it is known as *achiral*. If a molecule and its mirror image are non-super imposable on each other then it is recognised as chiral. A few examples are given in figure 2.5 to explain chirality.



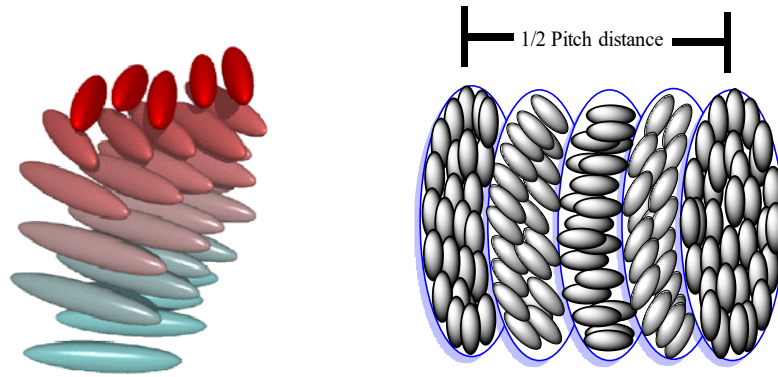
**Figure 2.5:** A few examples of chiral objects.

In liquid crystals, chirality can either be introduced by adding a chiral component in the molecular structure itself or by adding a small amount of chiral material to the host inducing chirality. This is usually known as a chiral dopant.

The cholesteric (or chiral nematic) liquid crystal phase denoted by  $N^*$  is characteristically composed of nematic mesogenic molecules. These molecules contain a chiral centre which produces intermolecular forces that favour alignment between molecules at a slight angle to one another. This leads to the formation of a structure which can be visualised as a stack of very thin 2-D nematic-like layers with the director in each layer twisted with respect to those above and below. In this structure, the directors actually form in a continuous helical pattern about the layer normal. [30]

The molecules shown are merely representations of the many chiral nematic mesogens lying in the slabs of infinitesimal thickness with a distribution of orientation around the director. An important characteristic of the cholesteric mesophase is the chiral pitch “p”.





(a) Molecular orientation in a chiral nematic helix



(b) Standing helix with pitch gradient in a planar cell



(c) Oily-streaks or Grandjean texture

**Figure 2.6:** Molecular arrangements in cholesteric or chiral nematic phase and textures under polarised optical microscope. Image (b) reproduced with permission from Dr. Malik Qasim

The pitch “ $p$ ” is defined as the distance; it takes for the director to rotate one full turn in the helix, as demonstrated in the above figure 2.6(a). A by product of the helical structure of the chiral nematic phase is its ability to selectively reflect light of wavelengths equal to the pitch length, so that a colour will be reflected when the pitch is equal to the corresponding wavelength of light in the visible spectrum. The effect is based on the gradual change in director orientation between successive layers which modifies the pitch length resulting in an alteration of the wavelength of reflected light according to temperature. The angle at which the director changes can be made larger, and thus tighten the pitch, by increasing the temperature of the molecules, hence giving them more thermal energy. Similarly, decreasing the temperature of the molecules increases the pitch length of the chiral nematic liquid crystal. This makes it possible to build a liquid crystal thermometer that displays the temperature of its environment by the reflected colour. Mixtures of various types of these liquid crystals are often used to create sensors with a wide variety of responses to temperature change.

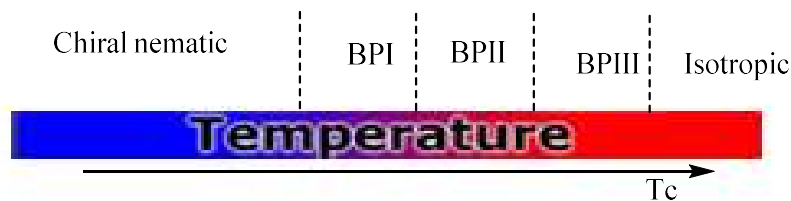
The wavelength of the reflected light can also be controlled by adjusting the chemical composition, since cholesterics can either consist of exclusively chiral molecules or of

nematic molecules with a chiral dopant dispersed throughout. In this case, the dopant concentration is used to adjust the chirality and thus the pitch of the nematic.

### 2.1.3.3 Blue Phases:

Blue phases, exhibited by high chiral liquid crystals were first observed by Reinitzer in 1888 upon cooling cholesteroyl benzoate. He observed a “bright blue-violet colour phenomenon” and was very quick in its appearance and disappearance.[31] However, it was not until the work of Armitage and Price in 1975 that blue phases were shown to be stable, distinct and thermodynamically stable phases of liquid crystals.

Blue phase usually appears within a small temperature range at the boundary of the isotropic and nematic phase as a mosaic of bright colours. Blue phases in contrast to the chiral nematic phases, acquires a three dimensional periodic structures. These phases, with a three dimensional structure, appears as platelets under an optical polarising microscope. These platelets appear in different colours because they reflect different wavelengths. So far, three types of blue phases [BI, BII, BIII (also known as fog)] are known and classified with respect to their symmetry. The number and types of blue phase varies from material to material. Figure 2.7 shows the typical pattern for the three types of blue phases with respect to the temperature appearing in a chiral nematic liquid crystal.

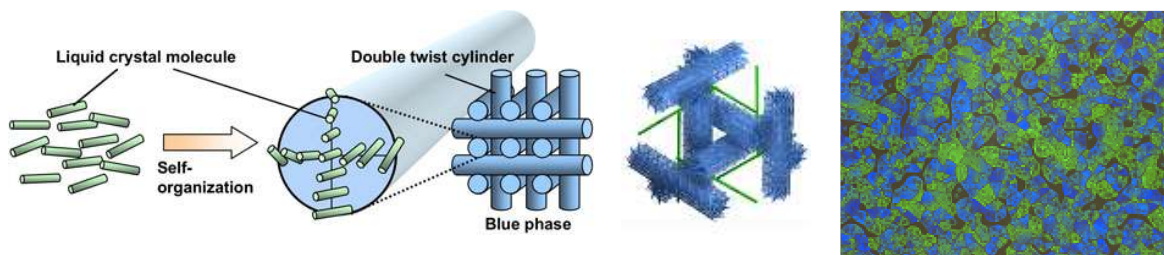


**Figure 2.7:** Phase diagram for three types of blue phase that appear in chiral nematic liquid crystals. Adapted from [28]

Blue phases are perturbed three dimensional cubic structures in which chirality and packing are in competition. Instead of a single helix in chiral nematic or cholesteric phase, the director in blue phase rotates in a helical manner about each axis perpendicular to a line in the middle matching the molecular longer axis orientation in its central point. This type of self assembly in a blue phase is referred to as a double twist structure, though there is no particular number of helical axes constituting this type of arrangement. The array of defects appears at the corners of stacked cubic structures due to the presence of the different directors.

Blue phase devices give a particular blue reflection due to Bragg's scattering when observed without the aid of an optical microscope. When blue phase is illuminated with linearly polarised light, it creates a narrow reflection band. This means that the reflected light does not change its polarisation. However, in chiral nematics Bragg's reflection depends on the chiral pitch of the nematic material.[32]

A general rule of thumb for the blue phase to appear in a chiral nematic material is that the pitch needs to be less than 500 nm.[33] Figure 2.8 shows an illustration and a simple cartoon of the self assembly of a blue phase [34], including basic disclination lines or defects and optical micrograph for combined BPI and BPII.



**Figure 2.8:**Blue phase self organisation, array of disclination lines [35] and the actual polarised optical micrograph.

The blue phase is of great interest in present modulation technology due to its selective Bragg's reflections of visible wavelengths and a photonic band which can be manipulated by an applied electric field. The blue phase can be utilised in devices such as high speed modulators or in tuneable photonic crystals and lasers. The blue phase is also optically isotropic and possesses a large *Kerr* constant because of the change in refractive index of the material with an applied electric field. [36]

Blue phase allows colour sequential display by using blue, green and red LEDs (light emitting diode) backlight so that the conventional filters can be abolished. It does not require any alignment layer so the process of fabrication can be simplified. The off state of blue phase is isotropic in nature, evolves wider viewing angle [37]–[39] Blue phase give a response time in micro second range which is ten times faster as compared to the nematic liquid crystals. [40]

However, the main obstacle to their practical application is the narrow band transition temperature. In situ polymer stabilisation of the blue phase can make it more practical but the polymer network in the system increases the threshold voltage several folds. By using an

appropriate composition and concentration of reactive mesogens, this issue can be resolved. One of the main aspects of this research is to obtain a low threshold switchable polymer stabilised blue phase.

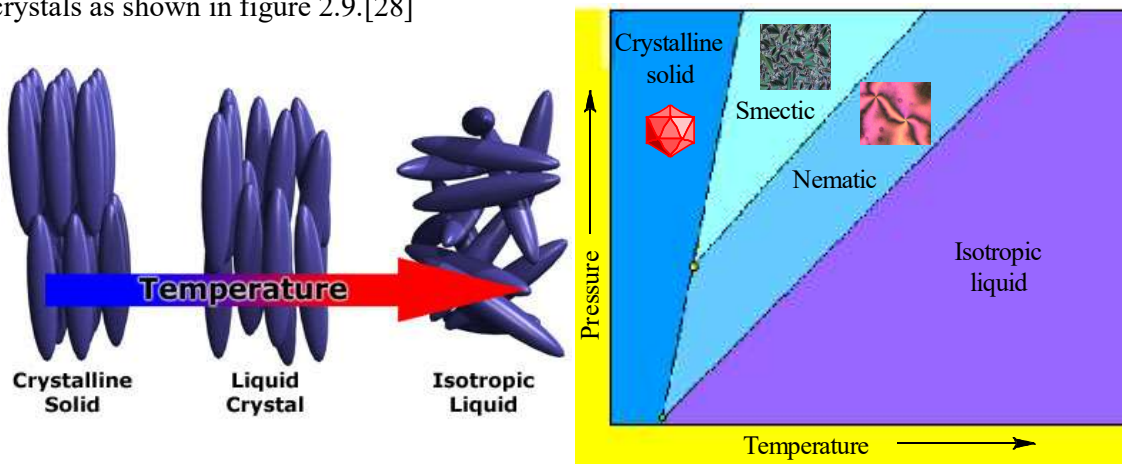
### 2.1.3.4 Smectic phases:

Like nematic, the word "smectic" is derived from the Latin word 'smecticus' means cleaning or soap like properties. This is explained by the fact that the thick, slippery substance often found at the bottom of a soap dish is actually a type of smectic liquid crystal.

The smectic state is another distinct mesophase of liquid crystal substances. Molecules in this phase show a higher degree of translational order and least symmetry. In the smectic state, the molecules not only maintain the general orientational order of nematics but also tend to align themselves in layers or planes. Motion is restricted to within these planes, and separate planes are observed to flow past each other. The increased order means that the smectic state is more viscous than the nematic. [41] Many compounds are observed to form more than one type of smectic phases and 12 different variations have been identified. These will not be discussed further as they are not relevant to this research work.

### 2.1.4 Characterisation of Liquid Crystals:

Crystalline materials exhibit long range periodic order in three dimensions. By definition, an isotropic liquid has no orientational order. [42] Substances that are not as ordered as a solid, and even have some degree of arrangement, are appropriately called liquid crystals as shown in figure 2.9.[28]

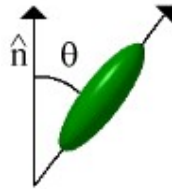


**Figure 2.9:** Molecular arrangement and phase description with respect to temperature change. Reproduced from [28]

To measure just how much order is present in a material, the order parameter (S) is defined as:

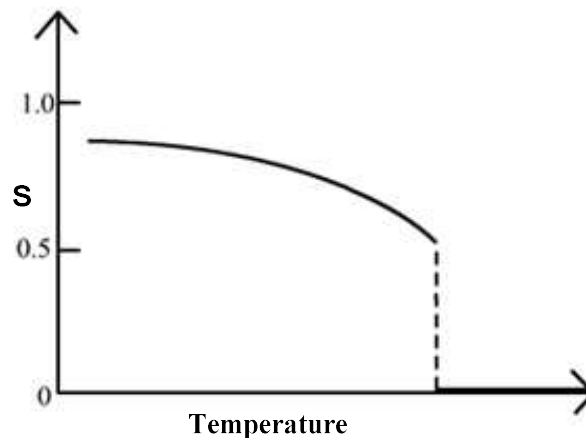
$$S = \frac{1}{2} \langle 3\cos^2\theta - 1 \rangle \quad \text{Equation 2.1}$$

Where,  $\theta$  is the angle between the director and the long axis of each molecule. The parentheses  $\langle \rangle$  represent an average orientation of the molecules in defined boundaries as shown in figure 2.10.



**Figure 2.10:** Pictorial representation of the molecular director.

In an isotropic liquid, the average of the cosine terms is zero, and so the order parameter is equal to zero. For a perfect crystal, the order parameter is one and generally, the order parameter of a liquid crystal falls between 0.3 and 0.9 and is a function of temperature. This is shown in figure 2.11 for a typical nematic liquid crystal material.



**Figure 2.11:** Order parameter versus temperature. [43]

Anisotropy is defined as the ability of molecules to align along with the director and is responsible for the unusual optical properties of the liquid crystal.

Three main factors are responsible for liquid crystal formation. “Positional order” refers to the extent to which an average molecule or group of molecules show translational symmetry (as a crystalline material would show). “Orientational order” represents a measure of the tendency of the molecules to align along the director on a long-range basis. “Bond Orientational Order” describes a line joining the centres of nearest-neighbour molecules without requiring a regular spacing along that line. Thus, these molecules show a relatively long-range order with respect to the line of centres but only short range positional order along that line.

Polymorphism is a condition where a liquid crystal compound demonstrates more than one phase in the liquid crystalline state. The term mesophase is used to describe the "sub phases" of such liquid crystal materials. Mesophases are formed by changing the amount of order in the sample, either by imposing order in only one or two dimensions, or by allowing the molecules to have a degree of translational motion.

#### 2.1.5 Thermal characterisation:

Liquid crystal phases are primarily identified under an optical polarising microscope and often with respect to variation in temperature.[28] There are two common thermal techniques that are often employed to do initial characterisation.

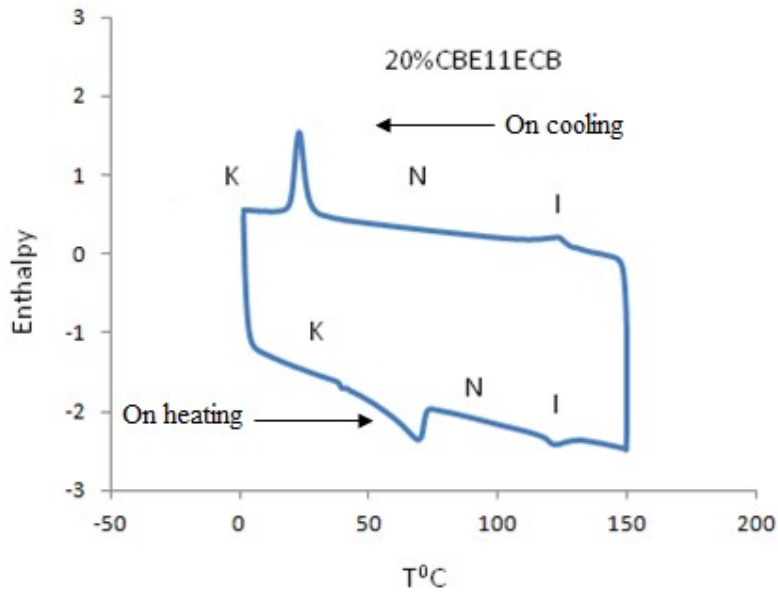
##### 2.1.5.1 Cover slip transition:

This method usually involves the identification of mesophases through optical polarising microscopy. A thin sample of mesogenic material is placed between glass slide and a glass cover slip. This glass slide is then placed in a stage which is accurately temperature controlled. To view the texture of each mesophase, polarisers are set at  $90^\circ$  to each other and hence known as crossed. If an isotropic material is analysed, there will be no change in the polarised light. However, anisotropic birefringent materials give an optical texture which is used to determine the arrangement of the molecules within that medium. [28]

##### 2.1.5.2 Differential scanning calorimetry (DSC):

DSC is used as a complementary tool to optical polarised microscopy to determine the presence of mesophases by detecting the enthalpy change associated with a phase transition. A DSC instrument contains two furnaces, one to heat the sample in an inert reference pan and

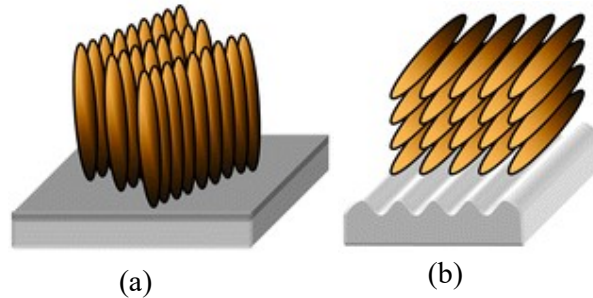
the other to heat the reference (empty) pan. The sample is weighed (5-10mg) into a small aluminium pan and then sealed with an aluminium top. Enthalpy changes associated with a transition cannot identify the type of phase. However, the magnitude of enthalpy change is proportional to the change in ordering of the phase involved. [28] A DSC thermogram for 20%CBE11ECB in BL006 is shown in figure 2.12. Transitions have been marked through cover slip characterisation using POM.



**Figure 2.12:** DSC thermal scan for 20%CBE11ECB in BL006

### 2.1.6 Polarised optical microscopic characterisation:

The polarised optical microscope (POM) is an important tool for the identification of liquid crystalline material and different mesophases. It also plays a vital role in evaluating the physical properties such as spontaneous polarisation, tilt angle and response time of liquid crystals. The texture of a mesogen depends upon how the material is aligned. [28] There are two basic types of alignment of liquid crystalline material. In homeotropic alignment, the orientation of the long axes of molecules is normal (perpendicular) to the substrate and in a planar alignment it is parallel to the substrate plane. Figure 2.13 represents the homeotropic and planar alignment of liquid crystals.



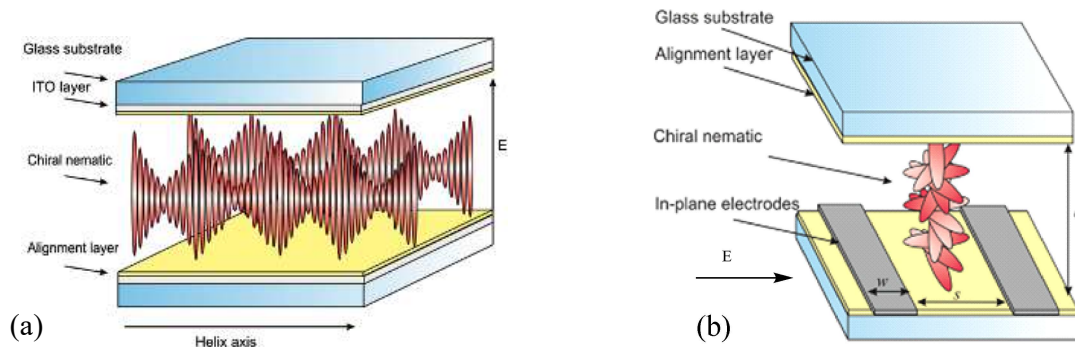
**Figure 2.13:** Representation of (a) homeotropic and (b) planar alignment.

## 2.2 Electro-optic properties (ULH & USH):

Liquid crystals change their optical properties when subjected to an externally applied electric field. The elongated molecules in nematic liquid crystals are likely to have ordered orientations, which are altered upon applying mechanical change or electrical field. The ‘*electro-optic effect*’ is the change in the refractive index resulting from molecular reorientation due to the applied electric field. This in turn changes the observed optical effect of the liquid crystal when light travels through it.

If the refractive index changes are proportional to the applied electric field, it is known as a ‘*linear electro-optic*’ effect or ‘*Pockels effect*’. Whereas, if the refractive index changes are in proportion to the square of an applied electric field is known as a ‘*quadratic electro-optic effect*’ or the ‘*Kerr effect*’.[44]

There are two modes of operation of the flexoelectro-optic effect. One is the uniform lying helix (ULH) configuration in which helix axis is aligned parallel to the substrate and the field applied is orthogonal to the helix axis. As seen in figure 2.14(a). The other orientation is the uniform standing helix (USH) where the helix axis is orthogonal to the substrate as shown in figure 2.14(b). In this case the electric field is applied perpendicular to the helical axis using in-plane electrodes. Figure 2.14 shows the representation of ULH and USH configurations.



**Figure 2.14:** Chiral nematic liquid crystal in a sandwich cell geometry, (a) uniform lying helix, ULH,



configuration and (b) uniform standing helix, USH, configuration [45].

One of the main advantages of the USH mode over the ULH is that the alignment is not that important as Grandjean texture is the lowest energy state when using rubbed polyamide alignment planar layer. Flexoelectro-optic switching in both ULH and USH modes shows that the helix axis tilt angles are comparable for these two modes. However, USH display devices require a larger tilt angle for full modulation than  $22.5^\circ$ , which is more desirable in the ULH mode. Tilt angle for full phase modulation depends on flexoelastic ratio, birefringence and the cell thickness.[46]

### 2.2.1 Dielectric properties:

A polar material which is a non conductor of electricity is known as a dielectric material. Most of the industrial applications of liquid crystals are based on the interaction and reorientation of these materials on an applied electric field. The dielectric properties of liquid crystals give an insight to their basic molecular properties and response to the applied electric field. In liquid crystals, anisotropy is responsible for the dielectric properties and has two components of permittivity. A nematic liquid crystal has a component of dielectric permittivity along the director axis and is represented by  $\epsilon_{||}$  whereas; the component perpendicular to the director is denoted by  $\epsilon_{\perp}$ . Dielectric anisotropy is given by:

$$\Delta\epsilon = \epsilon_{||} - \epsilon_{\perp} \quad \text{Equation 2.2}$$

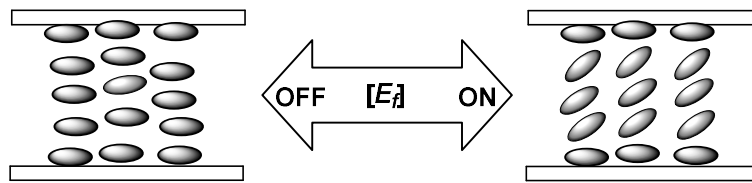
This difference is a very important parameter, like birefringence, to characterise nematic liquid crystals. In positive dielectric materials molecules align their long axis with the direction of an applied electric field. In contrast, for a negative dielectric anisotropic material, the molecules align in such a way that the director is perpendicular to the direction of the applied electric field. [28] The orientation of molecules in the liquid crystal also has a strong effect under an applied electric field. For instance, if the molecules have a strong permanent dipole parallel to the long axis of the molecules, the anisotropy of the dielectric constant is very large. The molecular orientation contribution to the dielectric constant dominates and anisotropy in the dielectric constant follows the order parameter and increases with decreasing temperature.

### 2.2.1.1 The Fréedericksz Transition:

The phase transition in an anisotropic liquid upon applying a sufficiently strong applied electric field was first observed by Fréedericksz and Repiewa in 1927.[47] When a liquid crystalline material is incarcerated in two parallel plates having an alignment layer, the anisotropic material purely follow the surface anchoring conditions. Applying an external electric field across the plates induces reorientation of the liquid crystal molecules, being a dielectric liquid material. This change is frequently known as Fréedericksz transition and can be calculated by the following relation.

$$E_f = \frac{\pi}{h} \sqrt{\frac{K_{11}}{\epsilon_0 \Delta \epsilon}} \quad \text{Equation 2.3}$$

Where  $E_f$  stands for external electric field and is inversely proportional to the dielectric anisotropy  $\Delta \epsilon$  and cell gap  $h$ .  $K_{11}$  is the splay elastic constant and  $\epsilon_0$  is the vacuum permittivity.

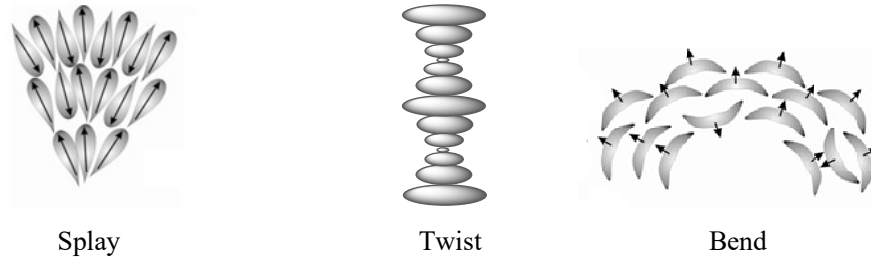


**Figure 2.15:** Freedericksz transition for liquid crystalline material with positive dielectric anisotropy.

With the application of an electric field, the liquid crystal molecules reorient in the middle of the device however, they are constrained along the surfaces by the alignment layers. This phenomenon of reorientation of molecules is shown in figure 2.15. The reorientation of liquid crystalline molecules can be tracked by measuring the change in capacitance with an applied voltage.

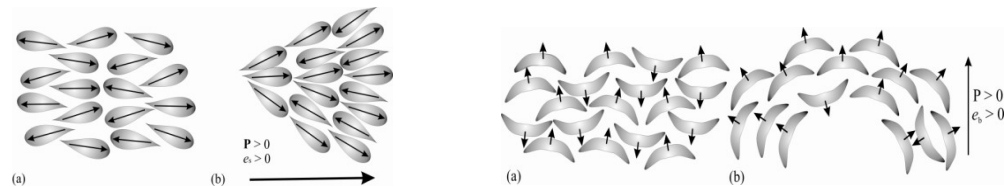
### 2.2.2 Polar effects and flexoelectric coupling:

The discovery and introduction of polar effects in liquid crystals originated from the ideas of Meyer.[48] In 1969 he published a paper entitled the ‘*Piezoelectric Effects*’ in liquid crystals. There are three types of possible deformations, splay, bend and twist and a representation is shown in figure 2.16.



**Figure 2.16:** Three possible deformations in the molecules.

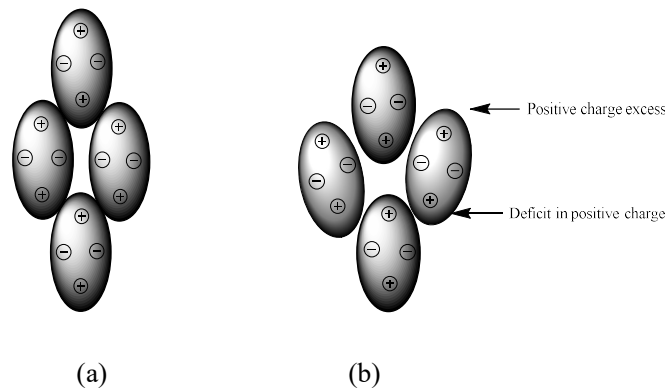
The phenomenon in liquid crystals which is somehow analogous to the piezoelectric effect in solids is termed as flexoelectric effect by Meyer. The molecular structure and geometry of a liquid crystal is imperative for observable flexoelectricity and in turn has many effects on its flexoelectro-optic properties. If molecules possess shape polarity and also have a permanent electric dipole moment, this will polarise the material and conversely an electric field will induce the deformations. Flexoelectricity is the generation of a spontaneous polarisation in a liquid crystal, due to deformation of the director profile. Classically, the flexoelectric effect arises from molecules with a shape asymmetry. Pear shaped molecules with longitudinal dipoles show spontaneous polarisation when splayed. Likewise, banana-shaped molecules with transverse dipoles exhibit spontaneous polarisation under bend deformation. It has been recommended by Rudquist[49] that a material with a combined pear-banana shape hybrid asymmetry and a molecular dipole at  $\sim 45^\circ$  to the molecular long axis will have a low dielectric anisotropy. This type of materials holds a strong molecular dipole and high shape asymmetry. Due to its hybrid shape and its dipole moment, the molecule will have non-zero values for both the splay and bend flexoelectric coefficients. Figure 2.17 shows the Meyer model to explain the deformations in an overall non-polar un-deformed state upon applied electric field for banana and pear shaped molecules[50].



**Figure 2.17:** Meyer's model of curvature electricity, (a) un-deformed and (b) with deformations [46].

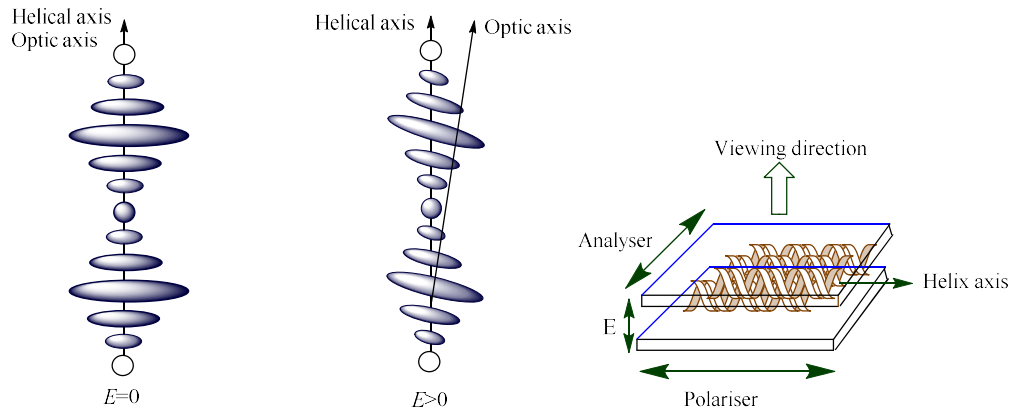
Later it was found that flexoelectricity was not limited only to asymmetric molecules with strong dipoles. Prost and Marcerou [51] showed that quadrupolar flexoelectric coupling is also possible and it does not require the shape asymmetry or the presence of a permanent

dipole. It means that flexoelectricity is possible in all nematic materials. Figure 2.18 shows the effect of a splay deformation in a nematic material with non-polar symmetric molecules. It is obvious that the splay deformation of a group of quadrupoles creates a non-uniform charge distribution therefore leading to a bulk polarisation.



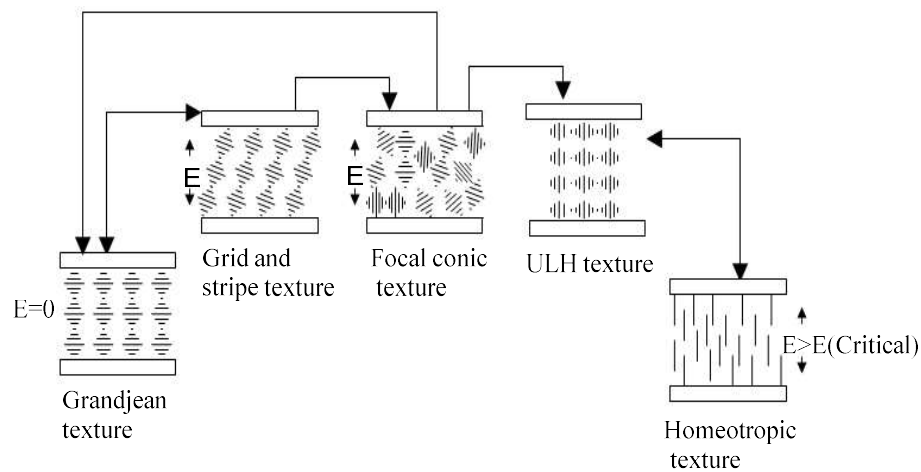
**Figure 2.18:** An illustration of quadrupolar flexoelectricity; a) shows the un-deformed system, while b) shows a splay curvature.

As explained earlier, the optic axis of a material in a short pitch chiral nematic is positioned perpendicular to the director plane and hence any rotation of the director plane ends up in an equivalent rotation of the optical axis. Applying an appropriate external electric field, perpendicular to the helix axis, produces strains due to the coupling of molecular dipoles flexoelectrically to the applied field. The resulting rotation of director planes through an angle (often called the tilt angle) signifies the rotation of the optic axis by an equivalent angle. This flexoelectrically induced rotation of the optic axis is referred to as the flexoelectro-optic effect and is illustrated in figure 2.19 along with the uniform lying helix (ULH) orientation of short pitch chiral nematic liquid crystals. In order to view the flexoelectro-optic effect, the alignment of the short pitch chiral nematic liquid crystalline material should be in the uniform lying helix (ULH) orientation and is potentially desirable in an electro-optic device or application.



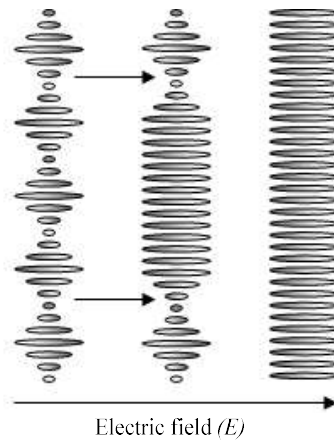
**Figure 2.19:** An illustration of the flexoelectro-optic effect.

A chiral nematic liquid crystal with a positive dielectric anisotropy aligned in the standing helix texture generates a sequence of texture changes upon an applied electric field as illustrated in figure 2.20. Usually, without any external electric field, the chiral nematic material in a test cell having a planar alignment layer, exhibits the Grandjean texture. The helix axis in this texture is perpendicular to the substrate. On employing an external electric field up to a critical point across the device, a grid and stripe texture appears as a result of tilt in the helices. Upon further increment of the applied field, nucleation of the focal conic texture is observed. The relaxation of the focal conic texture by an adequate decrease in the electric field depends on the pitch ( $p$ ) of chiral nematic liquid crystal material and the device thickness ( $d$ ). When the ratio between these two parameters is small, the focal conic texture will relax back faster than when compared to a large  $d/P$  ratio.



**Figure 2.20:** A graphic representation of texture changes demonstrated by the short pitch chiral nematic with respect to an external applied electric field.

When the external electric field amplitude is increased consistently, there is a point where helices will unwind completely and will adopt the homeotropically aligned chiral nematic liquid crystal texture. This helix unwinding is a persistent process with a consistent increment in the applied field due to the annihilation of the focal conic texture[52]. The sooner the amplitude of the external field is reduced below the unwinding voltage, the sooner the focal conic texture reappears and a further decrease in field leads to the reappearance of standing helices. Figure 2.21 shows unwinding of helices with the increase in applied field.



**Figure 2.21:** An illustration of unwinding of helix by increasing electric field amplitude.

### 2.2.3 Response time:

Speed of an optical response is equally important along with other parameters in any electro-optic application and is normally regarded as the switching speed when related to the change in the orientation of the optic axis. The time taken by the liquid crystalline medium to relax back to its equilibrium or stable state is recognised as response time. The response time can be explained through following mathematical expression.

$$\tau = \frac{\gamma}{K} \frac{p^2}{4\pi^2} \quad \text{Equation 2.4}$$

Where  $\tau$  is response time  $\gamma$  is the viscosity coefficient,  $p$  is the pitch length and  $K$  is an elastic coefficient. From this expression it is evident that the response time is independent of the external applied field. Considering an increase in the applied field, there will be a comparative increase in the torque exerted on the liquid crystalline molecules.[53] On the other hand, the increase in the applied field also increases the rotational molecular speed to the same extent. This in turn balances the rotational angle of the molecules and hence the response time is effectively independent of the applied field. The above relation also demonstrates that the response time of the material can be optimised by using a short pitch material with low

viscosity coefficient and high elastic coefficient. Usually, a bigger tilt angle, large flexoelectric coefficient, a lengthy pitch and low elastic constant are essential.[53] So response time and a large tilt angle can be traded off while selecting a material by optimising the material composition by incorporating components with high flexoelectric coefficients and components with low viscosity.

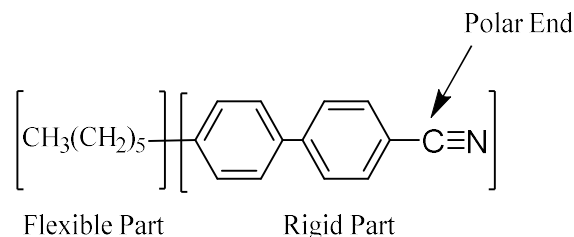
Another approach to achieve a faster response time is to control the device thickness and by using a high birefringent with low viscosity LC mixture. High birefringence provide a boost to brightness and contrast in polymer dispersed liquid crystals (PDLC) and cholesteric liquid crystal displays. Using a reduced cell gap below 4 $\mu$ m results in the faster response time and has already been reported [54]. Therefore in general, above mentioned factors can be summarised below in table 2.2.

Factors	Rise time	Decay time
Low viscosity ( $\gamma$ )	Decrease	Decrease
High elastic constant ( $K_{11}$ )	Increase	Decrease
High dielectric anisotropy ( $\Delta\epsilon$ )	Decrease	Decrease
Small device thickness (d)	Decrease	Decrease
Low tilt angle ( $\theta$ )	Increase	Decrease
High surface anchoring	Increase	Decrease
High temperature (T)	Decrease	Decrease
High Applied field (V)	Decrease	Decrease

**Table 2.2:** Factors affecting the response time of liquid crystal.

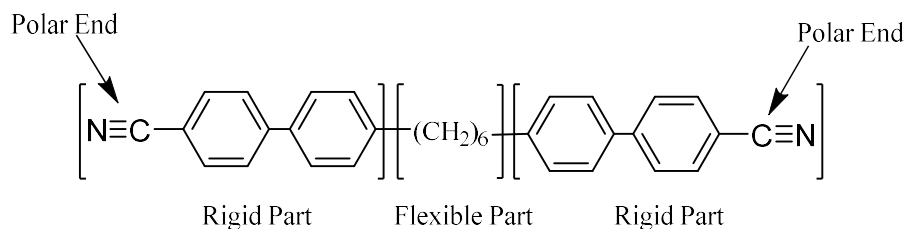
### 2.3 Chemical Structure of Liquid Crystals:

In general, liquid crystal molecules are consist of two main components, one is the rigid part manly coming from aromatic rings and the other is the flexible part derived from long hydrocarbon chain(s) and polar group(s) as shown in figure 2.22.



**Figure 2.22:** Generic structure of liquid crystal p-n-Hexyl-p'-cyanobiphenyl (6CB).

The above mentioned generic structure of liquid crystals is often referred as monomesogenic whereas, a mesogenic dimer is two rigid cores flanked by a flexible chain as shown in figure 2.23.



**Figure 2.23:** Generic molecular structure of a mesogenic dimer 4',4'''-(hexane-1,6-diyl)bis([1,1'-biphenyl]-4-carbonitrile).

## 2.4 Optical properties:

Due to the anisotropic nature of liquid crystalline molecules some interesting optical properties are demonstrated. The most important and interesting are Bragg-type scattering, circular dichroism, waveguiding and birefringence. [55]

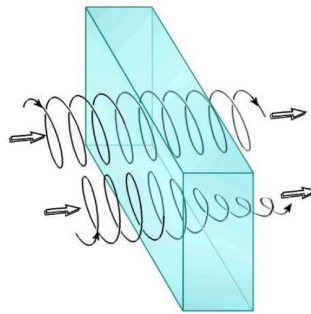
### 2.4.1 Bragg scattering:

When illuminated with white light, the chiral nematic structure scatters light to give an iridescent colour which varies with temperature, angle of incidence and angle of observation. In many ways chiral nematic liquid crystals behave like a multiple layer interference filter. At any given temperature the predominant wavelength depends upon the angle of incidence and the angle of scattering. [28] The scattered light behaves as if it were coming from a number of regularly spaced planes existing in a medium having a refracting index equal to 1.5. This is comparable to the Bragg scattering of X-rays from a crystal.



### 2.4.2 Circular dichroism:

In a chiral nematic standing helix or Grandjean plane texture; if the propagating incident light ( $\lambda_0$ ) is equal to the pitch length ( $p$ ) of the helix then it shows a strong selective reflection of circularly polarised light. Furthermore, this selective reflection corresponds to the same handedness and wavelength as the pitch inside the chiral nematic medium. [28] The reflected light is circularly polarised with the same handedness as the incident light, the exact opposite of a normal reflection. The oppositely circularly polarised light is almost wholly transmitted through the medium. This is called circular dichroism; figure 2.24 shows an example of such phenomenon.



**Figure 2.24:** Right-hand circularly polarised light (bottom) being absorbed by a material more strongly than left- hand circularly polarised light (top). (Image by Wikipedia Commons)

### 2.4.3 Waveguide properties:

In a waveguide the diffraction of a light beam is suppressed by the in-homogeneity of the optical medium and hence depends on the pitch of the LC material. Waveguiding takes place when the pitch of the chiral nematic is larger than the wavelength of the incident light. The LC helix can be considered as a layered structure. In a helix LC, molecules are arranged in such a way that each subsequent layer is at a very small increase in angle to the previous one. The polarised light upon entering each layer is slightly deviated owing to the angle increment in each layer. Polarisation of light remains linear as the phase difference between the two components is very small. This offers a waveguiding effect as the extent of rotation in polarisation corresponds to the amount of twist in the chiral LC. The same practice has been used in the twisted nematic display devices. Liquid crystals are promising, because their optical properties are easily influenced by temperature change or an electric field. Their presence can be used to modify the effective refractive index of light in a waveguide. So it is possible to generate a wave guide in a bulk liquid crystal by modulating the director orientation[56]. There are many applications where light propagation is not necessary in free space like optical communication and sensing.

#### 2.4.4 Birefringence:

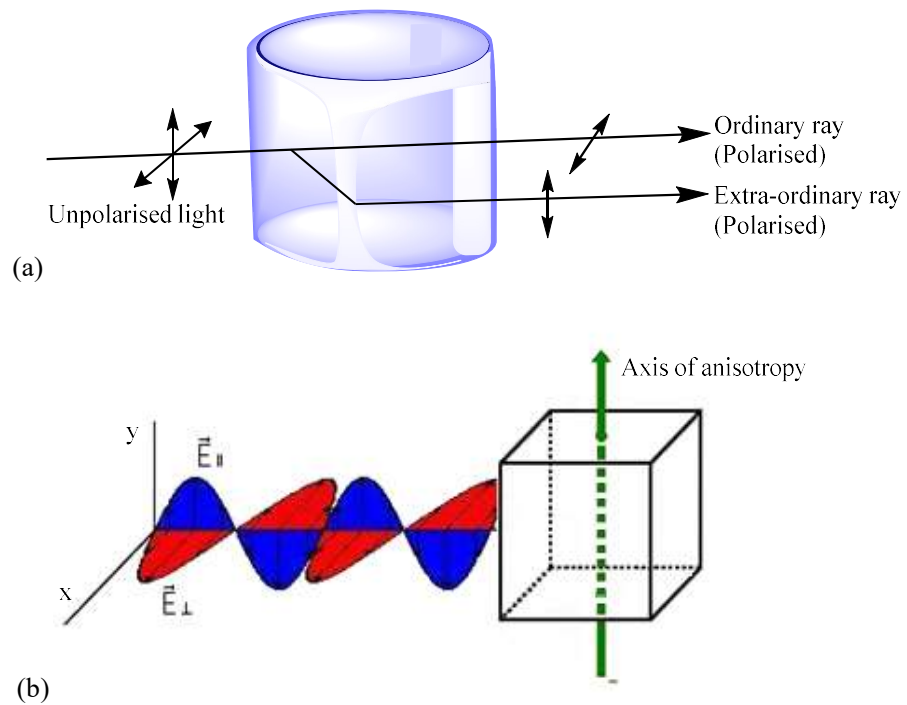
Birefringence is a characteristic of liquid crystals and is dependent on the presence of conjugated  $\pi$ -electrons in the molecule. It is very important for display applications to keep the birefringence at its optimum value as extended conjugation can impart dispersion leading colour generation under polarised white light[28].

When light enters nematic liquid crystal sample, the process is modelled in terms of the light being split into the fast (called the ordinary ray “*o*”) and slow (called the extraordinary ray “*e*”) components. Because the two components travel at different velocities, the waves get out of phase. When the rays are recombined as they exit the birefringent or doubly-refracting material, the polarisation state has changed because of this phase difference.

The birefringence of a material is characterised by the difference,  $\Delta n$ , in the indices of refraction for the ordinary and extraordinary rays. To be a little more quantitative, the index of refraction of a material is defined as the ratio of the speed of light in a vacuum to that in the material. For this case,  $n_e = c/v_{\parallel}$  and  $n_o = c/v_{\perp}$  for the velocities of a wave travelling perpendicular to the director and polarised parallel and perpendicular to the director. The maximum value for the birefringence,  $\Delta n = n_e - n_o$ .  $\Delta n$  varies from zero to a maximum value, depending on the direction of travel. The condition  $n_e > n_o$  describes a positive uniaxial material, and nematic liquid crystals are in this category. For typical nematic liquid crystals,  $n_o$  is approximately 1.5 and the maximum difference,  $\Delta n$ , may range between 0.05 and 0.5 [43].

The thickness of the sample is another important parameter because the phase shift accumulates as long as the light propagates in the birefringent material. Any polarisation state can be produced with the right combination of the birefringence and path length parameters. Since for the two wave components travelling with different velocities in a birefringent material, the difference in optical paths will lead to a change in the polarisation state of the wave as it progresses through the medium. We define the optical path for a wave travelling a distance  $L$  in a liquid crystal as  $nL$  so that the optical path difference for the two wave components mentioned above will be  $L(n_e - n_o) = L\Delta n$ . The resultant phase difference between the two components (the amount by which the slow, extraordinary component lags behind the fast, ordinary one) is just  $2\pi L\Delta n/\lambda_o$  where  $\lambda_o$  is the wavelength in vacuum. The following simulation demonstrates the optical properties of a birefringent material. A linearly polarised light wave enters a crystal whose extraordinary (slow) index of refraction can be controlled by the user. The path length of the sample can also be varied, and the outgoing

polarisation state is shown in figure 2.25a. Figure 2.25b shows light entering a birefringent material.

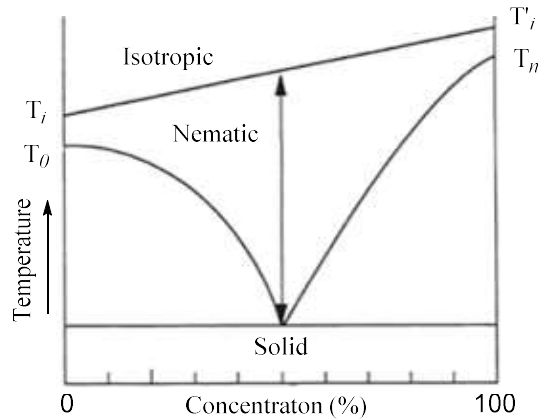


**Figure 2.25:** A schematics of birefringence, (a) An Ordinary light travelling through a nematic liquid crystal and (b) Light entering a birefringent material.

## 2.5 Eutectic Mixtures:

There is no single liquid crystal compound that can fulfil all requirements for a liquid crystal display available at present. For example, 5CB has melting point  $24^{\circ}\text{C}$  and clearing point is  $35.3^{\circ}\text{C}$ . It is obvious that such a narrow transition is inadequate for the industrial application with an operation temperature of  $-20$  to  $80^{\circ}\text{C}$ . It is well established that a binary mixture of compounds shows a lower melting point when compared to the either of its components and depends on the mixture ratio. At a eutectic point, melting point reaches its minimum. Clearing point of the liquid crystalline mixture is generally the linear average of the composition. A binary mixture of liquid crystal can offer a much wider nematic transition range for use in display applications. For example, a mixture of MBBA and EBBA offers a range of  $0^{\circ}\text{C}$  to  $60^{\circ}\text{C}$ .<sup>[57]</sup> Besides melting point, other physical parameters such as dielectric constant, dielectric anisotropy, elastic constants, birefringence and viscosity are also dependent on the mixture ratio. Typical liquid crystal mixtures are designed to provide the



optimum physical parameters for liquid crystal display applications. A typical example of a eutectic mixture is shown in figure 2.26 in the form of phase diagram.



**Figure 2.26:** Phase diagram of the binary mixture of liquid crystals. [58]

### 2.6 Phase Modulation:

Light is an electromagnetic radiation and the primary properties of visible light are intensity, propagation direction, frequency or wavelength spectrum and polarisation. [59] Further, packets of this electromagnetic radiation are also known as photons and they exhibit both particle and wave nature. This dual nature of light has been explained by its behaviours which are listed in below table 2.3.

Phenomenon	Wave nature of photon 	Particle nature of photon 
Reflection	✓	✓
Refraction	✓	✓
Interference	✓	✗
Diffraction	✓	✗
Polarisation	✓	✗
Photoelectric effect	✗	✓

**Table 2.3:** Dual nature phenomenon of light

In display technology phase modulation relates to the wavelength modulation of the light and gives a metric of colour whereas amplitude modulation relates to intensity of the light and hence controls the contrast or brightness. A change in phase and / or amplitude of light influenced by a medium or electric addressing is known as modulation of light. In a typical

LCoS (liquid crystal on silicon) device light modulation is harnessed by employing two principles either utilising the amplitude modulation, where linear variations in the polarised light are achieved in the direction of polarisers. Or by the phase modulation, where phase delay is achieved by electrically altering the optical refractive index along the direction of light [60][61].

### 2.6.1 Spatial light modulators and Holograms:

Devices which are used to convert electrical signals to the optical signals are known as spatial light modulators (SLMs). The electrical signals are used to convert the light by modulating the phase, amplitude or polarisation (or combinations of these) of light. In liquid crystal based SLMs the modulation depends on the type, chemical structure, electrical and optical anisotropy of the liquid crystal used. In addition, their electro-optic properties are significant in spatial applications where each pixel is able to change the properties of reflected or transmitted light. A digital micro mirror device (DMD) is an optical micro-electrical-mechanical system (MEMS) that contains an array of highly reflective micro mirrors. These micro mirrors are made out of Aluminium, to obtain gray scale mirrors are toggled on and off very quickly.[62] Liquid crystal on silicon (LCoS) technology is used in micro displays and pixel sizes are between 4-6  $\mu\text{m}$  whereas, in micro electro mechanical systems (MEMS) the pixel size is around 10  $\mu\text{m}$ .[63]–[65]

MEMS device relies on micro mirrors to control the direction of reflected light, often are used in data projectors but they are complex to manufacture and require high degrees of precision. Also this method only manipulates the amplitude of the light and hence cannot easily be used in diffraction devices. LC SLMs can be fabricated with less complexity, are more versatile than MEMS and are highly suitable for diffraction based device applications.

The generation of an image by the interaction of light waves through diffraction to create a defined intensity distribution in a required arrangement known as hologram and the technique is recognised as holography.

For a coherent light source such as laser, there is no need of complicated optics as an image is created by interference of diffracted light and can be controlled in depth as well. The image obtained by this method is often known as a computer generated hologram (CGH) and the generation method is known as computer generated holography. Also, the optics used in this type of diffractive system does not need to be of particularly high quality or alignment as a CGH has the ability to correct for aberrations and imperfections in the hologram.

Liquid crystal based SLMs proffer numerous benefits such a large modulation depth, no movable components, potential for large aperture functions and low manufacturing cost. For phase modulation of incident light, a nematic liquid crystal modulator is usually aligned in a planar mode in such a way that the director is aligned parallel with respect to the polarisation of the incident light. With the application of an external field, the liquid crystal molecules tilt in parallel to the direction of the applied field and hence change the refractive index. This changes optical path and subsequently creates a phase shift on the incident light.

#### 2.6.1.1 Applications of SLMs:

The continuous expansion of SLM technology has opened up many applications, in amplitude modulation such as conventional video projection and also some potential applications such as holography using phase modulation. Applications based on phase modulation includes holographic optical tweezers, holographic optical storage media and holographic image projection for head-up-displays (HUD) [66].

Liquid crystal properties limit the performance of LC based SLMs such as ferroelectric liquid crystals only have binary modulation but have faster response times whereas, nematic liquid crystals can continuously change their orientation with respect to the change in applied electric field. This in turn provides a full range of controls for the pixels in the SLM, yet with a slower response usually 1-15ms [66].

Other SLM applications also include optical communications, image projection, optical correlation [67], optical tweezers [68] and pulse shaping [69].

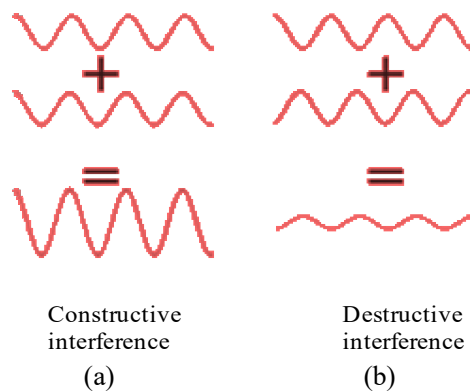
### **2.7 Phase Measurement:**

Phase measurement can be done in two ways in order to get the desired phase modulation properties of liquid crystals. In first method, light is divided in to two or more parts by partial reflection or refraction to obtain two coherent beams produced by amplitude division. These beams travel through different paths before recombining together to get an interference pattern. In the second method a wavefront from a narrow slit source is divided in to two by employing mirrors, biprisms or lenses e.g. Young's double slit interferometer.

This technique has been employed carefully to measure the phase modulation in the blue phase on silicon device.

### 2.7.1 Young's double slit experiment:

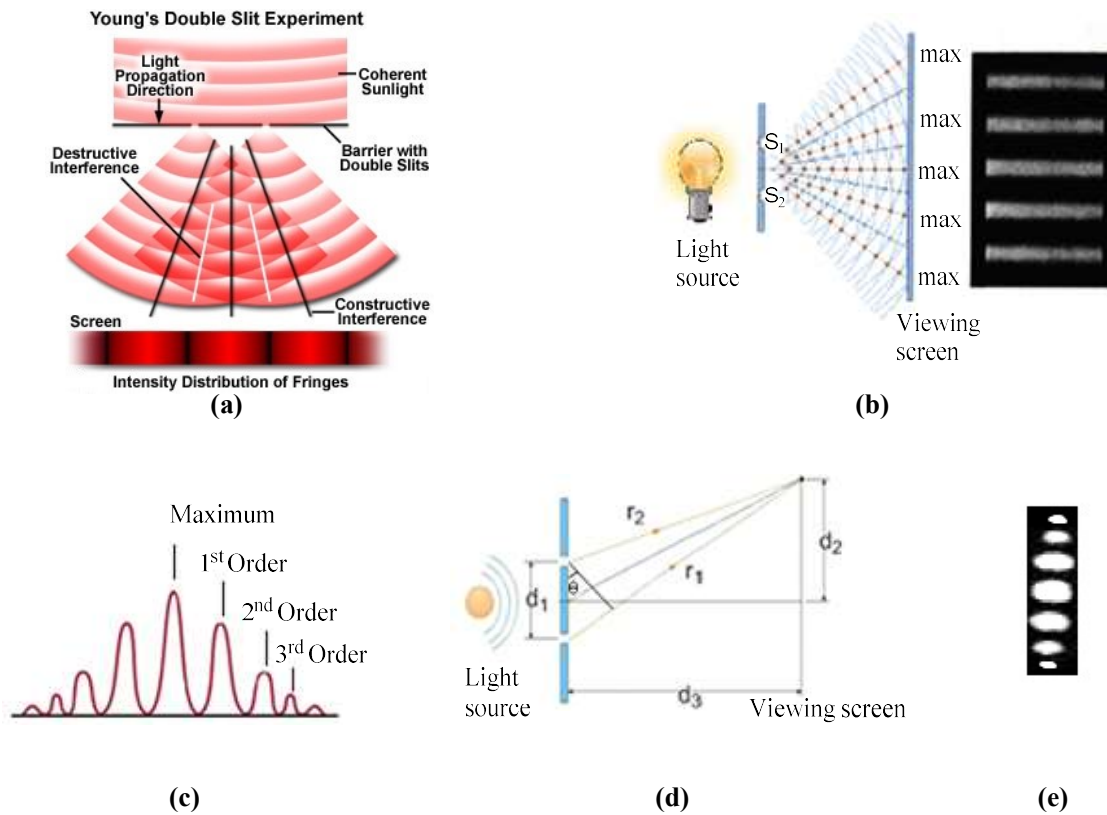
Thomas Young was an English physicist - in the early 18<sup>th</sup> century who did the famous double slit experiment to first observe diffraction of light and most importantly established the wave theory of light. When the light wave passes through a slit or hole it spreads out instead of travelling straight. This spreading out phenomenon is known as diffraction. A double slit shows that light can have a wave like interference pattern when the light from two slits overlap or interferes. The points where these waves overlap constructively always gives a brighter spot and where these overlap destructively, we get a dark spot as shown in figure 2.27 ( a, b). Where it is half constructive, half destructive overlapping a less bright spot is acquired.



**Figure 2.27:** The occurrence of constructive and destructive interference.

The image created is composed of maxima and minima due to the variation in the optical path length. The wave travelling from the centre of each slit is most intense at the middle and hence gives the brightest central spot. This due to the fact that the distance travelled from each slit is same and the phase difference will be zero. Or in other words that both light waves have the same wavelength and phase. This creates the maximum or the zero order. For the first order the difference will be one wavelength, for second order the difference will be two wavelengths and so on. Therefore the greater the difference in the distance travelled by two light waves and hence the intensity of observed pattern will be least, eventually it dies off as shown in figure 2.28 (c).

When the distance between the two slits is increased the angle between two light waves emerging from each of the slits is decreased and vice versa. So this angle is inversely proportional to the distance between the two slits.



**Figure 2.28:** The phenomenon of diffraction of light through a double slit. (a) Explains the diffraction trend through a double slit. (b) Shows the detailed constructive and destructive interference pattern. (c) The graphical representation of the diffraction pattern observed through a double slit indicating order of brightness observed. (d) Elucidate the relationship among the angle and the distance between the slits. Image (a) is taken from <http://www.daviddarling.info/encyclopedia/L/light.html> (e) Actual diffraction image observed during experiment.

When light shines on a reflective device having a double slit arrangement of pixels, an applied electric field induces a change in the liquid crystal birefringence for the light that goes through one of the slits compare to the light passing through the other slit. This induces a phase shift and can be ultimately calculated by the change in position of the maxima in the far field diffraction pattern. That is why Young's double slits can be considered as the simplest hologram and hence can be used to specify the device performance for use in holographic applications.

In this research work silicon substrates were used to carry out phase modulation as liquid crystalline material behaves differently on silicon being reflective when compared to the glass.



## **Chapter 3: Instrumentation and Devices**

This chapter includes all the instrumental techniques utilised to do electro-optic characterisation of all formulated mesogenic mixtures. Further to this, it also describes the device fabrication processes and types of devices used during this research work.

### **3.1 Instrumentation:**

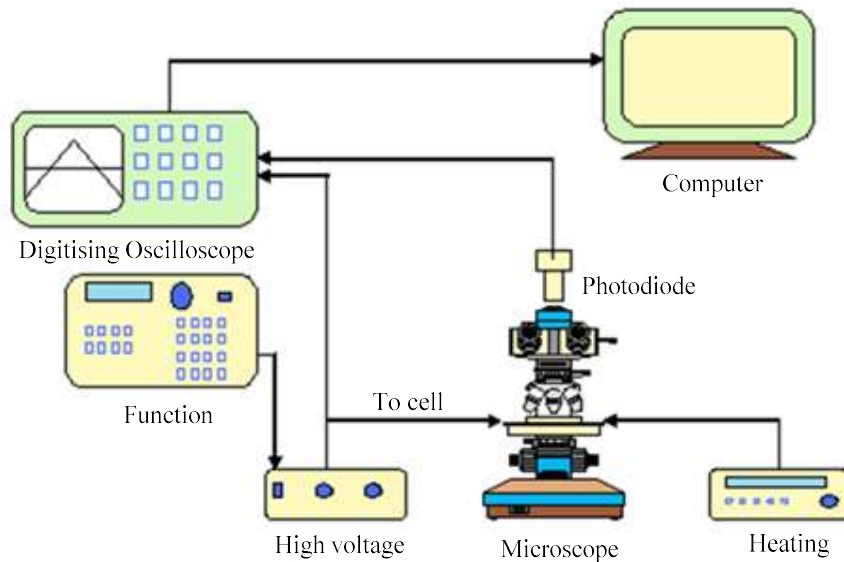
The details of instrumental setups used to study optical and electro-optical properties of all formulated mixtures are as follows.

#### **3.1.1 Optical setup for electro-optic measurements:**

The most commonly used instrument in this work is the hot stage optical polarising microscope. Samples are placed on a heating stage between the microscope's polarisers aligned at 90° to each other, usually known as crossed polarisers. Only optically anisotropic material can be observed under the crossed polarisers. Therefore quite often polarising microscopy is used to identify and characterise liquid crystal phases, to establish phase transition temperatures and to carry out electro-optic measurements. A hot stage attached to the rotation stage of the microscope and this allows temperature dependent measurements.

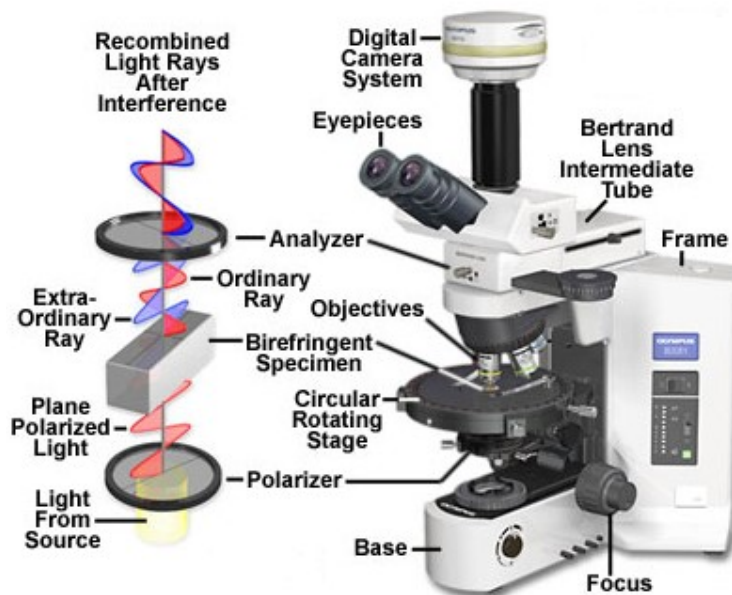
For electro-optic measurements, a function generator is used to apply electric fields to the sample. The signals from the function generator are amplified using an in house built wide band voltage amplifier. A photodiode is used to detect the intensity of light transmitted through the sample.

The applied electric field and photodiode signals are monitored using a digital oscilloscope and the resultant data can be analysed using a computer connected to the oscilloscope. The general set-up of instruments used to characterise the liquid crystals optic and electro-optic properties is shown in the figure 3.1.



**Figure 3.1:** General experimental set-up for electro-optic studies.

The Olympus microscope and schematic of the principal how light interacts with the anisotropic sample is shown in figure 3.2.



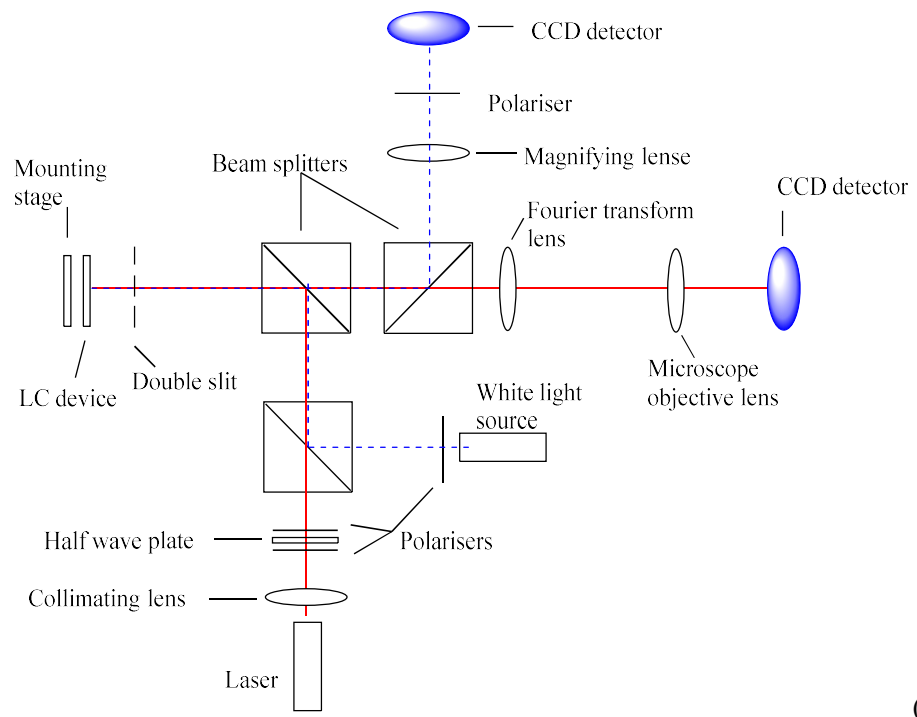
**Figure 3.2:** The Olympus polarising microscope. (Figure from supplier website)

### 3.1.2 Young's slit Interferometer Setup:

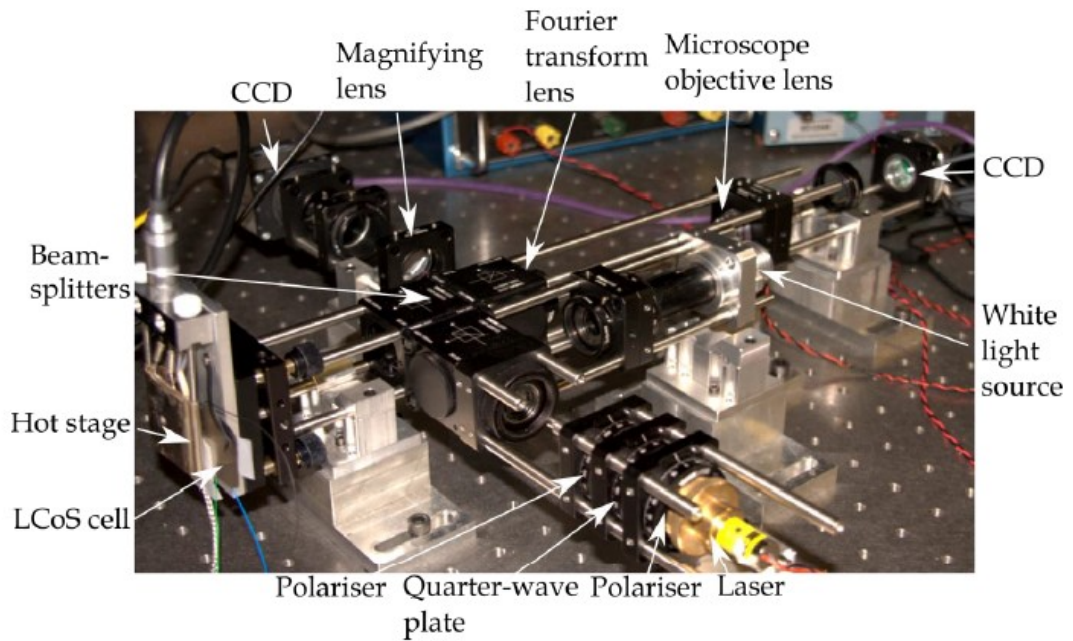
The Young's double slit experiment is based on the wavefront division using slits on a reflective surface. The details and theoretical aspects of the Young's double slit experiment are already explained in chapter 2. It is based on the principle that light passing through a double slit focuses on the screen in such a way that resultant image consists of minima and maxima. This is mainly due to the variation in the difference of the two optical path lengths.

Young's slit experimental setup has already been established and studied in detail by a former PhD student in the group [70] and has been selected to study this phase modulation without further changes.

The instrument setup consists of a coherent laser light to illuminate the area through narrow slits to result in the diffraction and interference pattern. The resultant image was enhanced by using a microscope objective lens and to bring the image closer a Fourier transform lens was used. A charge couple device (CCD) camera was used to capture the image. A white light source (LED) was also used to study the orientation of the liquid crystal. It was collimated using an ocular lens before it has passed through a polariser. Light was then directed to the device and to the further optics upon reflection using a beam splitter. A movable lens was used to magnify the image and a high speed colour camera by Edmund Optics to collect the images. A schematic diagram and the actual photograph of the complete experimental setup based on the Young's double slit diffraction grating are shown in figure 3.3. Laser light source path is shown in red whereas white light path is shown in blue.



(a)



(b)

**Figure 3.3:**(a) Schematics of Young's slit interferometer. (b) Young's slit experimental setup. [70]

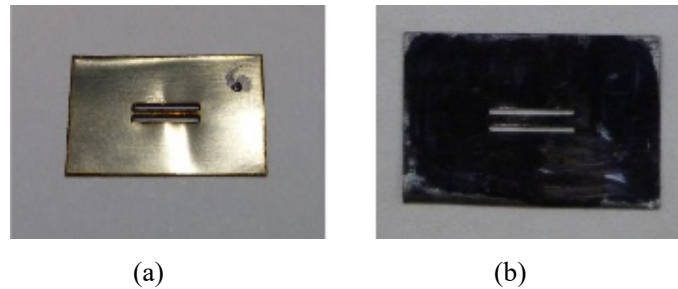
### 3.1.2.1 Alignment in optics and precautions:

It is a tricky process to align the optical components, but practically it is the foundation to precise results. To achieve the desired results, the whole setup was cage mounted on an isolated optical bench enclosed in cardboard sections. This was then further concealed in black curtains to minimise the interference background of light and to reduce the air flow caused by the air conditioning system. Minute flaws in alignment and heights of the optical components of the Young's slit interferometer makes it more difficult to align both the laser and white light at the same instance. The white light source has been beneficial for alignment of optical components as well as to observe the device switching upon applying a field.

The test device was mounted onto a kinematic stage which allowed the device to be tilted or tipped by a few degrees. This minor alteration was desired as the device was not perfectly flat on to the mount. Taking all these precautions made the entire process reliable with reproduce able results.

### 3.1.2.2 Slit mask:

In order to create a perfect diffraction pattern from blue phase LCoS Young's slit device, a mask was placed at the front of the device aligned with the patterned pixels. It was carefully and uniformly laser cut from 1mm thick stainless steel sheet with slit length at 5mm, slit width at 0.3mm and slit separation at 0.7mm. This mask is very useful in grating formation so that the diffraction pattern in the form of spots can be seen in the replay field. By covering the edges of the two patterned pixels, it also helps to remove the edge field effects. At the pixel edges, the electric field is not as uniform as it is in the centre of the pixel and hence response is not uniform throughout the device. In order to address this issue, the mask has been intentionally kept smaller than that of the patterned pixel dimensions to conceal the edges.



**Figure 3.4:** Metal grating used to conceal the device. (a) Novel reflective metal surface slit mask. (b) Same mask coloured in black to reduce reflections. [70]

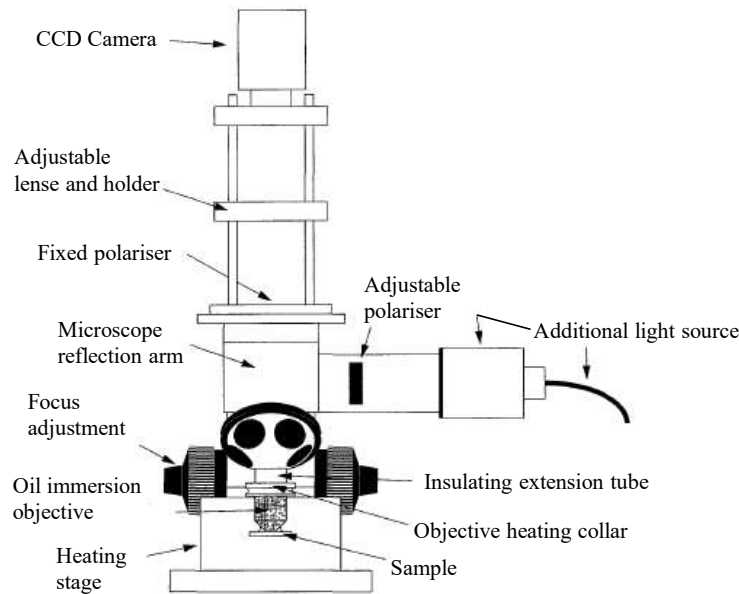
Stainless steel is a reflective surface and can interfere with the diffraction through the slit. To reduce unnecessary reflections, the mask has been stained with permanent black marker. Spray paint has been avoided in this case to retain smooth edges of the mask.

The LCoS device to be investigated, was mounted behind a slit mask, and will be discussed in section 3.2.2 and a 652nm laser light source was used to illuminate on the device along with Thorlabs polarisers, waveplate and non-polarising beam splitters. LeCroy wavestation 2012 10 MHz signal generator and in-house built amplifier were used and the applied voltage was recorded through an Agilent 54624A oscilloscope.

### 3.1.3 Kossel diagram Setup:

The optical setup to obtain a Kossel diagram involves an optical microscope with a provision to include an additional laser or a blue light source.[71] A high resolution oil immersion objective lens was used to obtain the diffraction pattern from the sample. An additional 450nm blue LED light source (Thorlabs) coupled with an optical microscope in a holder attached to the reflection arm was used to observe the diffraction pattern. The speckle pattern which appeared due to coherence has been effectively reduced by slowly shaking the cable of the blue LED. A CCD camera (Pixelink PL-B622CU-KIT camera, Aegis) was mounted onto the microscope to capture images produced after diffraction.

A high resolution (60X) oil immersion lens is vital to eliminate any thermal gradient between the objective and the blue phase sample and with a controllable aperture, light intensity and focus can be controlled. Figure 3.5 shows the optical setup for Kossel diagram.



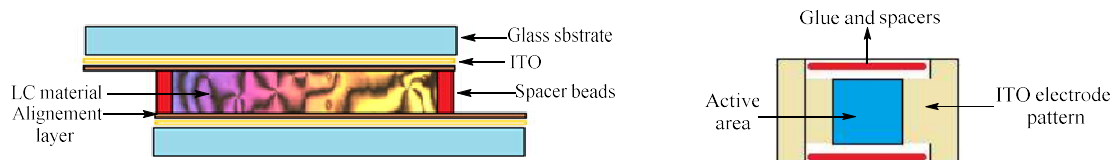
**Figure 3.5:** Optical setup to observe Kossel diagram.

## 3.2 Device Fabrication:

### 3.2.1 Glass cells:

All the flexoelectro-optic measurements have been recorded with the LC mixture confined between two glass substrates. These glass substrates were patterned with indium tin oxide (ITO), an optically transparent conductive layer. Polyamide alignment layer was applied in the inner surface and rubbed in to induce the planar alignment. The two substrates were then glued together using cure able glue (NOA 68 UV, Norland) containing spacer beads (2-20 $\mu\text{m}$ ). The cell was then filled by LC material through capillary action

Two types of cell were fabricated, one with uniform thickness throughout the cell depicted in figure 3.6 whereas, second type is fabricated in a wedge shape. In this case two different sizes of spacer beads are used.

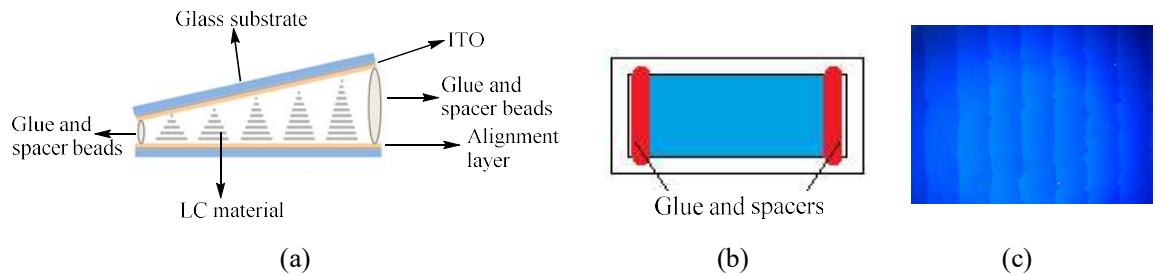


**Figure 3.6:** Lateral view and top view of AP (anti parallel planar) cell used in the LC material characterisation.



When a cholesteric LC material is confined between two glass plates with rubbed surface alignment layer inclined at a small angle, ridges or striations appeared. These ridges can be clearly seen under optical polarising microscope and are referred to as a Grandjean-Cano pattern or *Cano Wedge* as first developed by the French scientist R. Cano in 1960s. This technique of pitch measurement is called the Grandjean – Cano wedge method. [72]

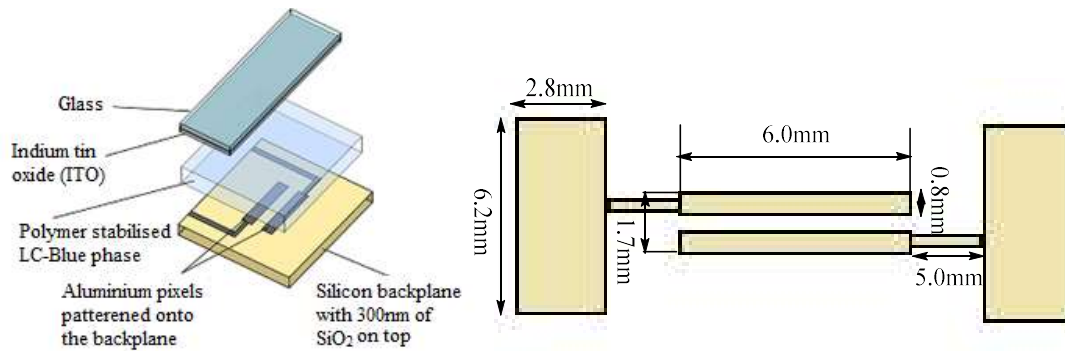
Three different types of wedge cells were fabricated, one without any alignment layer, second with alignment layer on one side and the third one with polyamide alignment layers on both sides. It was found that best result, prominent disclination lines, was observed from wedge cells with the alignment layers on both substrates. These cells were constructed from 20x30mm substrates glued together using optically cured glue (NOA 68 UV, Norland) containing spacer beads. Along one side 2 $\mu$ m spacer beads were used whereas, 20 $\mu$ m beads were employed on the other side to induce the wedge angle in the cell. A typical wedge cell is shown in figure 3.7.



**Figure 3.7:** A schematics of wedges cell (a) Lateral view (b) top view of a wedge cell (c) optical polarising micrograph for 20% FFE9ECB in BL006 showing typical pattern of domain separation by the defect lines.

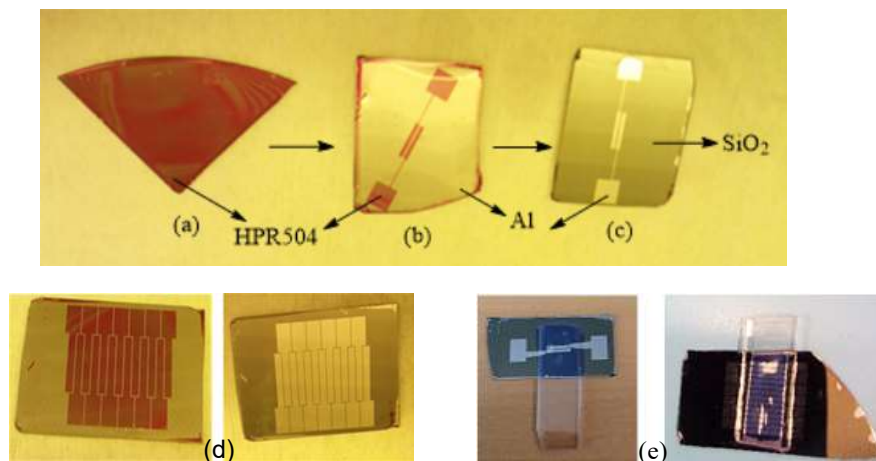
### 3.2.2 Silicon Backplane devices:

Silicon backplane devices are very similar to conventional devices except a silicon backplane constitutes one of the substrate with pixels patterned on it by photolithography. The required pixel structure has been obtained by the specially designed mask and the dimension of the mask used is given in the figure 3.8. The pixel length has been kept long to ensure good consistency for testing area and the rest was covered with the external pixal mask.



**Figure 3.8:** The LCoS device assembly and mask dimensions for the pixel pattern.

Silicon wafers containing 300 nm of  $\text{SiO}_2$ , whilst complementary metal oxide surface as an insulating layer, were used and 200 nm of aluminium metal was evaporated on the surface of the wafers. The entire fabrication process has been carried out in UV free environment due to light sensitive photoresist. The wafer was cut into pieces big enough to complement the pixel pattern mask. A positive photoresist (HPR504) spin coated uniformly on the aluminium surface of the substrate followed by baking at  $95^\circ\text{C}$  for 10 minutes as beyond this temperature aluminium would oxidise. This subsequently was UV cured with the chrome pixel mask placed on top followed by another baking for 3 minutes. These substrates were then developed in 15%AZ351 developer in DI water as developing solution and then placed in 40% orthophosphoric acid solution for etching process of the superfluous exposed aluminium. Figure 3.9 shows the step wise fabrication method and final devices.



**Figure 3.9:** (a) Substrate with photoresist spin coated on the surface. (b) UV cured with pixel mask and developed silicon substrate. (c) Finalised backplane with aluminium pixels after etching process. (d) Multi-pixel substrate. (e) Completed two pixel and multi pixel devices.

To complete the device, cleaned ITO coated glass was glued on to the developed silicon substrate in the same manner as in normal ITO glass cells but only to cover pixel area leaving exposed connection pads. In the similar way multi pixel devices have been fabricated, shown in figure 3.9 (d) to see the effect of polymer stabilisation of the blue phase on a more reflective pixel area. It was ensured to have a uniform thickness throughout the device and has been confirmed by the thickness measurement using Fabry-Perot technique.[73] The optical microscope coupled with a spectrometer was used to obtain a spectrum for at least four points across the cell. The spectrum peaks appeared due to the constructive interference of waves across the cell and were utilised to measure the device thickness.

## **Chapter 4: Synthesis and characterisation of materials**

This chapter covers the synthesis of new mesogenic materials aimed at flexo-electric and blue phase properties with percentage yields, transition temperatures and their structural confirmation through nuclear magnetic resonance spectroscopy ( $^1\text{H-NMR}$  and  $^{13}\text{C-NMR}$ ).

#### 4.1 Synthesis of Mesogenic dimers:

Some mesogenic dimers were synthesised and categorised with respect to their linkage. Synthetic routes and NMR data for the newly synthesised dimers are as follows.

##### 4.1.1 Mesogenic dimers with ester linkage:

The ester linked mesogenic dimers were synthesised using DCC coupling reaction. Desired dioic acid, *N,N'*-dicyclohexylcarbodiimide (DCC) and 4-dimethylaminopyridine (DMAP) were dissolved in chilled dichloromethane (DCM) in equimolar quantities. Then one part of the appropriate aryl phenol was added, whilst stirring the reaction mixture for 20 minutes at a temperature of  $\sim 5^\circ\text{C}$ . The reaction mixture was then brought to room temperature and stirred for 24 hours in a sealed round bottom flask. Equimolar quantities of second aryl phenol and remaining equimolar DCC were then added. Then the mixture was left on stirring at room temperature for another 72 hours. The reaction was monitored using thin layer chromatography (TLC). Once the reaction completed, it was then filtered over celite 545 using sintered funnel. The filtrate was then evaporated to dryness under reduced pressure. The resultant crude material was chromatographed (silica gel, DCM) and the fractions were collected and evaporated to obtain the desired products. The complete synthetic scheme is shown in figure 4.1. The final product has been characterised through NMR data given below.

##### Bis (4'-cyano[1,1'biphenyl]-4-yl) undecanedioate (CBE11ECB) (3)

Yield is 73%, on heating K 130 N 160 I and on cooling I 160 N 110 K ( $5^\circ\text{C}/\text{minute}$ )

$^1\text{H NMR}$  (500 MHz,  $\text{CDCl}_3$ )  $\delta$  7.93 – 7.87 (m, 4H), 7.88 – 7.83 (m, 4H), 7.74 – 7.69 (m, 4H), 7.22 – 7.16 (m, 4H), 2.60 (t,  $J = 7.1$  Hz, 4H), 1.80 (p,  $J = 7.0$  Hz, 4H) and 1.29 – 1.21 (m, 10H).

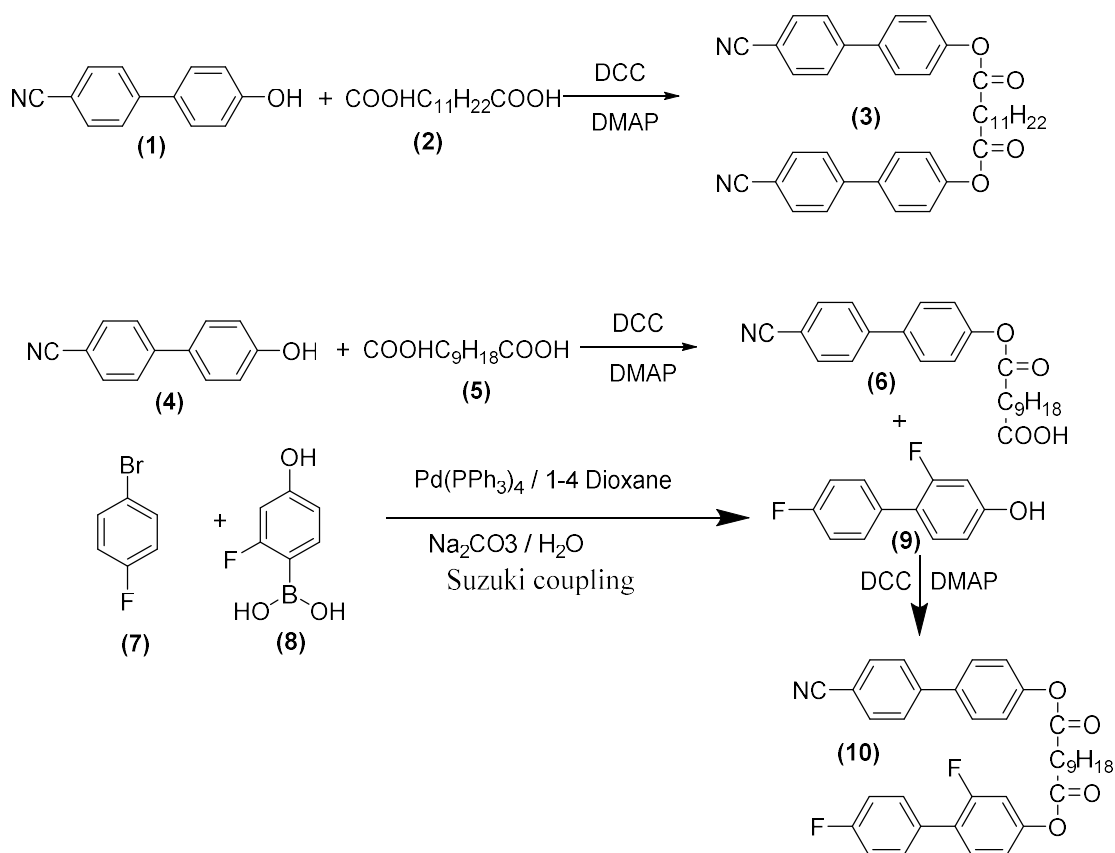
$^{13}\text{C NMR}$  (126 MHz,  $\text{CDCl}_3$ )  $\delta$  171.74 9(C=O), 151.97, 144.88, 134.20, 132.63, 128.48, 127.30, 122.52, 118.50 (C-N), 110.12, 34.55, 29.53, 29.18, 29.09 and 25.05.

1(4'-Cyano-[1,1'-biphenyl]-4-yl)-9-(2,4'-difluoro-[1,1'-biphenyl]-4-yl)  
nonanedionate (FFE9ECB) (**10**) [74]

Yield is 52%, on heating K 87.7 N 117.2 I and on cooling I 118.7 N 63.7 K (5°C/minute)

<sup>1</sup>H NMR (500 MHz, CDCl<sub>3</sub>) δ H 7.71 (dd, J = 8.8, 2.1 Hz, 2H), 7.65 (dd, J = 8.8, 2.1 Hz, 2H), 7.58 (dd, J = 7.0, 2.0 Hz, 2H), 7.48 (ddd, J = 8.8, 5.3, 1.6 Hz, 2H), 7.39 (t, J = 8.7 Hz, 1H), 7.21 (m, 2H), 7.16–7.09 (m, 2H), 7.00–6.92 (m, 2H), 2.59 (t, J = 7.1 Hz, 4H), 1.74–1.81 (m, 4H), and 1.49–1.35 (m, 10H).

<sup>13</sup>C NMR (126 MHz, CDCl<sub>3</sub>) δ 172.32, 172.06, 162.60 (d, J = 247.4 Hz), 159.53 (d, J = 247.4 Hz), 151.33, 150.80 (d, J = 8.1 Hz), 144.91, 136.88, 132.77, 131.19 (d, J = 3.6 Hz), 130.93 (d, J = 3.6 Hz), 130.74 (dd, J = 8.1, 3.6 Hz), 128.45, 127.79, 125.84 (d, J = 13.6 Hz), 122.45, 118.98, 117.87 (d, J = 3.6 Hz), 115.62 (d, J = 13.6 Hz), 111.15, 110.36 (d, J = 13.6 Hz), 34.51, 34.44, 29.36, 29.30, 29.19, 29.17, 25.02 and 24.97.



**Figure 4.1:** Synthesis of ester linked mesogenic dimers.

#### 4.1.2 Ester bridged-ether linked mesogenic dimers:

As it has been reported earlier [75] ether linked mesogenic dimers are monotropic with wide temperature range nematic transition. Whereas, ester linked mesogenic dimers are mostly reported as enantiotropic nematic liquid crystals with a narrow transition. Further, ether linked mesogenic dimers exhibit a nematic transition at low temperature as compared to ester linked mesogenic dimers which give a nematic transition at high temperature. However, ester linked mesogenic dimers display higher flexoelectric ratio than ether linked dimers.

Keeping these views in mind, a new family of mesogenic dimers containing both ether and ester linkage has been synthesised. Their synthesis is as follows.

One equivalent of 1,9-dibromononane (**12**) and two equivalents of ethyl 4-hydroxybenzoate (**11**) were dissolved together in acetone, before adding potassium carbonate. The resultant mixture was then refluxed. The reaction was monitored using thin layer chromatography (TLC). Upon completion of this reaction, the reaction mixture was filtered and washed with copious amount of acetone. Then the filtrate was evaporated to dryness under reduced pressure. This dried powder was then dissolved in 40% KOH ethanol solution and refluxed for 30 minutes to convert ester (**13**) in to carboxylic acid (**14**). Then the reaction mixture was acidified with 1 molar HCl to obtain the desired dioic acid as white precipitate. The resultant material was used in the further reaction without any purification.

In the next step one equivalent of dioic acid (**14**), two equivalents of DCC and one equivalent of DMAP were dissolved in chilled DCM. Then one or two parts of the appropriate phenol were added on stirring the reaction mixture for 20 minutes at a temperature of  $\sim 5^{\circ}\text{C}$ . The reaction mixture was then brought to room temperature and stirred for 72 hours in a sealed round bottom flask. The reaction was monitored using thin layer chromatography (TLC). Once the reaction completed, it was then filtered over celite 545 using sintered funnel. The filtrate was then evaporated to dryness under reduced pressure. The resultant crude material was chromatographed (silica gel, ethyl acetate: DCM, 1:1) and the major fractions were collected and evaporated to obtain the desired products. Complete synthetic scheme is shown in figure 4.2.

Bis (4-cyanophenyl) 4,4'-(nonane-1,9-diylbis(oxy))dibenzoate (**17**) [76]

Yield is 70%, on heating K 165.5 N 181.5 I and on cooling I 182.5 N 154.5 K ( $5^{\circ}\text{C}/\text{minute}$ )

$^1\text{H}$  NMR (500 MHz,  $\text{CDCl}_3$ )  $\delta$  8.12 – 8.10 (m, 4H), 7.91 – 7.85 (m, 4H), 7.46 – 7.40 (m, 4H), 7.10 – 7.03 (m, 4H), 3.98 (t,  $J = 6.1$  Hz, 4H), 1.78 – 1.73 (m, 4H), 1.43 (p,  $J = 6.8$  Hz, 4H) and 1.36 – 1.19 (m, 6H).

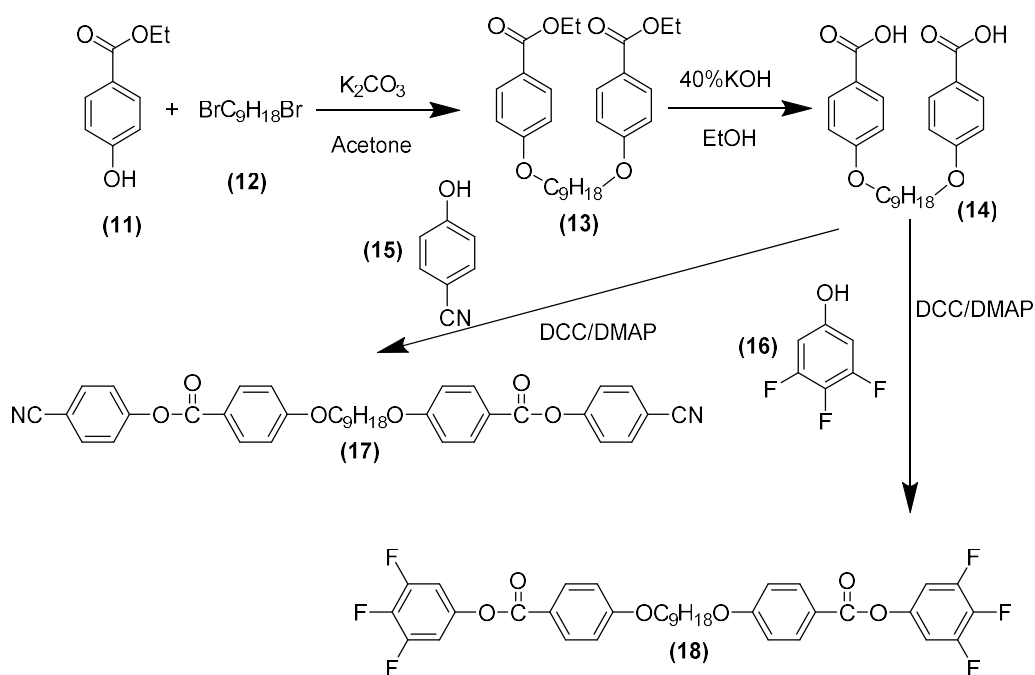
$^{13}\text{C}$  NMR (125 MHz,  $\text{CDCl}_3$ )  $\delta$  163.89 (C=O), 163.06, 153.70, 133.97, 133.96, 121.97, 121.57, 118.48(C-N), 112.31, 107.92, 68.39 ( $\text{CH}_2\text{-O}$ ), 29.52, 29.51, 29.09 and 26.03.

### Bis (3,4,5-trifluorophenyl) 4,4'-(nonane-1,9-diylbis(oxy))dibenzoate (**18**)

Yield is 51%, single melting at  $85^\circ\text{C}$  ( $5^\circ\text{C}/\text{minute}$ )

$^1\text{H}$  NMR (500 MHz,  $\text{CDCl}_3$ )  $\delta$  8.16 – 8.09 (m, 4H), 7.07 – 7.02 (m, 4H), 6.70 – 6.62 (m, 4H), 3.99 (t,  $J = 6.1$  Hz, 4H), 1.80 – 1.71 (m, 4H), 1.41 (p,  $J = 6.8$  Hz, 4H), 1.35 – 1.20 (m, 6H).

$^{13}\text{C}$  NMR (125 MHz,  $\text{CDCl}_3$ )  $\delta$  164.61 (C=O), 163.06, 152.13 (ddd,  $J = 252.1, 20.0, 8.0$  Hz C-F), 148.11 (td,  $J = 8.1, 3.1$  Hz), 138.05 (d,  $J = 252.1$  Hz C-F), 133.15, 123.32, 112.31, 107.19 (ddd,  $J = 20.0, 8.1, 3.1$  Hz), 68.39 ( $\text{CH}_2\text{-O}$ ), 29.52, 29.51, 29.09, 26.03.



**Figure 4.2:** Synthesis of ester bridged ether linked mesogenic dimers.



### 4.1.3 Synthesis of Mesogenic monomers:

To enhance the dielectric properties with intrinsic structure of dimer some mesogenic monomers have also been synthesised.

For the first type of synthesis, equimolar quantities of ethyl 4-hydroxy benzoate (**19**) and butyl bromide (**20**) were dissolved together in acetone before adding potassium carbonate. The resultant mixture was then refluxed. Upon completion of the reaction, the ester product (**21**) was re-crystallised in ethanol as white solid. In the next phase, ethyl butyloxy benzoate (**21**) was dissolved in 40% KOH ethanol solution and refluxed for 30 minutes to convert ester in to carboxylic acid (**22**). Then the reaction mixture was acidified with 1 molar HCl to obtain the desired carboxylic acid (**22**) as white precipitate. The resultant material was used in the further reaction without any purification.

In the next step acid (**22**), DCC and DMAP were dissolved in chilled DCM in equimolar quantities. Then one parts of the appropriate phenol {(**23**) 3,4,5 trifluoro phenol or (**24**) 4'-hydroxy[1,1'-biphenyl]-4-carbonitrile or (**25**) 2,6-difluoro-4-hydroxybenzonitrile or (**26**) 4-hydroxy benzonitrile} was added on stirring the reaction mixture for 20 minutes at a temperature of ~5 °C. The reaction mixture was then brought to room temperature and stirred for 24 hours in a sealed round bottom flask. The reaction was monitored using thin layer chromatography (TLC). Once the reaction completed, it was then filtered over celite 545 using sintered funnel. The filtrate was then evaporated to dryness under reduced pressure. The resultant crude material was chromatographed (silica gel, DCM) and the major fraction was collected and evaporated to obtain the desired product [(**27**) or (**28**) or (**29**) or (**30**)]. For product (**31**) the synthesis of a single monomer has been carried out with commercially available reactants through above mentioned DCC coupling method. Complete synthetic scheme is shown in figure 4.3.

#### 3,4,5-trifluorophenyl 4-butoxybenzoate (**27**)

Yield is 85%, single melting at 71°C (5°C/minute)

<sup>1</sup>H NMR (500 MHz, CDCl<sub>3</sub>) δ 8.13 – 8.06 (m, 2H), 7.10 – 7.03 (m, 2H), 6.70 – 6.63 (m, 2H), 3.97 (t, *J* = 6.1 Hz, 2H), 1.84 – 1.75 (m, 2H), 1.46-1.42 (m, *J* = 14.5, 2H) and 0.96 (t, *J* = 7.7 Hz, 3H).

$^{13}\text{C}$  NMR (126 MHz,  $\text{CDCl}_3$ )  $\delta$  164.61 (C=O), 163.39, 152.13 (ddd,  $J = 252.1, 20.0, 8.0$  Hz, C-F), 148.11 (td,  $J = 8.1, 3.1$  Hz), 133.15, 123.32, 112.6, 107.19 (ddd,  $J = 20.0, 8.1, 3.1$  Hz) 69.89 ( $\text{CH}_2\text{-O}$ ), 30.48, 18.83 and 13.77.

#### 4'-Cyano-[1,1'-biphenyl]-4-yl 4-butoxybenzoate (**28**) [77]

Yield is 81%, on heating K 124 N 285 I and on cooling I 283N 121 K (5°C/minute)

$^1\text{H}$  NMR (500 MHz,  $\text{CDCl}_3$ )  $\delta$  8.14 – 8.07 (m, 2H), 7.95 – 7.88 (m, 2H), 7.88 – 7.83 (m, 2H), 7.81 – 7.74 (m, 2H), 7.24 – 7.17 (m, 2H), 7.09 – 7.02 (m, 2H), 3.97 (t,  $J = 6.1$  Hz, 2H), 1.83 – 1.74 (m, 2H), 1.46-1.38 (m, 2H) and 0.95 (t,  $J = 7.7$  Hz, 3H).

$^{13}\text{C}$  NMR (126 MHz,  $\text{CDCl}_3$ )  $\delta$  164.19 (C=O), 163.39, 152.26, 144.88, 134.17, 133.97, 132.63, 128.43, 127.30, 122.47, 121.57, 118.50 (C-N), 112.67, 110.12, 69.89(C-O) 30.48, 18.83 and 13.77.

#### 4-Cyano-3,5-difluorophenyl 4-butoxybenzoate (**29**) [77]

Yield is 89%, single melting at 76.8°C (5°C/minute)

$^1\text{H}$  NMR (500 MHz,  $\text{CDCl}_3$ )  $\delta$  8.15 – 8.10 (m, 2H), 7.1 – 7.04 (m, 2H), 6.83 – 6.78 (m, 2H), 3.97 (t,  $J = 6.1$  Hz, 2H), 1.85 – 1.76 (m, 2H), 1.48-1.43 (m, 2H) and 0.95 (t,  $J = 7.7$  Hz, 3H).

$^{13}\text{C}$  NMR (126 MHz,  $\text{CDCl}_3$ )  $\delta$  167.00 (dd,  $J = 252.0, 8.0$  Hz, C-F), 164.61(C=O), 163.39, 155.62 (t,  $J = 8.0$  Hz), 133.15, 123.32, 112.67, 110.01 (t,  $J = 3.9$  Hz), 108.35 (dd,  $J = 20.0, 2.9$  Hz), 88.64 (t,  $J = 20.0$  Hz), 69.89( $\text{CH}_2\text{-O}$ ), 30.48, 18.83 and 13.77.

#### 4-Cyanophenyl 4-butoxybenzoate (**30**) [77]

Yield is 92%, single melting at 115°C (5°C/minute)

$^1\text{H}$  NMR (500 MHz,  $\text{CDCl}_3$ )  $\delta$  8.16 – 8.09 (m, 2H), 7.92 – 7.85 (m, 2H), 7.47 – 7.41 (m, 2H), 7.10 – 7.03 (m, 2H), 3.97 (t,  $J = 6.1$  Hz, 2H), 1.84 – 1.75 (m, 2H), 1.51-1.43 (m, 2H) and 0.97 (t,  $J = 7.7$  Hz, 3H).

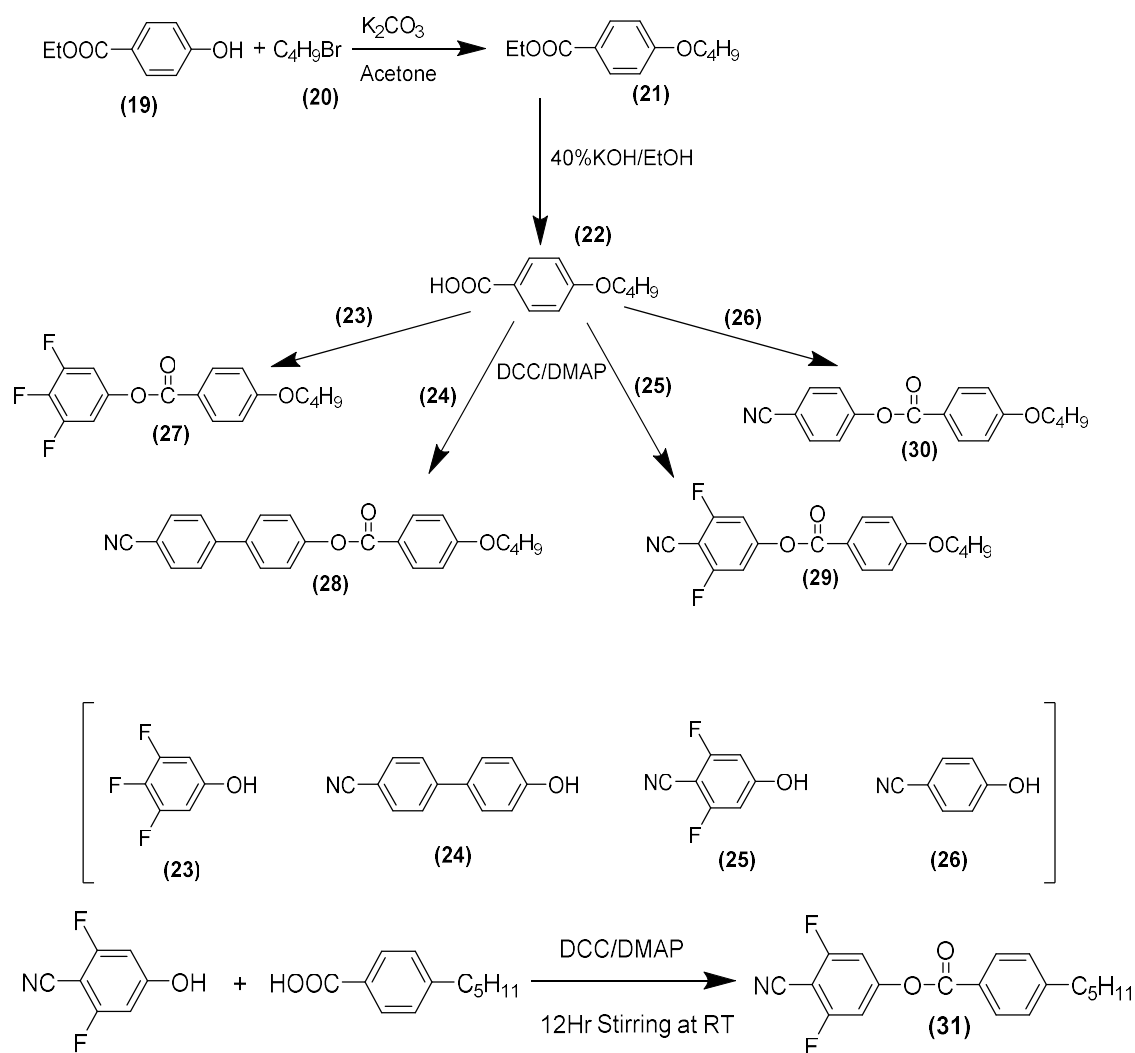
$^{13}\text{C}$  NMR (126 MHz,  $\text{CDCl}_3$ )  $\delta$  163.89 (C=O) 163.39, 153.70, 133.97, 133.96, 121.97, 121.57, 118.48 112.67, 107.92, 69.89 ( $\text{CH}_2\text{-O}$ ), 30.48, 18.83 and 13.77.

#### 4-Cyano-3,5-difluorophenyl 4-pentylbenzoate (**31**) [77]

Yield is 86%, single melting at 28.5°C (5°C/minute)

$^1\text{H}$  NMR (500 MHz,  $\text{CDCl}_3$ )  $\delta$  7.95 – 7.90 (m, 2H), 7.23 (dt,  $J = 8.4, 1.0$  Hz, 2H), 6.81 – 6.75 (m, 2H), 2.63 (tt,  $J = 6.4, 1.0$  Hz, 1H), 1.52 (p,  $J = 6.6$  Hz, 1H), 1.39 – 1.27 (m, 2H) and 0.93 – 0.86 (m, 2H).

$^{13}\text{C}$  NMR (125 MHz,  $\text{CDCl}_3$ )  $\delta$  167.00 (dd,  $J = 252.0, 8.0$  Hz C-F), 164.72 (C=O), 155.62 (t,  $J = 8.0$  Hz), 145.53, 130.79, 128.44, 128.07, 110.01 (t,  $J = 3.9$  Hz), 108.35 (dd,  $J = 20.0, 2.9$  Hz), 88.64 (t,  $J = 20.0$  Hz), 35.30, 31.47, 31.18, 22.48 and 14.07.



**Figure 4.3:** Synthesis of mesogenic monomers.

## 4.2 Mixture formulation:

The main focus in this chapter was to formulate an ideal mixture with reasonable flexo- and dielectric properties to get a stable and switchable blue phase. Further to this, the newly synthesised monomers and mesogenic dimers will be doped in an ideal mixture composition to study the effect on flexo and dielectric properties in detail.

For this purpose and to keep the composition simple, primarily 5CB (crystalline to nematic then to isotropic state at 18°C and 35°C respectively) was used as a base liquid crystal to make the mixtures by doping FFE9ECB and CBE11ECB between 10 and 80% by weight. But compounds were precipitated out and have shown immiscibility in the host material (5CB). The next readily available commercial candidate was E7 (mixture of 5CB 51%, 7CB 25%, 8OCB 16%, 5CT 8%). It was selected due to its well characterised properties however; no homogenous mixture was obtained when mixed with above mentioned dimers. In search for an appropriate base liquid crystal, BL006 (another well characterised liquid crystal, Merck Germany, Clearing point 113°C,  $\Delta n = 0.28$  and  $\Delta \epsilon = 17.3$ ) was successfully used to make the mixtures between 10 and 80% in composition by weight for FFE9ECB, and 10 and 20% for CBE11ECB separately. These mixtures were then heated and brought to their clearing point and further kept in oven at 90°C for two hours. Thermal transitions of mixtures have been presented in the table 4.1.

Mixture Reference	LC-Host %W	Mesogenic dimer %W	Transition °C		
			DSC		Heating stage
			On cooling	On heating	
Mix-1	90	10 <sup>a</sup>	-25 - 115	-25 - 115.4	25 - 126
Mix-2	80	20 <sup>a</sup>	-25 - 119	-25 - 119	25 - 124.1
Mix-3	60	40 <sup>a</sup>	-15 - 116.5	41.5 - 111	55 - 118
Mix-4	40	60 <sup>a</sup>	10.75 - 114.5	60 - 109	60 - 119
Mix-5	20	80 <sup>a</sup>	52.3 - 135.3	89.4 - 125	75 - 121
Mix-6	90	10 <sup>b</sup>	1.25 - 126.4	54 - 118	33 - 135
Mix-7	80	20 <sup>b</sup>	25 - 128.4	65.5 - 120	71 - 133

**Table 4.1:** <sup>a</sup>(FFE9ECB) and <sup>b</sup>(CBE11ECB) in LC Host BL006.

### 4.3 Characterisation of Mixtures:

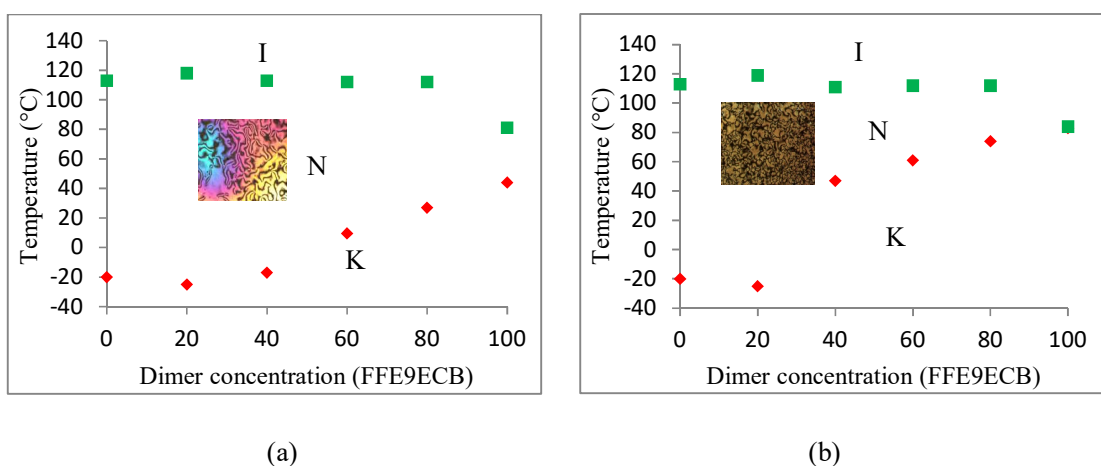
Characterisation of each mixture was carried out on three physical parameters. Thermal transitions were determined by the hot stage optical polarised microscope and further confirmed by the differential scanning calorimeter (DSC). Dielectric measurements were obtained from the Wayne Kerr and for flexoelectro-optic response; the optical polarised microscope setup was used. This apparatus setup has been already explained in chapter 3. Below is the experimental detail for thermal characterisation.

### 4.3.1 Thermal characterisation:

At first cover slip transitions were carefully recorded using an optical polarised microscope with hot stage. These results were then confirmed by the DSC transitions. 10 and 20% mixtures of FFE9ECB showed wide temperature LC transitions which were then confirmed by DSC thermograms obtained from  $-25$  to  $150^{\circ}\text{C}$ . A phase diagram in a liquid crystal material shows the existence of different liquid crystalline phases in the given conditions. In this part of the research a phase diagram deals with the changes in phase with respect to temperature. The DSC thermo scan data was utilised to obtain a phase diagram to do the initial thermal characterisation of the formulated mixtures.

Polarised optical micrographs were recorded using the hot stage of the optical microscope for all the corresponding mixtures of FFE9ECB and CBE11ECB in BL006 as a host liquid crystal. From these micrographs their LC phase transitions were established and are shown in table 4.1

DSC thermograms were scanned using the Mettler Toledo DSC822e differential scanning calorimeter from  $-50$  to  $150^{\circ}\text{C}$ . LC transitions obtained through coverslip were confirmed by the DSC thermograms and results are shown in table 4.1 Figure 4.4 shows the phase diagram obtained through DSC data. Modern DSCs have uncertainties of  $0.1 - 0.5$  degree Kelvin over a temperature range from  $200$  to  $800$  degree Kelvin,  $0.5 - 1.0$  % in enthalpy changes and  $1 - 2$  % in heat capacity. [78]



**Figure 4.4:** Phase diagrams for FFE9ECB mixtures based on DSC thermal traces (a) on cooling and (b) on heating.

**Conclusion:**

In this chapter the synthesis of some mesogen materials and their structural characterisation through  $^1\text{H-NMR}$  and  $^{13}\text{C-NMR}$  techniques has been presented. Further to this, mixture formulation steps have been illustrated and successfully formulated using BL006 as a commercial nematic host between 10 and 80% of the dimer concentration. Thermal transitions were recorded through POM and confirmed through DSC. Textures of the formulated mixtures have been observed through POM. On the basis of thermal data, their phase diagram has been finalised to find out the mixture composition with the wide nematic transition.

## **Chapter 5: Electro-optic Properties of formulated mixtures**

Physical and optical properties of the nematic liquid crystals can be manipulated by an applied electric field. On applying a voltage, the molecules tend to align themselves parallel to the applied field with the molecular axis possessing greatest polarity. This realignment of the liquid crystalline molecules is due to the presence of permanent and electrically induced dipoles that correspond to the Kerr effect. This phenomenon is the basis for applications based on the electro-optic properties of liquid crystals. The following are analysis of formulated mixtures through dielectric anisotropy; flexoelectro-optic properties and response time of all of the formulated mixtures.

### 5.1 Dielectric anisotropy:

The dielectric anisotropy of the samples has been determined as a function of capacitance verses voltage for a given area and can be expressed by the following relation for the perpendicular dielectric permittivity.

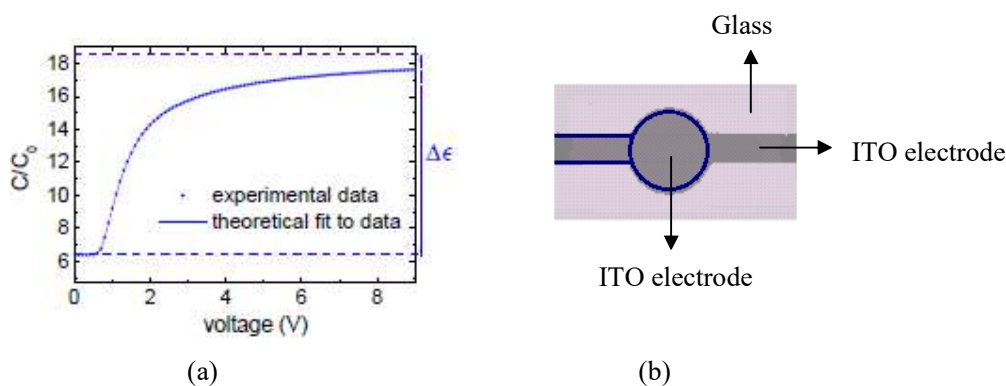
$$\epsilon_{\perp} = \frac{C_{\perp}}{C_0} \quad \text{Equation 5.1}$$

Where  $\epsilon_{\perp}$  is perpendicular permittivity,  $C_{\perp}$  is perpendicular capacitance of the filled device and  $C_0$  is the empty cell capacitance. In a similar way parallel permittivity can be determined.

A precision component analyser (6440A Wayne Kerr) was used to determine the capacitance as a function of voltage (0-10V) at different temperatures. The temperature of the cell was controlled using a hot-stage controller with a precision of  $\pm 0.1^{\circ}\text{C}$ .

At first, the capacitance of an empty cell with anti-parallel planar alignment (AP) was recorded at 10 kHz. The cell was then filled with sample mixture and capacitance of the filled cell was measured in the temperature range from  $30^{\circ}\text{C}$  -  $150^{\circ}\text{C}$ . Shifted temperature was taken from the isotropic point to the nematic transition upon cooling at a  $10^{\circ}\text{C}$  intervals. The voltage increment between measurements at a set temperature was 100mV. The capacitance ratio was determined by dividing filled cell capacitance by empty cell capacitance to finalise the measurements (equation 5.1). Figure 5.1 is a typical example of the capacitance curve normalised to the empty cell. It generally depends on the  $\epsilon_{\parallel}$  and  $\epsilon_{\perp}$  as well as  $K_{11}$  and  $K_{33}$ .





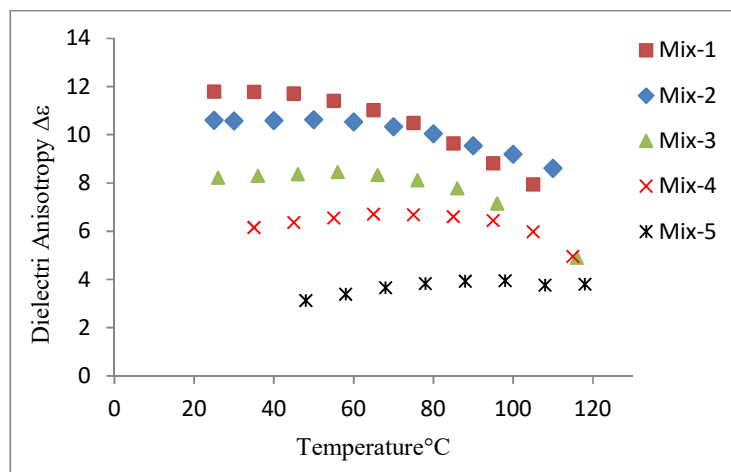
**Figure 5.1:** (a) The capacitance curve as a function of applied voltage. [79] (b) schematic of the device used to measure dielectric properties. (Supplied by Merck)

### 5.1.1 Result and Discussion:

#### 5.1.1.1 FFE9ECB Mixtures (**Mix-1** to **Mix-5**):

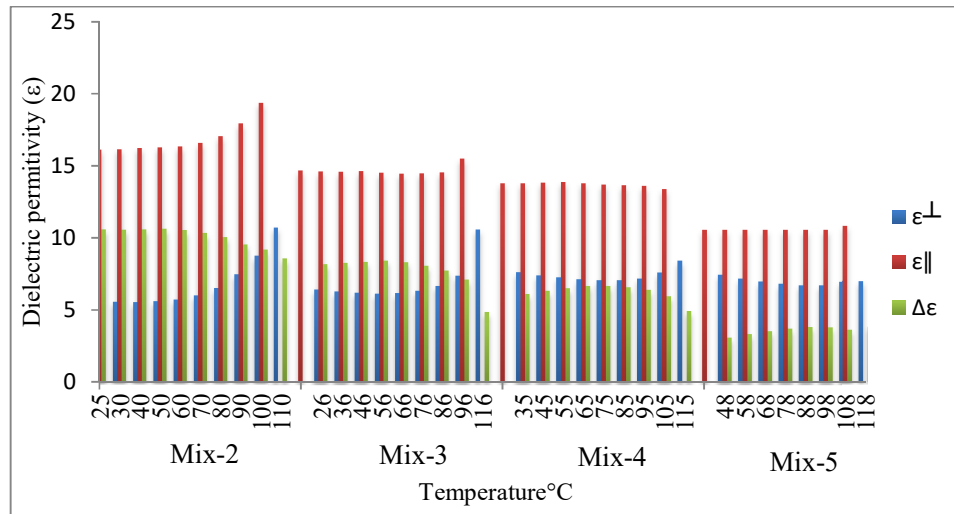
Dielectric properties of all the mixtures were recorded as a function of temperature. At low temperature a large difference in parallel and perpendicular permittivity was observed. Near the clearing temperature, the difference between parallel and perpendicular permittivity was marginal. This is due to the fact that mixture loses its anisotropy and becomes isotropic. Here in particular the additional factor was concentration of dimer in a dielectric nematic host (BL006). It was evident from the experimental data presented in figure 5.2 that the dielectric anisotropy had decreased significantly for the 80% dimer concentration in the mixture. This is owing to the molecular structural nature of dimer as it tends to cancel out the overall dipole moment and hence reduces the dielectric anisotropy- in an ideal scenario it tends to zero.

An overall trend was observed and can be clearly seen in figure 5.3. At room temperature BL006 has  $\Delta\epsilon$  of 17.3 (Merck Co., Germany), however, with the addition of the dimer mesogen FFE9ECB,  $\Delta\epsilon$  tends to decrease with respect to concentration. Furthermore, this trend seems to be linear, for 10% composition (**Mix-1**)  $\Delta\epsilon$  is 11.8, 20% composition (**Mix-2**)  $\Delta\epsilon$  10.6 and for 40% composition (**Mix-3**)  $\Delta\epsilon$  is lowered down to 8.2 at 25°C. Although, **Mix-4** and **Mix-5**, 60 and 80% composition respectively, crystallise out at room temperature but at higher temperatures the trend is similar. At 55°C **Mix-3** exhibits  $\Delta\epsilon$  8.5, **Mix-4** shows  $\Delta\epsilon$  6.5 whereas; **Mix-5** has the lowest  $\Delta\epsilon$  of 3.4. However, 20°C below their clearing point this trend diminishes, **Mix-1** shows maximum drop in  $\Delta\epsilon$  from 11.8 at 25°C to 7.9 at 105°C while for **Mix-5** there is no significant change and  $\Delta\epsilon$  stays between 3.9 and 3.1. Comprehensive measurements of  $\Delta\epsilon$  are given in figure 5.2.



**Figure 5.2:** Dielectric anisotropy for FFE9ECB mixtures in BL006.

Dielectric measurements show a significant change in the dielectric properties of **Mix-2** and **Mix-3**. For **Mix-2** up to 50°C, the difference in parallel and perpendicular dielectric permittivity is almost the same. As soon as the temperature is increased, the parallel and perpendicular dielectric permittivities also increased and are almost equal at 110°C with the lowest difference. This is due to the fact that mixture loses its anisotropic nature and becomes isotropic. For the **Mix-3**, up to 100°C the difference between parallel and perpendicular dielectric anisotropy stayed almost constant. However, beyond this temperature a similar trend was observed in the dielectric properties. Another point of focus from these results is that variations in the dielectric properties from room temperature to near clearing point are higher for those mixtures with least amount of dimer. It has been suggested that the addition of dimer components into a dielectric matrix enhances the packing of mesogenic components and is most pronounced when the dimer concentration is increased above 50%. However, it has an adverse effect on dielectric permittivity. Detailed results and comparisons are shown as bar graphs in figure 5.3.

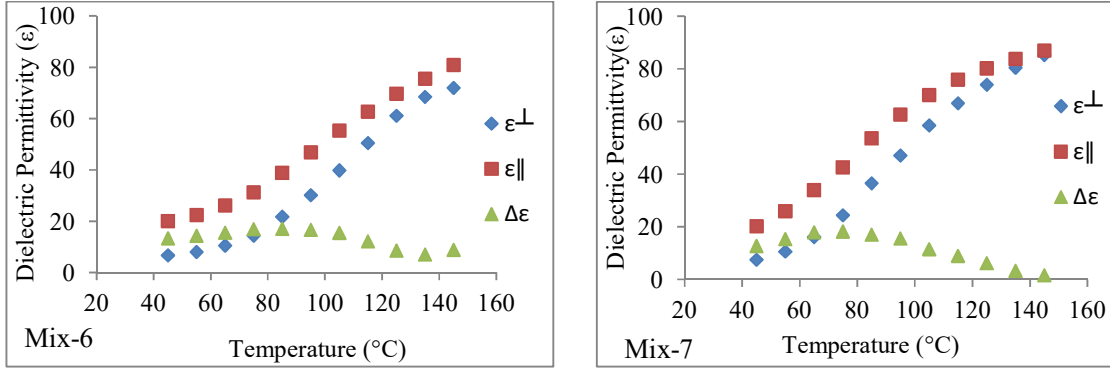


**Figure 5.3:** Dielectric permittivity comparison for mixtures (Mix-2 to Mix-5).

Among these mixtures, **Mix-2** seems to fill a few of the criteria of the desired formulation; (1) a wider transition temperature range (2) good dielectric properties with low variation. **Mix-1** has shown  $\Delta\epsilon$  from 11.8 to 8.8 whereas; **Mix-2**  $\Delta\epsilon$  changes less significantly from 10.5 to 9.5 over the temperature range of 25°C to 90°C. This in turn helps to understand the role of flexo coupling over dielectric optical switching.

#### 5.1.1.2 CB11ECB Mixtures (**Mix-6** and **Mix-7**):

CBE11ECB (**3**) demonstrated higher melting transitions and miscibility issues with only the 10 and 20% mixtures (**Mix-6** and **Mix-7**) having been formulated in BL006. These mixtures reveal peculiar behaviour when subjected to the dielectric measurements. Primarily, it seemed that **Mix-6** and **Mix-7** are ionic in nature. To conclude this, further experiments have been carried out to understand the nature of this material. After a DC swap which is the applied field at a fixed polarity, the same trend was observed and hence the ionic nature of the material was ruled out. Hence it can be concluded as an intrinsic property of this material and requires further investigation. Graphs in figure5.4 show the dielectric measurements for the 10 and 20% mixtures of CBE11ECB in BL006. Both of the mixtures have shown high  $\epsilon \sim 80$  but the differences between  $\epsilon_{\parallel}$  and  $\epsilon_{\perp}$  stayed under 20. The SI unit for permittivity is farad per meter (F/m or  $F \cdot m^{-1}$ ). However, here I have measured relative dielectric anisotropic permittivity ( $\epsilon_r$ ) so is unit less. This is also in accordance with the literature.[80]



**Figure 5.4:** Dielectric measurements for 10 and 20 % mixtures of CBE11ECB.

## 5.2 Flexoelectro-optic measurements:

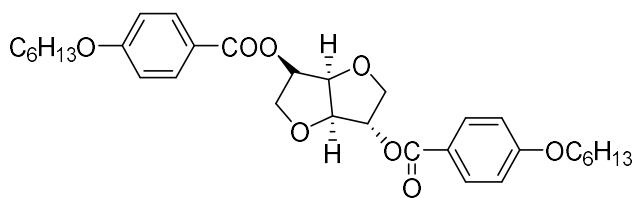
The flexoelectric coefficient ( $e/k$ ) of the material can be calculated from the tilt angle ( $\phi$ ) and the pitch ( $p$ ) using following equation where an external field  $E$  is applied.

$$\frac{e}{k} = \frac{2\pi \tan\phi}{Ep} \quad \text{Equation 5.2}$$

Literature suggests that two methods are often used to determine the tilt angle ( $\phi$ ), the hybrid aligned nematic (HAN) cell method and uniform lying helix (ULH) configuration in antiparallel planer (AP) cell. [81] There are a few drawbacks associated with the HAN cell method. Among these are complicated device fabrication and degradation of the alignment layer over time and high applied field are major adverse factors during the experiment. Whereas, the AP-cell ULH has easier device fabrication and the alignment layers are stable which does not interfere with the measurements. However, a stable ULH texture in AP cell needs to be optimised under an applied field near to the isotropic transition of the material which varies with material composition.

In this present work, as the formulated mixtures have both dielectric and flexo components, we use a very uniform and stable ULH configuration in an AP cell. Flexo properties help in packing of the material while dielectric components assist the molecules to align in the direction of an applied field. So the ULH method in AP cell has been followed to determine the tilt angle.

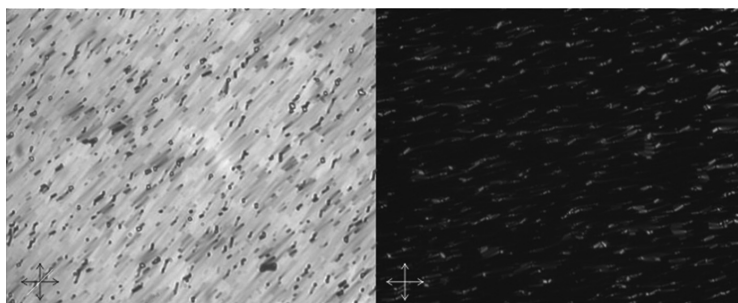
Chiral dopant (BDH1281, chemical structure shown in figure5.5) was added to the mixture 5.5 to 7.5% by weight to achieve a reflection band in the UV region which is a fundamental requirement for use as a ‘black-blue phase’ – a purely optically isotropic blue phase across the visible spectrum. These mixtures were then heated and brought to their clearing point and further kept in an oven at 90°C for two hours.



**Figure 5.5:** Chemical structure of BDH1281.

### 5.2.1 ULH mode for flexoelectro-optic switching:

For flexoelectro-optic switching, the uniform lying helix texture is commonly used. To obtain the uniform lying helix (ULH) mode, material is capillary filled into a cell with planar alignment. Then this cell is heated to its isotropic point under a high applied field. The cell is sheered and slowly cooled down to its anisotropic transition. This method induces a good uniform alignment although this is a tedious process and often requires a number of attempts to get a proper stable ULH alignment. Uniform lying helix texture upon bright (a) and dark (b) state is shown in figure 5.6.

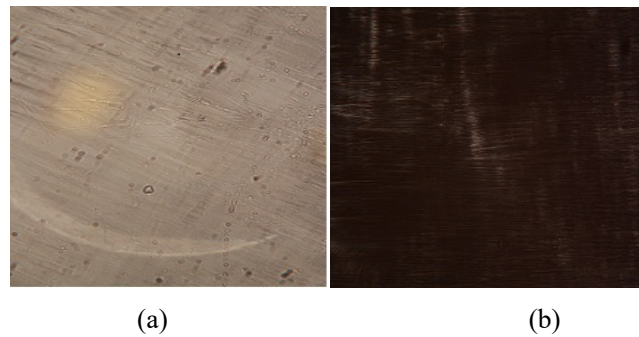


**Figure 5.6:** ULH alignment achieved by cooling a chiral nematic liquid crystal from isotropic phase with the application of electric field with orientation of optic axis at  $45^\circ$  and  $0^\circ$  with respect to polariser.[82]

Another alternative method of obtaining the uniform lying helix texture was developed by Coles *et al.* [83] This method involves a cell with hybrid alignment and the sample is cooled at a very slow rate (typically less than  $1^\circ\text{C}/\text{minute}$ ) from the isotropic phase with an electric field applied across the cell. This method can produce a very good alignment but takes longer to achieve the desired results.

Here a good method has been developed during this work to achieve an excellent and convenient stable ULH mode without the use of complicated cell geometry. This involves a moderate applied field ( $\sim 2\text{V}/\mu\text{m}$ , 1 kHz frequency) across the sample in a planar cell with a sheering at a rapid cooling rate ( $\sim 5\text{-}10^\circ\text{C}/\text{minute}$ ) depending on the material. This method has

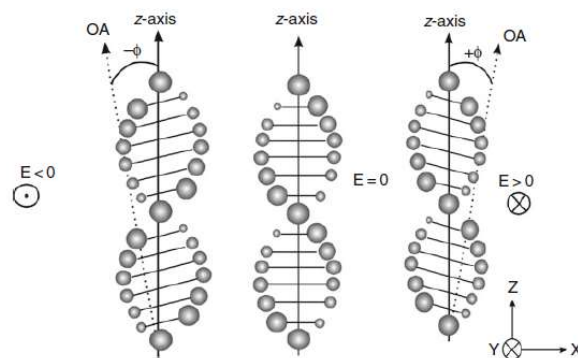
always proven to be quick and easy to get a good ULH texture for the further studies. Figure 5.7 shows both bright and dark states of the uniformly lying helices.



**Figure 5.7:** The texture observed for the uniformly lying helix geometry in **Mix-2** both bright and dark states.

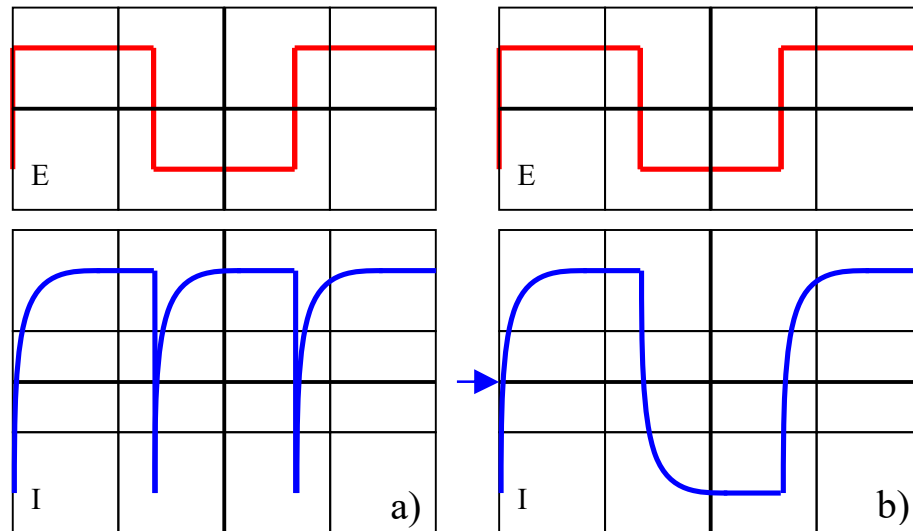
### 5.2.1.1 Flexoelectro-optic switching:

In 1987, Patel and Meyer were the first to observe an electro-optic switching effect in chiral nematics that was directly attributed to flexoelectricity; this is sometimes known as the “flexoelectro-optic effect.” [84] In a short-pitch chiral nematic, the optic axis of the material lies perpendicular to the director planes. Hence, any rotation of the director planes results in an equal rotation of the optical axis. The application of a suitable electric field in a direction normal to the helix axis induces curvature strains as the molecular dipoles couple flexoelectrically to the field. The resulting rotation of the director planes through an angle means that the optic axis also rotates by the same angle. This flexoelectrically induced rotation of the optic axis is known as the flexoelectro-optic effect, and is shown diagrammatically in figure.5.8



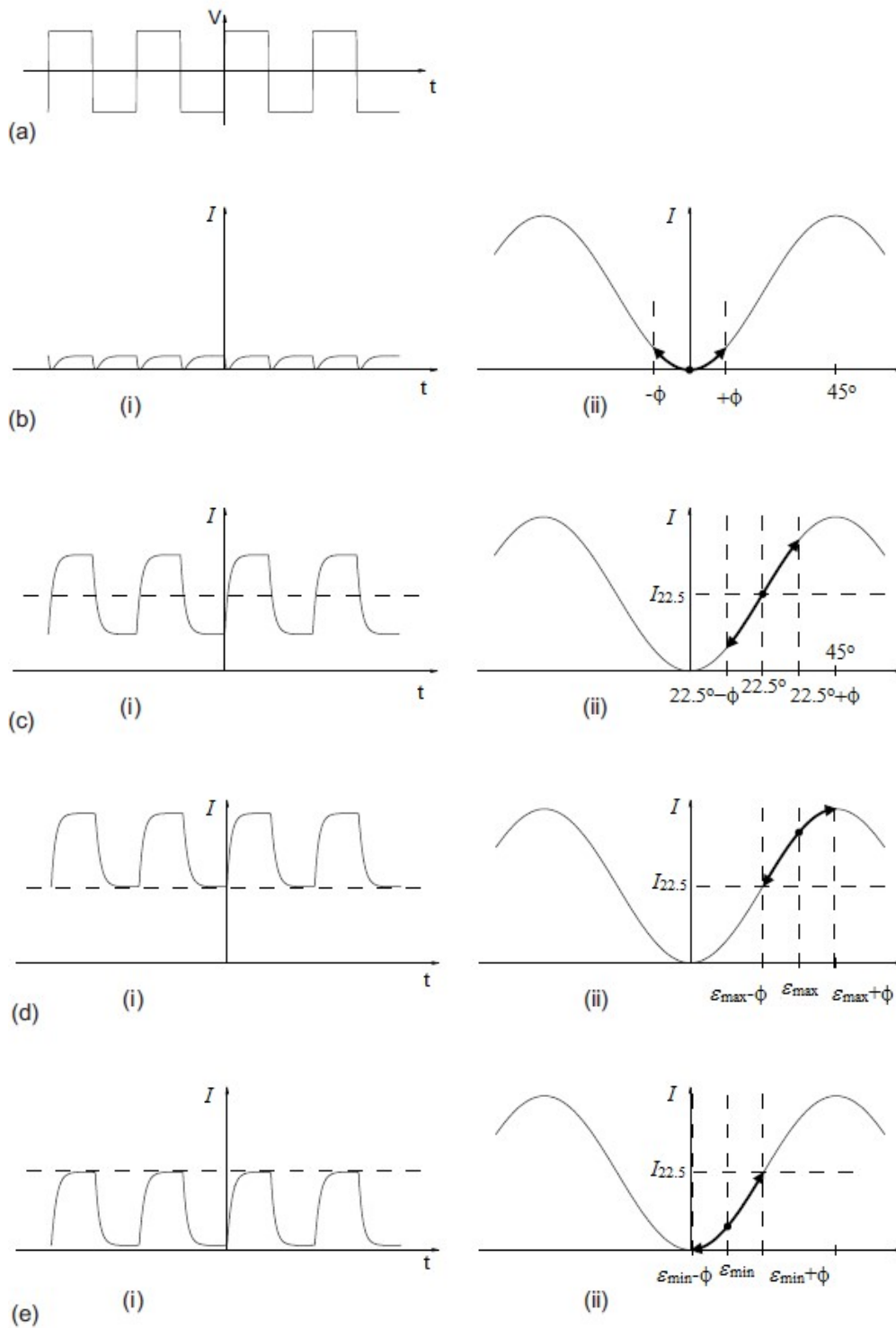
**Figure 5.8:** An example of the rotation of the optic axis in a chiral nematic liquid crystal with an applied electric field perpendicular to the helical axis.

The tilt angle  $\phi$  depends upon the direction and magnitude of the applied field. The direction of the rotation of the optic axis is determined by the direction of applied electric field. The tilt angle is defined as the maximum angle at which the optic axis rotates away from its equilibrium position for a certain applied electric field. The switching angle is the angle between the two switched states ( $2\phi$ ). An electric field is applied across the cell and the tilt angles are measured as a function of that applied electric field and temperature, using the polarising microscope set-up described in chapter 3.



**Figure 5.9:** A diagrammatic representation of the photodiode response, for a bipolar square wave applied field, when the zero position of the optic axis is a) parallel and b) at  $22.5^\circ$  to the transmission axis of one of the polarisers.

Initially, the sample is rotated until the equilibrium position of the optic axis is aligned with the transmission axis of one of the polarisers, figure 5.9a. Then the sample is rotated by  $22.5^\circ$ . The mid-point of the two switched positions is marked with a cursor on the oscilloscope, as shown on figure 5.9b. The sample is then rotated until the maximum of one of the switched positions lies level with the cursor; and the angle reading on the rotation stage is then noted. The sample is then rotated in the opposite direction until the maximum of the other switched positions lies level with the cursor and the new position of the rotation stage is noted. The tilt angle is equal to half the difference between the two noted positions. This method is very accurate especially for small angles, as a small rotation of the optic axis close to  $22.5^\circ$  produces a bigger change in light intensity. Figure 5.10 is the best illustration of the above mentioned method to determine tilt angle adapted from *F.Castles* PhD thesis (2010). [79]



**Figure 5.10:** An illustration applied voltage as a function of time, optical response in ULH mode to measure induced tilt as explained in text. [79]

The procedure for measuring tilt angles ( $< 22.5^\circ$ ) as explained by *F. Castles* is as follows:



1. Reduce the applied voltage to as low a value as possible while still maintaining the ULH configuration.
2. Rotate the microscope stage until the signal from the photodiode is the same for both polarities of driving voltage, and the change in polarity shows a dip in photodiode signal, as shown in figure 5.10(b)(i). This corresponds to oscillations of tilt about the  $\varepsilon = 0$  position shown in figure 5.10(b)(ii).
3. Rotate the stage to  $\varepsilon = 22.5^\circ$ . At this position a small tilt  $\phi$  creates maximum contrast in the photodiode modulation. The photodiode response is as shown in figure 5.10(c)(i). Note the average response  $I_{22.5}$ .
4. Rotate the stage until the minimum of the signal coincides with  $I_{22.5}$ . The situation is as shown in figure 5.10(d). Record the angle of the stage  $\varepsilon_{\max}$ .
5. Rotate the stage until the maximum of the signal coincides with  $I_{22.5}$ . The situation is as shown in figure 5.10(e). Record the angle of the stage  $\varepsilon_{\min}$ .
6. It can be seen from figures 5.10(d) and 5.10(e) that the flexoelectric tilt angle is given by  $\phi = (\varepsilon_{\max} - \varepsilon_{\min})/2$

### 5.2.2 Pitch measurements:

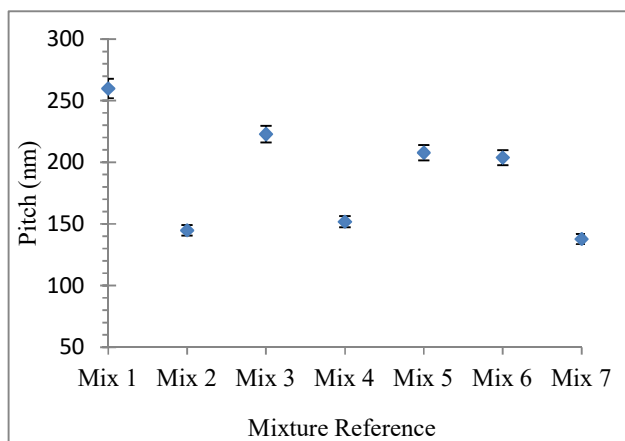
The pitch of the chiral nematic mixtures were determined by wedge cell geometry. These have non-uniform thickness and give a pitch gradient. To determine the pitch of material, two points  $A_1$  and  $A_2$  were marked near opposite edges and the thickness was measured at designated points ( $d_1, d_2$ ). After filling the cell with chiral nematic material, the number of disclination lines  $n$  was counted between  $A_1$  and  $A_2$  at different temperatures. Pitch was calculated using the relation below.

$$p = \frac{2[d_2 - d_1]}{n} \quad \text{Equation 5.3}$$

Where  $p$  is pitch,  $d_1$  and  $d_2$  are the thickness and  $n$  is number of disclinations.

Pitch was determined from the isotropic point to room temperature or crystallisation point whichever came first for the all corresponding mixtures and results shows that the pitch was independent of temperature in most of the cases. Detailed results are shown in the table 5.1.

Mixture Reference	Mixtures in BL006	Pitch (nm)
Mix-1	10% FFE9ECB	260
Mix-2	20% FFE9ECB	145
Mix-3	40% FFE9ECB	223
Mix-4	60% FFE9ECB	152
Mix-5	80% FFE9ECB	208
Mix-6	10% CBE11ECB	204
Mix-7	20% CBE11ECB	138



**Table 5.1:** Pitch for the FFE9ECB and CBE11ECB mixtures.

Each mixture has shown disclination lines under polarised optical microscope when filled in a wedge cell upon cooling from its isotropic point. The line count was different for each mixture so is the pitch. However pitch measurements have shown a very slight shift in the disclination lines with respect to temperature for a particular mixture. This trend was observed in almost all of the mixtures whereas; the number of lines was same for a mixture throughout its transition temperature. This is an intrinsic property of chiral dopant BDH1281. [85]–[87] The above graph shows the comparison of pitch at 60 °C for **Mix-1** to **Mix-7**.

To obtain desirable pitch in the UV reflection, in most of the mixtures, 5.5 %wt quantity of chiral dopant was sufficient. However, for mixture (Mix-2) 7.5 %wt chiral dopant was adequate to acquire the desired pitch.

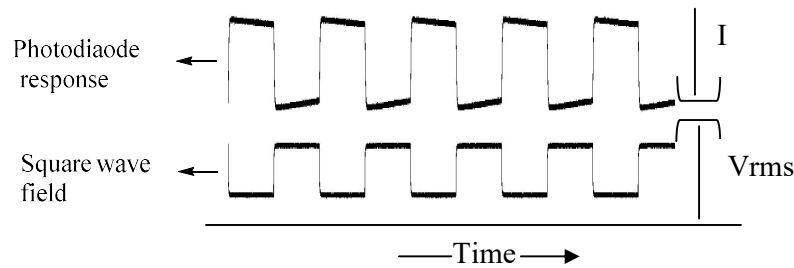
#### 5.2.2.1 Flexoelastic coefficient and results:

Using the measurements of tilt and pitch it is now possible to calculate the flexoelastic ratio of  $e/k$ . This is the ratio of the effective flexoelectric coefficient and the average of splay and bend elastic constants. The flexo-elastic ratio gives a direct indication of the flexoelectric properties of a material, with higher values corresponding with better flexoelectric properties. The flexoelastic ratio can be calculated using following relation.

$$\frac{e}{k} = \frac{2\pi \tan\phi}{Ep} \quad \text{Equation 5.4}$$

Tilt angles were recorded as a function of temperature and applied voltage by the method explained in section 5.2.2 (Flexoelectro-optic switching). The uniform lying helix (ULH) configuration has been attained by the method explained in section 5.2.1 (ULH Mode for flexoelectro-optic switching). All the mixtures showed a very uniform ULH texture formation. Commercial  $\sim 3.5\mu\text{m}$  thick *Instac* cells with an antiparallel planner alignment layer were used and their accurate thicknesses were carefully recorded using the Fabry-Perot technique explained in the chapter 2.

One particular finding in this work is that all the mixtures adequately followed the applied square wave field after obtaining the ULH configuration. Figure 5.11 is an example of a typical photo diode response of the ULH texture from **Mix-2** at a comparatively high temperature with an applied electric field of  $2.5\text{V}\mu\text{m}^{-1}$ . This particular type of response was used to determine the tilt angle.

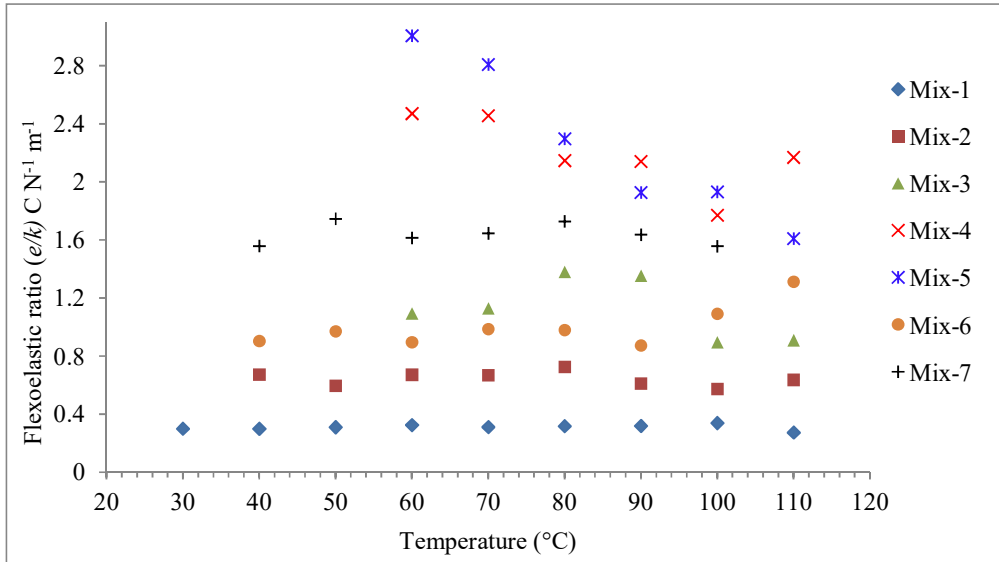


**Figure 5.11:** Photodiode response of Mix-2 and applied square wave electric field ( $2.5\text{V}\mu\text{m}^{-1}$ ) at  $90^\circ\text{C}$ .

There was a linear increase in the tilt angle with respect to applied electric field at the given temperature. However, at high applied voltages, the material tends to show dielectric unwinding of the helices before reaching a maximum tilt angle. The tilt angles were observed having a lowest value close to the clearing point with a stable ULH mode due to the dominance of the dielectric coupling leading to the unwinding of the helices.

Tilt angle magnitude increased with a gradual decrease in temperature and is the highest at the minimum temperature above the crystallisation point at the maximum applied field before the unwinding of the helices. **Mix-1** exhibited a stable ULH mode at  $30^\circ\text{C}$  but its flexoelastic ratio was  $0.30 \text{ C N}^{-1} \text{ m}^{-1}$  and at  $110^\circ\text{C}$  it was  $0.27 \text{ C N}^{-1} \text{ m}^{-1}$  with no significant change. For **Mix-2** there was three times increase in flexoelastic ratio with just an increase of 10% in the concentration of mesogenic dimer. **Mix-2** gives a wider temperature range among rest of the mixtures with better flexoelectric properties however, **Mix-3** to **Mix-5** crystallised

out below 60°C. It is clear from the results shown in figure 5.12 that by increasing the concentration of the mesogenic dimer in the high dielectric nematic, the flexoelastic ratio also increased. Hence for **Mix-5** with an 80% mesogenic dimer concentration, the flexoelastic ratio was 3.0 C N<sup>-1</sup> m<sup>-1</sup> at 60°C which was the maximum value for *e/k* coefficient among all the mixtures over all temperatures. **Mix-6** and **Mix-7** had better *e/k* values when compared to **Mix-2** with the elevation of the overall transition temperatures. However, their peculiar dielectric properties need to be investigated further before considering these mixtures for further blue phase research. To summarise, Mix-2 has a better values of *e/k* ratios over a wide temperature range which makes it a better candidate to investigate further for blue phase. It is worth mentioning here, in figure 5.12; the temperature range in the graph does not cover the full mesogenic transition of the mixture. However, these are the best points of interest where the mixtures exhibited an excellent ULH mode.



**Figure 5.12:** Flexo-elastic ratios (*e/k*) for Mix-1 to Mix-7.

Further to this, the ester linkage clearly plays an important role in the packing arrangement of molecules in the device. Literature study suggests [88] that ester linked mesogenic dimers give a better self-assembly of the materials compared to their corresponding ether linked dimer mesogens. An opposite trend has been observed for dielectric properties, already seen in the previous result and discussion section.

### 5.3 Response time:

The response time of a liquid crystal is an important parameter in applications particularly those involving the flexoelectro-optic effect. In principal, it is measured as the time taken for the light intensity at the photodiode to change as a function of applied field and

is measured from 10% to 90% of the maximum intensity. This is to compensate for the surface anchored material and to further negate any delays after the polarity of the field is switched. For this work, a bipolar square wave is used and response time is measured for the full switching angles only and not for the tilt angles as a function of applied voltage at different temperatures. At 60°C a comparison between all mixtures has revealed that as a flexo response, **Mix-2** showed a faster response  $\sim 25\mu\text{s}$  rise and decay time. **Mix-3** exhibited slower response (rise time  $239\mu\text{s}$  and decay time  $214\mu\text{s}$ ) compared to **Mix-4** (rise time  $164\mu\text{s}$  and decay time  $159\mu\text{s}$ ). However, **Mix-5** was the slowest among all the mixtures with a rise time of  $240\mu\text{s}$  and decay time  $275\mu\text{s}$ . It was determined that all mixtures exhibited a sub-millisecond response and they were found to be independent of applied voltage in most cases. Complete graphical results are given in the appendix section 9.1.

#### 5.4 Summary:

An optimised mixture composition has been established through analysing the electro-optical properties of all of the mixtures. The dielectric measurements showed that **Mix-2** has ample dielectric anisotropy with more stability at higher temperature than **Mix-1** which loses its anisotropy at high temperatures. Rest of the mixture compositions did not exhibit wider nematic transitions and their dielectric anisotropy was less than **Mix-2**. Flexoelectric properties of all mixtures were studied using the ULH configuration. From the results it is clear that the 80% dimer composition (**Mix-5**) has shown the highest flexoelastic ratio but it is far less dielectric compared to the 20% dimer composition in the commercial nematic LC host (BL006). Among all mixtures **Mix-2** has established a faster response time ( $25\mu\text{s}$ ) when compared at 60°C. The above criteria fit with the desired properties for a mixture to furnish a stable and switchable blue phase electro-optical effect.

**Chapter 6: Blue Phase, electro-optic study, polymer stabilisation and phase modulation**

### **6.1 Blue phase; advantages and short comings in display technology:**

In chapter 2, the blue phase was explained in generic terms. It consists of double twisted cylinders organised in cubic structures with a network of disclination lines which helps to steady the 3-D periodicity of the blue phase. The narrow transition temperature range can be explained by the fact that it is a metastable state between isotropic and chiral nematic LC phases. [89]

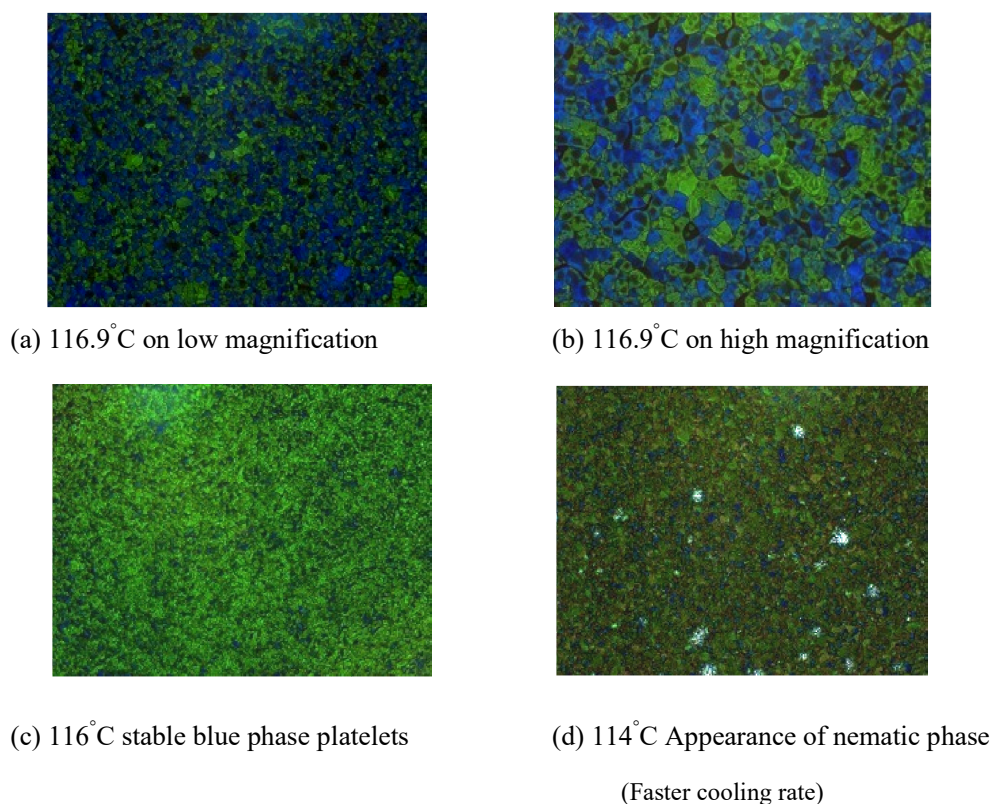
A polymer stabilised blue phase with a wide range transition temperature has several influences on device fabrication and applications, [90][91] for instance three dimensional mirror free lasers, [92] micro lens arrays, [93] Fabry Perot filters, [94] a dye-doped polariser independent display, [95] variable optical attenuators, [96] optical vortices [97] and gratings. [98]

Their structure, properties and applications in next generation display technology can be beneficial in several different ways. [99]–[102] For example their switching speed or response time is usually sub-millisecond, which is much faster than nematic liquid crystal which in turn helps to minimise image blur and artefacts and also makes colour sequential illumination a possibility. Another advantage is that an alignment layer is not required and hence makes the manufacturing process much simpler with an effective increase in yield and cost reduction. Most importantly, this phase is optically isotropic allowing wider viewing angles and insensitivity to cell gap thickness in an in-plane device. All the above mentioned advantages can make the potential system less bulky, light weight and polariser free.

Despite all these plus points, there are some problems with blue phase devices. At the moment, their threshold operation voltage is higher than that of nematic liquid crystals, and their transmittance is lower and also potential hysteresis effect must be tackled to improve display performance. Here we present research focused to address these issues.

### **6.2 Blue Phase mixture:**

Primarily, from the thermal and electro-optic studies in chapter 5, **Mix-2** appears to best fulfil the criteria of obtaining a stable blue phase. So, further studies have been carried out to investigate the appearance of blue phase near its isotropic point. This mixture exhibits a wider nematic transition and becomes isotropic at around 118°C. This mixture was heated up to its isotropic point and cooled by 1°C/min rate which was slightly higher than the literature value to obtain a blue phase in an ordinary liquid crystalline material. When the temperature reached 117°C, a dull green fog appeared and on further cooling to 116.9°C blue phase platelets was observed. Results can be seen in the figure 6.1.



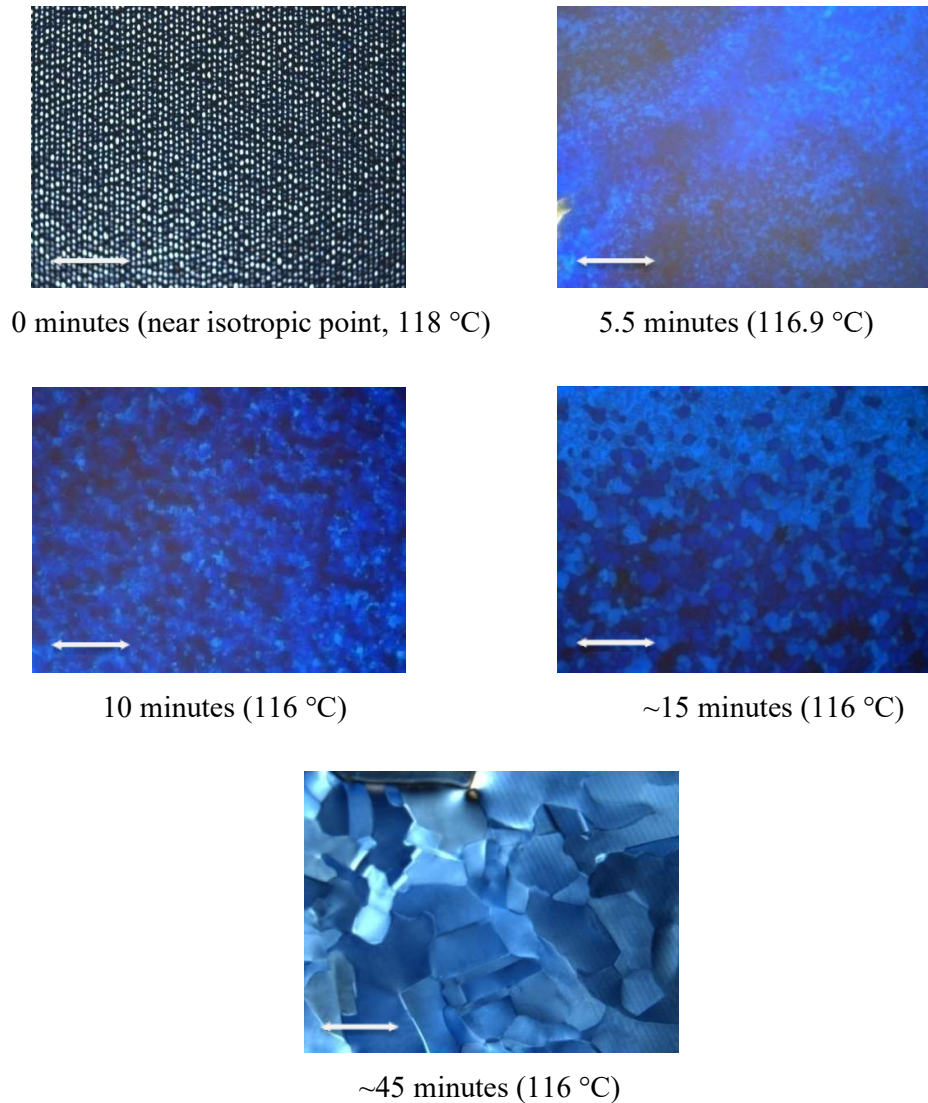
**Figure 6.1:** Appearance of a stable blue in **Mix-2**. (5.5% chiral dopant)

It was found that the blue phase from this mixture was robust in appearance even when moving the sample from the hot stage of the microscope and then replacing it back on the hot stage at the same temperature, the blue phase quickly reappeared. It is indeed a very promising result as according to a lot of literature, under normal circumstances any slight disturbance and the blue phase disappears quickly.

Additionally, **Mix-2** has shown a growth of bigger platelets under an hour when compared to the literature. Previous research suggests that obtaining blue phases is a very time consuming and tedious process. However, the appearance of these phases in **Mix-2** was much faster, well defined and bigger in domains. **Mix-2** started to become isotropic at 118 °C and prior to this temperature it appeared as nice droplets as shown in figure 6.2. To obtain a clear dark isotropic state under optical polarised microscope, the mixture was heated further up to 120 °C. Then the device was cooled at the rate of 0.2°C/ minute until reached to 116.9°C, here the device was held at this temperature for five minutes and a blue fog started appearing. Then around 10 minutes, this fog turned into blue phase platelets where the temperature was 116 °C. Another 15 minutes at this temperature, these platelets were well defined and ~ 20-50 µm in size. Holding the device at this temperature for another 45



minutes, yielded to very distinct large size blue phase platelets in the range of 300-500  $\mu\text{m}$  sizes. Results are depicted in the figure 6.2. Due to the tight pitch of the **Mix-2**, it was really hard to take clear images so these were captured with a slight variation in polarisers or a little change in the light intensity.



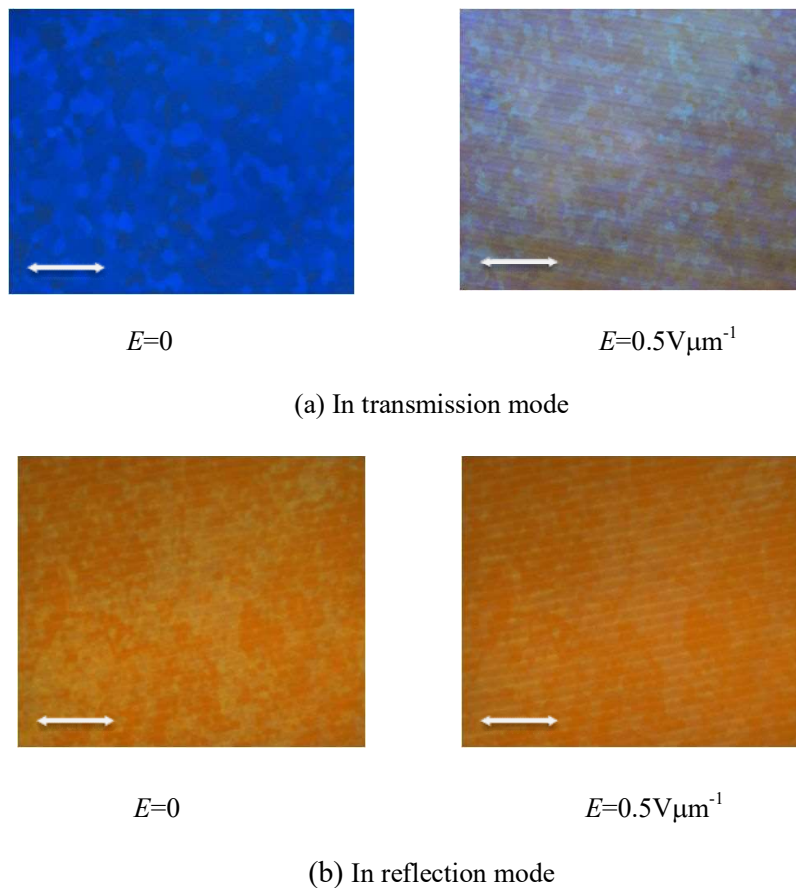
**Figure 6.2:** Growth of blue phase within one hour. (Scale bar: 200  $\mu\text{m}$  and 7.5% chiral dopant)

As discussed earlier, this mixture possesses both of the desirable properties such as dielectric anisotropy and flexoelasticity which help to facilitate to get the switchable stable blue phase.

### 6.3 Stability and polymer free switching of blue phase:

The mixture **Mix-2** gives a very robust and stable blue phase which was tested for initial polymer free switching at 114.3°C in an in-plane device. It only took a field of

$0.5\text{V}\mu\text{m}^{-1}$  to give stable switching and relax back to its initial blue phase platelets upon removing the applied field. The switching was observed in both transmission and reflection mode. This can be seen from the images taken through the optical microscope (figure 6.2). This resulting blue phase from Mix-2 is so stable that upon applying an electric field, the helices do not show any unwinding or distortion. Figure 6.2 shows the switching of blue phase platelets upon an applied voltage in both modes.

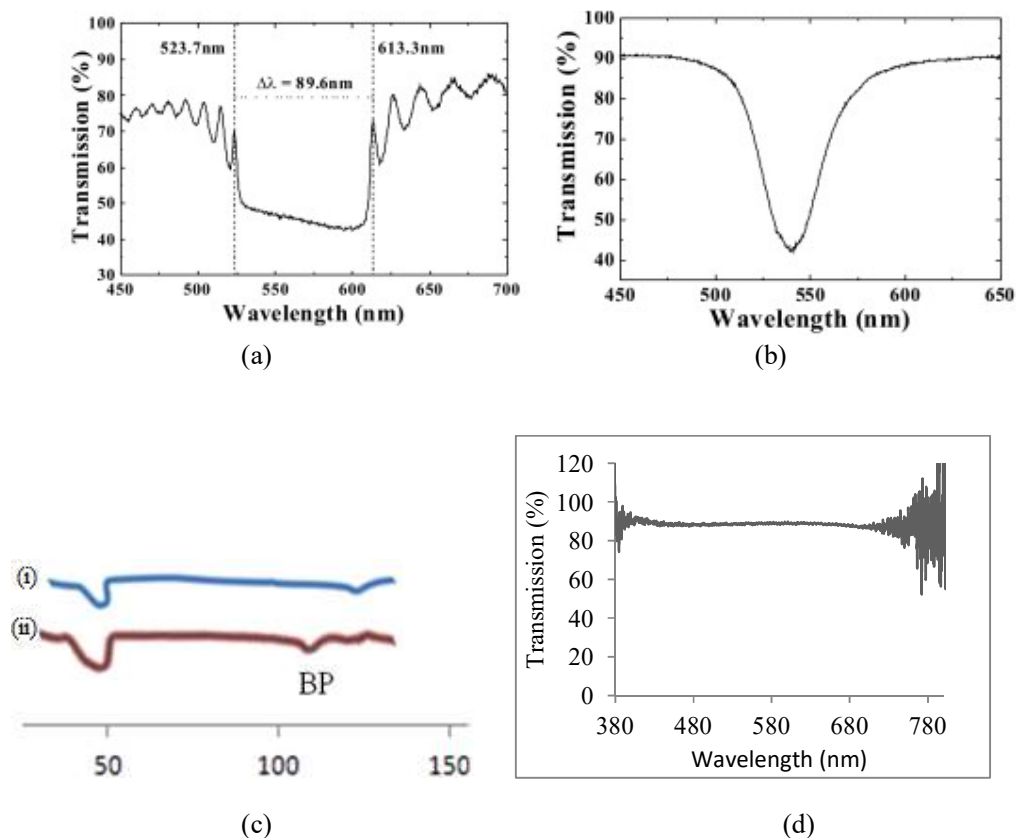


**Figure 6.3:** The switching of the polymer free blue phase using **Mix-2** at 114 °C. Scale bar: 400 $\mu\text{m}$

#### 6.4 Thermal scanning and band gap optimisation:

In order to study the blue phase appearance in Mix-2, a DSC thermal scan was recorded at a rate of 0.2°C/minute to identify any extra endotherms. A plot has been compared with the non-chiral mixture of Mix-2 and an extra peak can be clearly seen at 112°C in the plots in figure 6.3 (c) where (i) is the achiral mixture and (ii) is the chiral mixture.

Chiral nematic liquid crystals give a wider reflection band. A blue phase usually gives a peculiar narrow reflection band due to the presence of the 3D crystal lattice structure. In this case the reflection band has been pushed into the UV region due to its tighter pitch as was planned so as to avoid having the band gap in the visible spectrum.



**Figure 6.4:** The reflection bands of (a) nematic liquid crystals (b) blue phase respectively\*. (c) DSC traced showing an extra endotherm that belongs to blue phase and (d) the reflection band of the tight pitch Mix-2.]

### 6.5 Formulation of stabilised blue phase:

To obtain a polymer stabilised blue phase liquid crystal, a fraction of reactive mesogens and ultra violet (UV) curable photo initiator is usually added into the blue phase LC system. The temperature is then controlled to obtain blue phase which is followed by a UV curing process. After UV irradiation, the reactive mesogens are polymerised in the disclination lines to form a polymer network which in turn stabilises the blue phase lattice structure and facilitates the blue phase beyond its usual thermal transition. Important aspects to consider are that in the polymer stabilised, self assembled blue phase, all corresponding components properties are vital during the process of interacting with each other. However,

the polymer stabilised blue phase has a few limitations when it comes to platelet size and their electro-optic response. To address these additional controls in the blue phase polymer stabilisation, the following study has been carried out. This leads to obtaining a polymer stabilised switchable blue phase at room temperature.

### 6.5.1 Nematic liquid crystal:

A good photo and thermal stability is generally attained by incorporating 3 to 4 phenyl rings in mesogenic molecules which also brings a significant birefringence to the system. Moreover, polar groups enhance dielectric anisotropy by their dipole moment while fluoro compounds are preferred to reduce image flickering in displays [103] and reduce molecular packing due to their low polarisability.

To avoid image flickering, a high resistivity is another crucial requirement for obtaining a high voltage-holding-ratio for liquid crystal displays (LCDs). A significantly large  $\Delta\epsilon$  with a good birefringence tends to lower the driving voltage, which in turn lowers the power consumption of a display. Fluoro components offer an excellent resistivity [104], modest dipole moment with a low viscosity. Laterally substituted fluorinated liquid crystals [105], *i.e.*, (2,3) difluorinated biphenyl, terphenyl [106] and tolane [107] usually exhibit a high resistivity and a modest  $\Delta\epsilon$  [103].

For these reasons the present hybrid compound, FFE9ECB was selected. This compound encompasses many unique features, including a desirable formulation of a polymer stabilised blue phase, bearing both high polarised and low polarised ends with in a single mesogen.

Here, FFE9ECB (synthesised in house mentioned in Chapter 4), a nematic dimer has an excellent solubility in the high dielectric nematic liquid crystal host BL006 (Merck KGaA). Furthermore, a 20% composition has emerged as a potential blue phase mixture to study the stabilisation conditions and electro-optic properties. Additionally, the clearing temperature of this mixture ( $\sim 119$  °C) covers the desired temperature range ( $-40$  to  $85$  °C) which is an important aspect for the storage, displays and photonic commercial applications. The other main factors still need to be addressed are; low applied voltage and hysteresis free switching for precise grey scale after polymer stabilisation.

### 6.5.2 Chiral dopants:

Blue phases are highly three dimensional oriented chiral meso-phases. This chirality is often obtained by the addition of chiral dopants into the mixture. These chiral dopants or

twisting agents induce twist or helicity in normally achiral nematics. Blue phases often emerge when chirality exceeds a certain value. Furthermore, the helical twisting power (HTP) depends on the chiral dopant's molecular structure. The solubility of a chiral dopant limits its maximum concentration hence it is preferred to use high HTP chiral dopant where possible. Another important aspect is that twisting agents with low melting points tend to lower the clearing temperature of the LC host. So, to make a wider temperature range BPLC, the melting point of a chiral dopant should be higher than its host material with a good miscibility. To optimise the amount and obtain a blue phase; two types of chiral dopants BDH1281 and R5011 (both from Merck KGaA) have been studied. However, it was found that there was no significant difference in the required amount of both chiral dopants (BDH181 or R5011) to obtain the desirable short pitch UV region **Mix-2**. 7.5 % wt. of BDH1281 and 7.3 % wt. of R5011 were required respectively to achieve reflection band in UV region. BDH1281 was selected for further research because it was readily available.

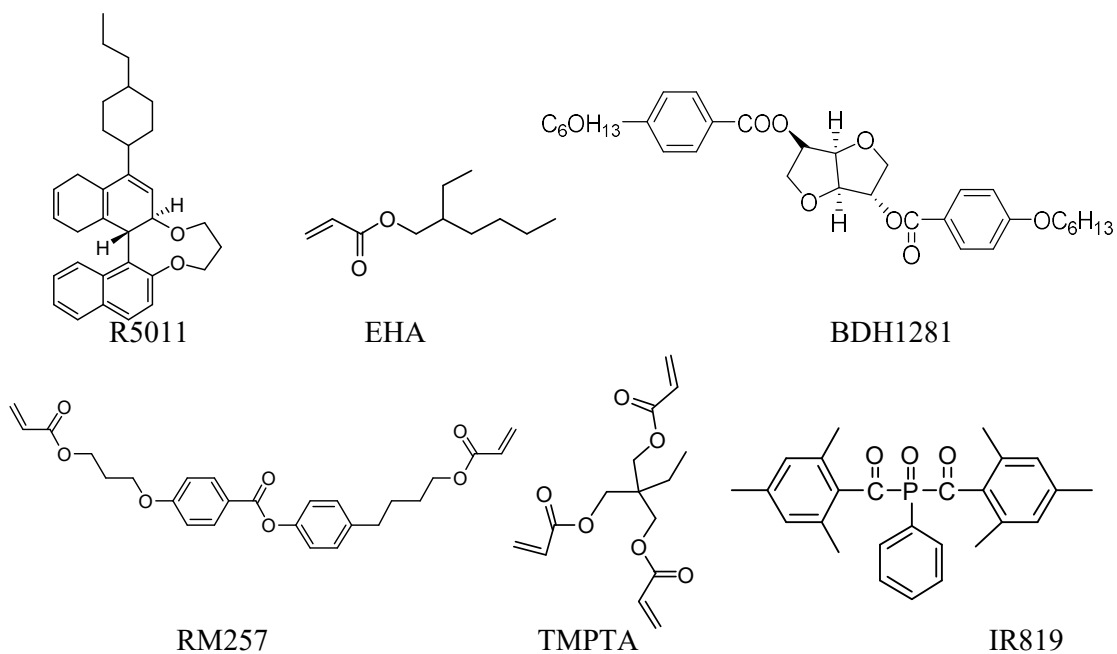
### 6.5.3 Reactive mesogens:

The choice of reactive mesogen plays an important role in determining the stability of blue phases in liquid crystal mixtures. Typically, two types of monomers are required to optimise the polymerisation process. Monomer concentration depends upon the number of reactive sites and ratio of both the monomer can be fixed to finalise the polymerisation process. Overall polymer concentration also affects the driving voltage and so has been limited to 10% for all sets of precursors. Four different sets of polymer precursors have been tested to achieve best results. Details are depicted in table 6.1.

Set	Reactive mesogens	Composition (mgs)
1	RM257 and EHA	5 each
		UCL-011-K1
2	(a) UCL-011-K1 and RM257	5 each
3	(b) RM257 and QM02-01	5 each
4	RM257 and TMPTA	(a) 8 and 2
		(b) 7 and 3
		(c) 6 and 4

**Table 6.1:** Reactive mesogens and their composition in a 100 mg mixture

The first set comprised of the bi-functional RM257 and mono functional ethyl hexyl acrylate (EHA) in equal %wt. The second set consisted of 6% bi-functional RM257 and 4% tri functional Trimethylolpropane triacrylate (TMPTA) and the third one was 10% UCL-011-K1 (Dai-Nippon Ink and Chemicals). In all three cases photo initiator (IR819, CIBA) was kept at 0.1%wt to control the polymerisation process. Chemical structures of the chiral dopants, reactive mesogens and photo initiator are shown in figure 6.4.



**Figure 6.5:** Chemical structure of components used in stabilisation of blue phase.

#### 6.5.4 RM257 and EHA [Set 1]:

The first set of monomers in a 1:1 ratio was thoroughly mixed in **Mix-2** along with 7.5% wt chiral dopant and 0.1%wt. photo initiator. The resulting blue phase mixture was then heated on a hot plate for 10 minutes in a dark environment up to its isotropic point at 105°C. It was then carefully capillary filled at the same temperature into an in-plane device of 14µm thickness. The cell was then cooled at the slightly faster rate of 2°C/minute to 99.5°C and then to 93.8°C at 0.1°C/minute till the blue phase platelets were observed. The device was then left at the same temperature for a further 10 minutes before UV curing using a handheld UV lamp, mounted on heating stage of the microscope and then left it for a further 30 minutes cure time at 365 nm. Then the sample was cooled down to the room temperature with the UV lamp illuminated on the heating stage.



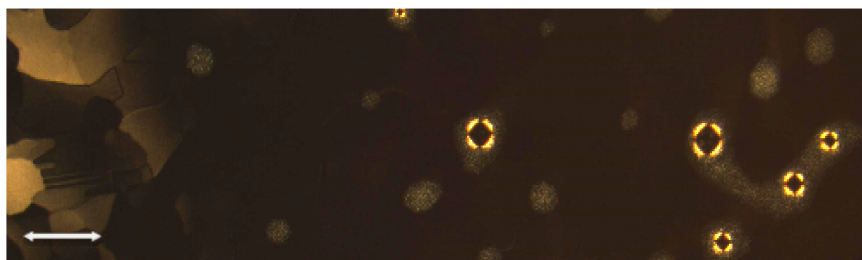
**Figure 6.6:** (a) Blue phase in an in-plane device (b) Degradation of polymer matrix on high voltage. Scale bar: 200µm.

EHA being a mono functional polymer precursor takes a long time to cure compared to the other multifunctional monomers. It gives a soft polymer network which tends to degrade at higher fields ( $\sim 15\text{V}\mu\text{m}^{-1}$ ). Figure 6.5 (b) shows the degradation of the polymer network and hence the distortion of blue phase platelets into the nematic liquid crystal phase. The blue phase material itself was very robust and easy to stabilise at the blue phase temperature. But with this polymer composition it was very slow and tedious to get uniform polymerisation. Due to the above mentioned limitations and associated phase separation, no further studies were carried out.

#### 6.5.5 UCL-011-K1 [Set 2 (a) and (b)]:

UCL-011-K1 is a mixture of monomers with photoinitiator obtained from Dai-Nippon Ink and Chemicals and has been utilised in two ways. Initially, 10%wt of this polymeric mixture was carefully mixed with the blue phase system in a UV free environment. After capillary filling, the device was tested for the blue phase followed by polymerisation. Although, the blue phase acquired was very uniform with bigger domains, the polymer

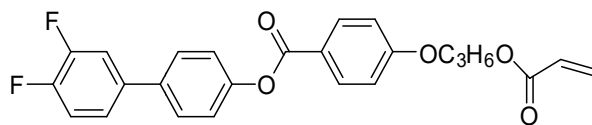
mixture led to phase separation and droplets appeared within the device. A second mixture composed of equal quantities (50:50 ratio) of UCL-011-K1 and RM257 which was mixed together with 0.1%wt. photoinitiator to form a new blue phase mixture. The effect of the RM257 in this mixture on the polymerisation process has been studied while keeping the reactive mesogens at 10%wt. Again there was no difference observed in the blue phase formation and phase separation viewed earlier for the case of the pure UCL-011-K1 in blue phase system. Hence, this polymer mixture has been disregarded for any further investigation. Droplet formation and phase separation can be seen in figure 6.6.



**Figure 6.7:** Phase separation and droplet formation in blue phase mixture with UCL-011-K1 under UV filter. Scale bar: 200 $\mu$ m

#### 6.5.6 RM257 and QM02-01 [Set 3]:

The reactive mesogen QM02-01 has been synthesised previously in-house by Dr. Malik Qasim and has a potential single reactive site with terminal fluoro groups similar to the dimer component of the **Mix-2**. This material has been utilised along with RM257 to study the polymerisation conditions and stability of **Mix-2**. The chemical structure is given in figure 6.7. Equal amounts in %wt. of both QM02-01 and RM257 were incorporated into **Mix-2** together with 0.1%wt IR819 as a photo-initiator. A stable blue phase appeared at 94.1 $^{\circ}$ C but the polymer composition was not compatible with **Mix-2** and underwent a phase separation. Again this mixture composition has been disregarded due to its immiscibility in the **Mix-2**.



**Figure 6.8:** Chemical structure of QM02-01

#### 6.5.7 RM257 and TMPTA [Set 4 (a), (b) and (c)]:

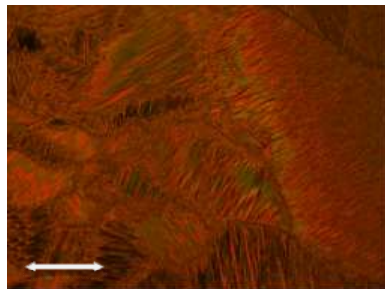
TMPTA is a triacrylate and when mixed with RM257 gives a cross linking due to active sites available in this polymeric system. RM257 and TMPTA with varied concentrations have been tested in order to optimise curing conditions, lower the threshold



voltage and to get a uniformly polymerised blue phase. Three sets of RM257 and TMPTA in varying weight percentage compositions were mixed (a) 8%wt. and 2%wt., (b) 7%wt. and 3%wt., (c) 6%wt. and 4%wt. respectively. The first two compositions were not proven to satisfy the desired criteria. A lesser amount of TMPTA in a polymer mixture has shown a similar behaviour as seen with the RM257 and EHA. For these reasons no further studies have been carried out for the first two mixtures.

The 6%wt. RM257 and 4%wt. TMPTA along with 0.1%wt. photo initiator turned out to be an excellent option to match the required performance. For this composition, filled into an in-plane device, the blue phase started to appear at 99.5°C and kept stable at 98.9°C for another 10 minutes to allow a 3D photonic structure to stabilise further before UV curing at the same temperature. This composition proved to be excellent at generating a uniform curing state in the device and blue phase appeared within minutes at the correct temperature. A complete device was ready within an hour from capillary filling of the blue phase material into the device. Normally, it takes several hours to get a stable blue phase, but with this material composition it has been easily achieved.

To find a better polymerisation process, the sample was left overnight on a heating stage at a very slow cooling rate (0.01°C) to 98.9°C under a UV filter. Instead of having a fine blue phase texture, an unusual texture was observed which cured at 98.9°C and can be seen in figure 6.8.



**Figure 6.9:** Blue phase device left overnight to optimise polymerisation process. (Scale bar: 200μm)

Based on the previous observations, the (50:50) ratio of EHA and RM257 is workable but a bit sluggish in polymerisation conditions. A blue phase in the in-plane device was stabilised in patches but was not uniform throughout the device. On the other hand, RM257 6%wt. and TMPTA 4% has emerged as the best potential composition for further characterisation. It was easy to polymerise and the fabricated device was very uniform. Hence

for the blue phase system, a mixture of 6%wt. RM257 and 4%wt. TMPTA will be used from here on to obtain an electro-optic response and test optical phase modulation.

Results for all the above mentioned reactive mesogen compositions are summarised in the table 6.2.

Reactive mesogen mixture	Ease in polymerisation	Curing temperature °C
Set 1	Sluggish polymerisation	93.8
Set 2	(a) Did not work (Phase separation)	-
	(b) Did not work (Phase separation)	-
Set 3	Did not work (Phase separation)	-
Set 4	(a) Soft matrix formation	-
	(b) Sluggish polymerisation	-
	(c) Easy to polymerise with very uniform blue phase	98.9

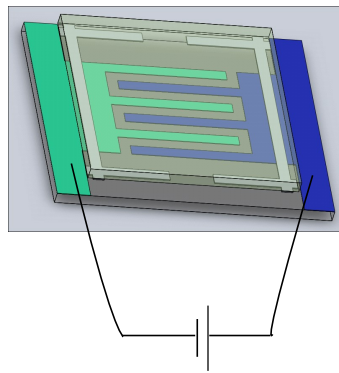
**Table 6.2:** Curing conditions of reactive mesogens.

## 6.6 Electro-optic properties of polymer stabilised blue phase:

A blue phase mixture has been devised that it has suitable dielectric properties as well as a reasonable flexoelastic ratio as explained in chapter 5. Previous research to obtain a switchable blue phase involved polymer templating which itself is a painstaking step and has several flaws.[18] In the templating process, a blue phase polymer network is created from the high flexo material and then washed with appropriate solvent to reveal the template. Then this template is filled with high dielectric liquid crystalline material to obtain electro-optic switching response. Often during the washing process, the polymer network alters itself either by swelling or by leeching into the solvent and hence changing initial stabilisation. A second important factor is the high amount of polymer (~40%) utilised in constructing the polymer

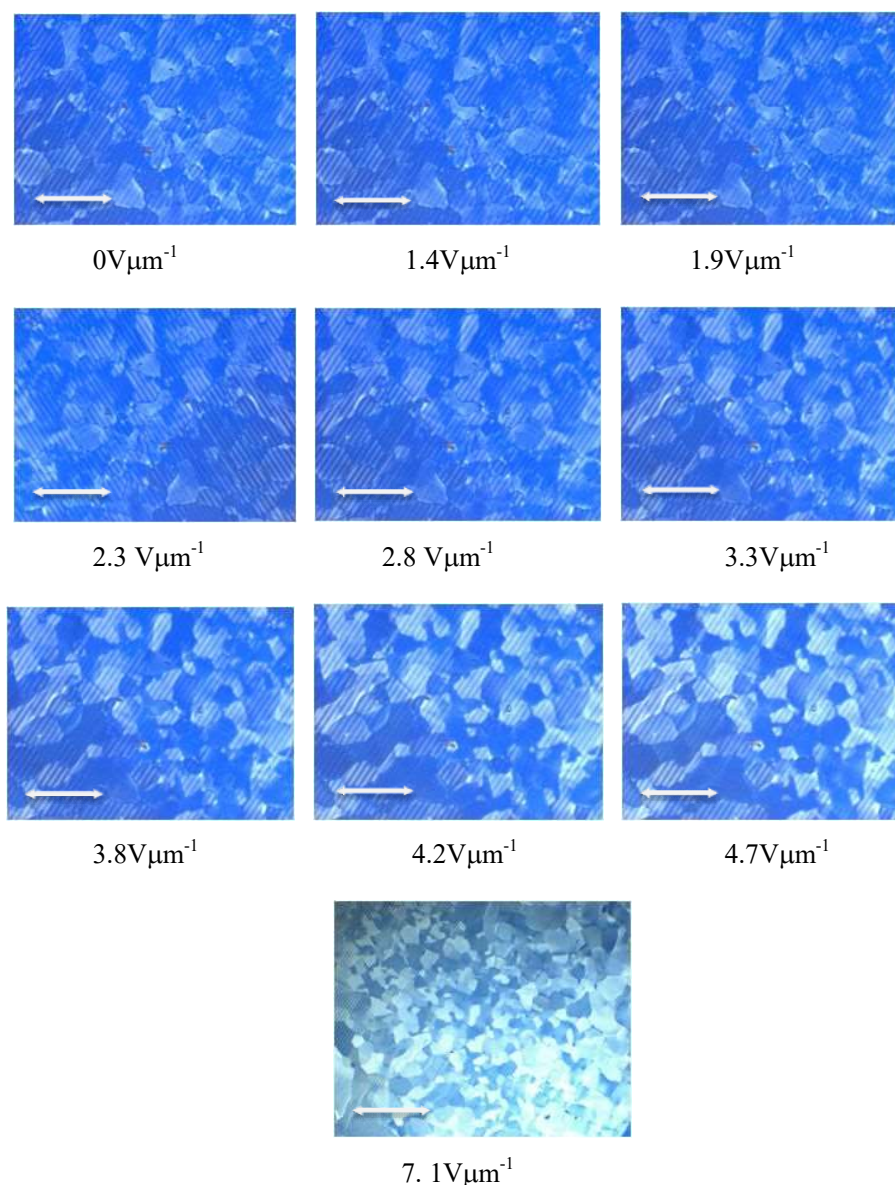
network in the template ramps up the threshold voltage several folds. In fact, polymer template blue phases have not been able to switch at all. In this work, a switchable blue phase device has been fabricated in a single step by incorporating flexo and dielectric components in the same mixture. Device fabrication and its detailed components have been explained in the previous section.

The in-plane device has pixel addressing on one substrate. The pixel size and gap between pixels constitutes the overall dimensions of the device. The device has no alignment layers on either of the substrates. Plain glass constitutes the top substrate so that it only covers the pixel area and leaving exposed connectors as shown in figure 6.9 below.



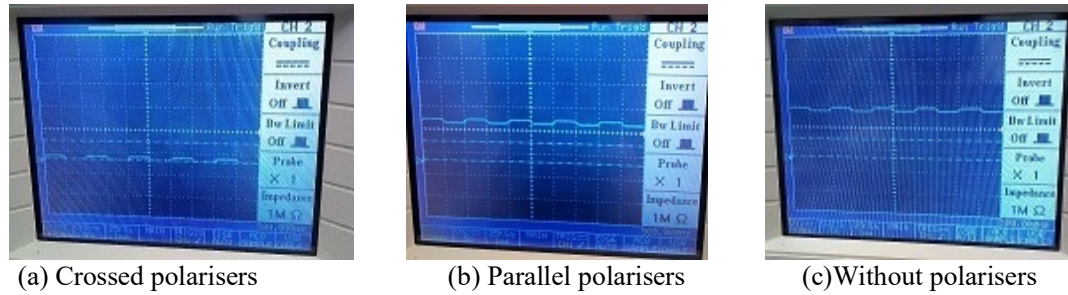
**Figure 6.10:** In-plane device assembly for polymer stabilised blue phase. (Image has been adapted from Instec supplier website.)

As it is well known that in-plane switching is insensitive to the cell gap but in this case to grow bigger platelets, a  $25\mu\text{m}$  thick cell was fabricated. To get the electro-optic response of the blue phase, an in-plane device was made by capillary filling the blue phase mixture followed by polymer stabilisation. The device was subjected to an incremental applied voltage to observe the switching of the platelets. It was evident from the series of pictures shown in figure 6.10 that there was no significant change up to  $2.3\text{V}\mu\text{m}^{-1}$ . As the voltage increased, the switching of platelets was observed. For the first time BP II switching has been observed as the light intensity changed significantly from  $0\text{V}\mu\text{m}^{-1}$  to  $4.7\text{V}\mu\text{m}^{-1}$ . At  $7.1\text{V}\mu\text{m}^{-1}$  this material still showed stability and withstood high voltages above its saturation point, without changing the polymer network. This was a very promising result with a lower threshold voltage when compared to previously reported results.[70] Figure 6.10 shows series of changes in the light intensity and switching of the cubic structure.



**Figure 6.11:** In-plane switching of polymer stabilised blue phase at 20X (scale: 200 $\mu\text{m}$ ) and 10X (scale: 400 $\mu\text{m}$ ) magnification.

Electro-optic switching of a polymer stabilised blue phase was observed under three polarisation conditions to confirm its optically isotropic nature. There was no significant difference in the photodiode response as it followed the applied field and the only difference was in the intensity of light passing through the device. Under the influence of crossed polarisers, a minimum of light passed through the device and switching response was independent of the orientation of the polarisers. Figure 6.11 indicates the response in three different polarisation states.



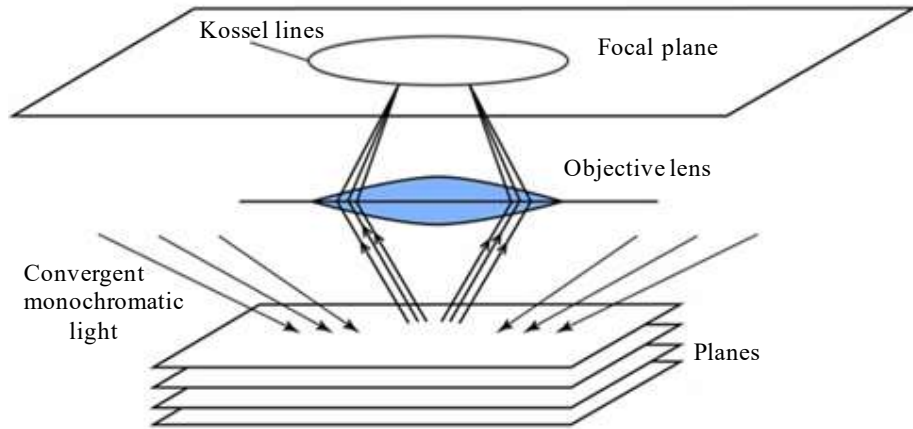
**Figure 6.12:** In-plane switching of the polymer stabilised blue phase with respect to three different polarisation states.

The above result indicates that polariser independent electro-optic switching can be achieved by these polymer stabilised blue phase devices at low applied field. This could reduce the cost of display device fabrication and hence the device could be less bulky and cheaper without polarisers. This mixture also delivers further ease in blue phase device fabrication when compared to more complicated conventional display devices.

### 6.7 Optical characterisation of polymer stabilised blue phase:

A Kossel diffraction diagram technique is often used to study the three dimensional cubic structure of blue phases based on Bragg's selective refraction. Blue phases exhibit three dimensional periodicities of the order of visible wavelengths and hence Bragg's diffraction is a very useful mechanism to study them. Since it has been proposed that blue phases exhibit cubic structures, several attempts have been made theoretically and experimentally to establish the structure.[108][71] Either highly convergent or divergent light induces Bragg's diffraction and develops a pattern by diffracting light due to parts of the crystal lattice structure. This patterned diffracted light relates to the facets of the crystal (or cubic) lattice.

When a coherent light is used through a high magnification objective lens, some of the light interacts with the lattice and is then diffracted forming a part of a cone. Kossel lines are observed in the reflection which come to a focus in the rear focal plane and appear as circles ellipses or lines. These lines depend on the wavelength of the incident light, orientation and size of the lattice. The image produced in this way is known as a Kossel diagram. A schematic diagram demonstrating the Kossel diagram method is shown in figure 6.12.



**Figure 6.13:** Schematic diagram illustrates Kossel diagram when parallel coherent light is reflected from sample.

The entire setup and method has been adapted from *Millar and Gleeson's* procedure to measure lattice parameters from Kossel diagrams in blue phase [71] and is shown in Chapter 3. The experimental results and literature comparison with respect to Miller indices are shown in table 6.3.

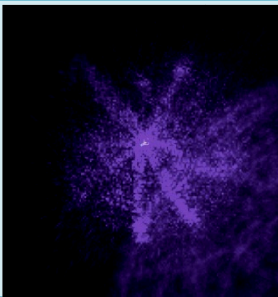
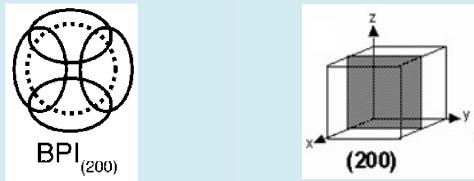
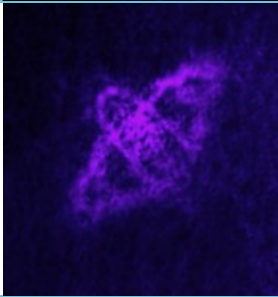

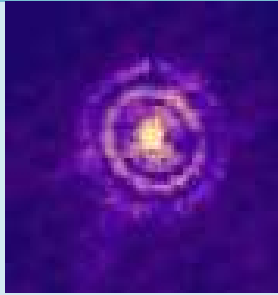

### 6.8 Bigger domains:

The physical and electro-optic properties of **Mix-2** have been already explained in the previous chapter. This specific mixture has the ability to self organise in a stable 3-D arranged photonic structure. It exhibits a wider workable temperature range blue phase transition and is easy to polymerise depending on the types and concentration of reactive mesogens as explained earlier in this chapter. To observe a clear Kossel diagram, an attempt was made to grow bigger platelets for phase modulation to avoid light scattering and interference with the visible light. Upon careful cooling, bigger domains appeared around 200 $\mu\text{m}$  in size after the polymerisation process which can be seen in the figure 6.13 at just 10x magnification.



**Figure 6.14:** Optical micrographs of bigger platelets at 20X (scale bar: 200 $\mu\text{m}$ ) and 40X (Scale bar: 100 $\mu\text{m}$ ) magnifications.

The observed Kossel diagrams are indicative of the presence of cubic platelets which are characteristic of a blue phase transition. Table 6.3 shows a set of diffraction patterns which have been observed as a Kossel diagram from the bigger blue phase domains after polymer stabilisation. Focus and setup steadiness plays an important role in obtaining an exact image and even a very small vibration can influence the results. Further, these images are the most commonly observed patterns which were carefully recorded.

No	Kossel diffraction pattern	Schematic illustration [109]	Miller indices
1			
2			
3			

**Table 6.3:** Observed Kossel diffraction pattern and schematic illustration.

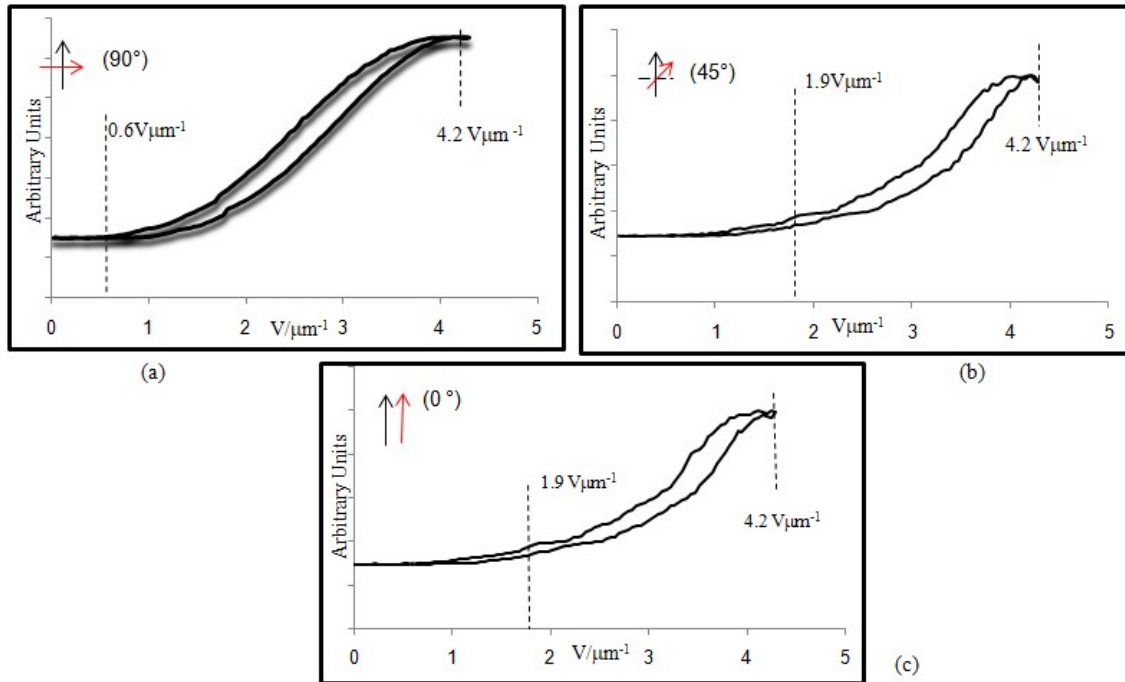
The observed Kossel diffraction patterns of polymerised **Mix-2** when compared to literature, suggest the presence of predominant blue phase BPI and BP II. However for the comprehensive Kossel diffraction pattern study with respect to thermal scan, under applied field and RGB wavelengths interaction requires a new electro optical setup as a part of future plan.

## 6.9 Electro-optic properties of polymer stabilised blue phase:

Any display technology based on a blue phase requires a low driving voltage as well as minimal hysteresis. Large hysteresis appears due to deformation in the blue phase platelets and polymer network by the application of a high applied electric field. It is important to have a strong polymer network which can withstand higher voltages. Hence, there is always a compromise between the polymer composition and driving voltage. Further to this, disclination lines are also responsible for hysteresis because light leaks out through these disclination lines and hence generate the effects of hysteresis. It is already explained that the blue phases here are optically isotropic and can switch with sub millisecond response times.

It has already been shown in figure 6.11 that there is no difference in the blue phase optical response in three separate polarisation states, except the overall intensity of light that is scattered through the sample. With crossed polarisers the minimum intensity passed through the sample while it was at maximum without any polariser at all. Voltage transmission data was recorded for the polymer stabilised blue phase in order to check its stability and hysteresis. In figure 6.14; (a) it was observed when the polarisers were crossed, (b) was the 45° polarisation state and (c) was the parallel polarisation state. These graphs were reordered over more than ten runs of each VT cycle until no change in the results was observed. Additionally, these VT graphs also depict the presence of least hysteresis effect, as a least change in the light transmission during this on-off switching cycle together with repetition of the curves after each complete run. Likewise, VT response in all three polarisation states is an indication of the optically isotropic nature of this blue phase material. These results have shown quite promising electro optic responses which further suggest a stable polymerisation of blue phase in this formulated mixture **Mix-2** (Set-4c).





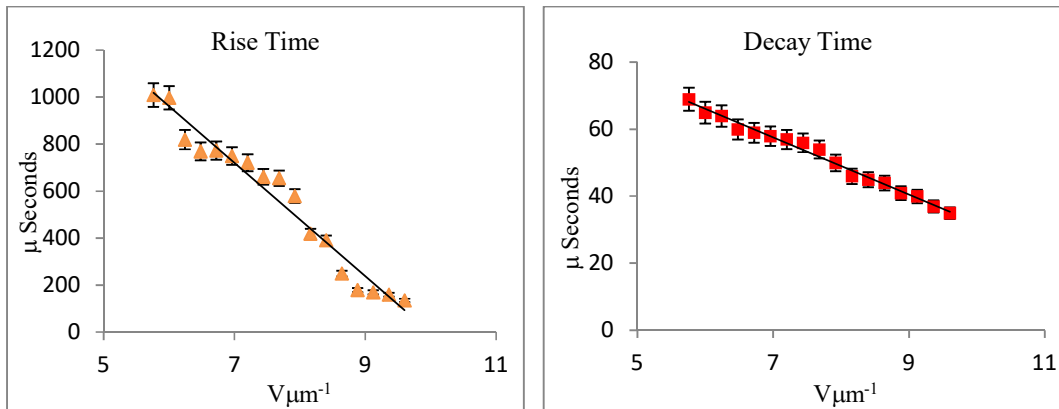
**Figure 6.15:** Voltage transmission data for the PSBP in an in-plane device at three polarisation states. VT curve (a), at  $90^\circ$  polarisers, grey line (—) is the first run, whereas, the darker line (—) is the tenth and onward runs of the sample. VT curve (b), at  $45^\circ$  polarisers and VT curve (c), is at parallel polarisation state.

### 6.9.1.1 Response time of the polymer stabilised blue phase:

A conventional nematic liquid crystal display exhibits response times of the order of tens of milliseconds which is not sufficient for high frame rate sequential displays. Hence it is equally important to improve the response time of material under the influence of applied field and it should be fast enough to address the requirement for faster displays. The Kerr effect of a material is a fast response which is the transition from isotropic to anisotropic states under the influence of an applied field. As blue phase is a three dimensional arrangement of helices, on applied field those helices which align with the direction of the applied electric field are affected more and get more distorted. This distortion of helices in the 3D lattice induces anisotropy.

The polymer stabilised **Mix-2** in an in-plane device has shown micro second response times without significantly distorting the polymer matrix up to fields of  $10\text{V}\mu\text{m}^{-1}$ . This particular mixture forms a stable blue phase with a high dielectric component and at high voltages dielectric coupling dominates inducing anisotropy. Whereas, the mesogenic dimer provides the flexo component which stabilises the blue phase and hence dominates at

relatively low applied field and gives an isotropic nature to the blue phase. This is one theory to explain the fast rise and decay times of this in-plane device.



**Figure 6.16:** Switching times in micro seconds with respect to the field a 1 kHz signal applied at room temperature.

The above plot shows a minimum rise time of  $136\mu s$  and decay time of  $35\mu s$  at  $9.25V\mu m^{-1}$  whereas, the highest response observed at  $5.5V\mu m^{-1}$  was  $\sim 1$  millisecond and  $\sim 70\mu s$  as rise time and decay time respectively. The linear trend was also observed, with a decreasing response by an increase in applied field. The response was measured at a 1 kHz frequency from  $5.5V\mu m^{-1}$  to  $9.25V\mu m^{-1}$ .

### 6.10 Effect of polymer concentration on response time of PSBP:

The use of reactive mesogens is inevitable as these materials give stability to the desired configuration of liquid crystals whether it is in the ULH mode or blue phase. In the case of the blue phase, the reactive mesogens are polymerised and provide permanence to the photonic crystal structure. The use of polymer not only lowered the appearance of the blue phase transition temperature (by at least  $\sim 19^\circ C$  in case of **Mix-2**) but also provided thermo dynamical stability over a wider temperature range.

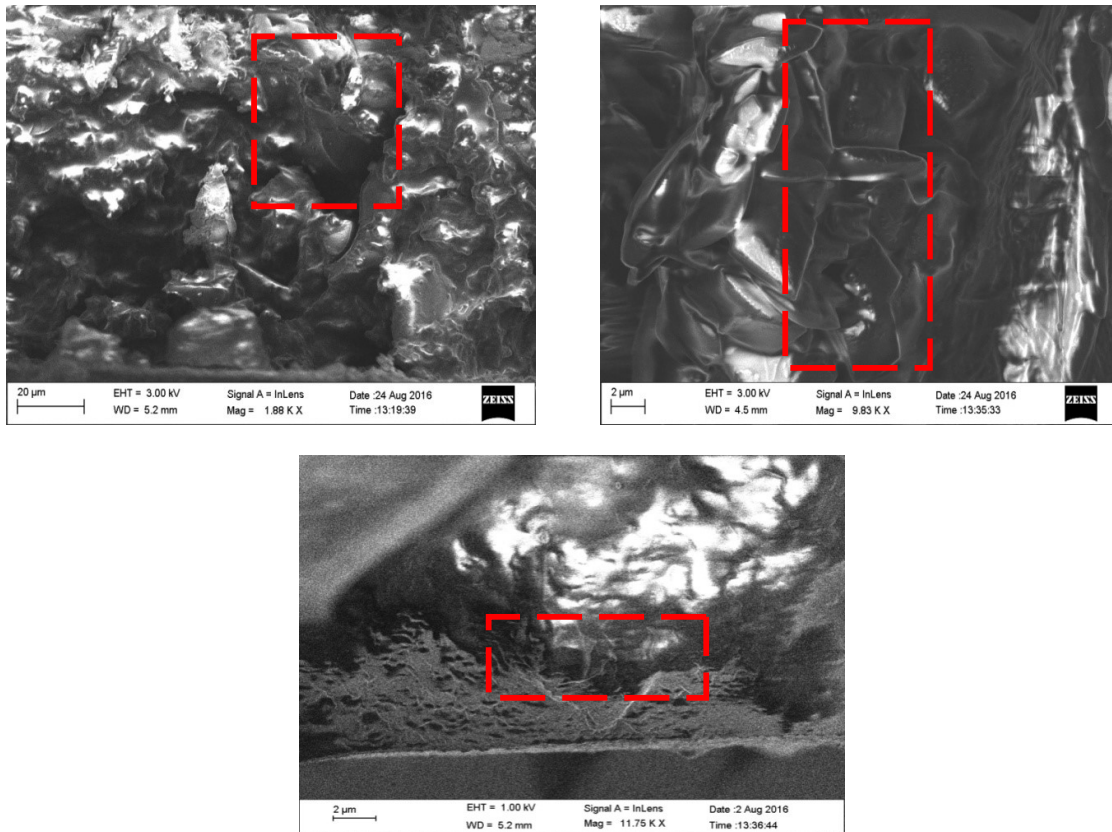
The polymer interlocks the geometry of the blue phase in a cubic structure by sitting in the disclination lines to stabilise it. But it also affects the applied field by increasing it and so it is important to optimise the concentration of polymer material in the system. Minimal concentrations of polymer would not stabilise the blue phase over a wide enough temperature range and excessive amounts of polymer would not lead to an optical response upon applied field.

Keeping these points in view, a polymer concentration has been optimised and significantly reduced by over 50% as compared to blue phase templating.[18]

### 6.11 SEM micrographs for polymer stabilised blue phase:

SEM images have been recorded through a Zeiss Sigma FE-scanning electron microscope. For these images, the final polymer stabilised blue phase device was prepared in order to fit on the SEM mount. Initially the device was cleaved in to pieces by immersing in liquid nitrogen followed by sputtering ~10nm Ni layer on each piece to act as a contact layer.

The amount of reactive mesogen was only the 10% wt. of the total blue phase mixture and hence the device was quite fragile. In figure 6.16, SEM images show some obvious layering and stacking indicating the orientation of blue phase platelets and the bright area in the images is the polymer network. These images have been recorded to observe the orientation of blue phase lattices and polymer network sitting in the disclination lines to lock the platelets. These images were recorded at 2 and 20 $\mu$ m scale and repetitive pattern of platelets was observed, highlighted as a red box area on images.



**Figure 6.17:** SEM micrographs of polymer stabilised blue phase revealing inside texture of the device.

## 6.12 Phase modulation of light using PSBP:

In 2010, a polarisation independent  $\pi$  phase shift of light by means of a polymer stabilised blue phase in a transmissive device was first reported by Lin *et al.* [93] Specific electro-optical properties of the blue phase have been explained earlier, and to achieve desirable results an appropriate mixture was formulated.

### 6.12.1 Polymer stabilised blue phase:

A blue phase mixture has been described in section 6.2 and gave blue phase upon slow cooling from its isotropic phase. By adding the reactive mesogens into the **Mix-2**, the isotropic point was decreased further (by almost 19°C) from its original isotropic transition of 118°C. Hence an LCoS device was capillary filled at 103°C to make sure that mixture containing reactive mesogens was in the isotropic state. Afterwards, the cell was cooled down at the rate of 3°C/minute till 100°C then 1°C/minute to 98°C followed by 0.1°C/minute until the 97.8°C temperature was achieved. Then the device was left at this temperature for ten minutes so that bigger platelets of blue phase were formed. Subsequently, the device was cured by a heating mountable 365nm (80mW output) light source for 10 minutes followed by cooling at 5°C/minute rate to room temperature while the light source was kept mounted on the heating stage. UV was illuminated from top of the devices as a diffused light source to lock the blue phase platelets by polymerisation of reactive mesogens. The hand held UV curer is shown in figure 6.17 and the mount was made in house.



**Figure 6.18:** Hand held UV curer and its mount. Image copied from the supplier's web site (Mightex).

Finally, each device was checked by driving each pixel at  $7V\mu\text{m}^{-1}$  in order to make sure that the final devices properly switched and there was no short circuit before subjecting them to the Young's slit diffraction experiment.

### 6.12.1.1 Factors affecting phase modulation of light using PSBP:

As discussed earlier, polarisation independent phase modulation of light using a polymer stabilised blue phase has been studied since 2010 and has been a point of interest for several photonic applications. There are certain factors already explained in the literature using different types of devices, platelet sizes and device thicknesses.[110][70] It has also been reported that two types of devices were used to observe the phase shift; one with a rubbed polyimide alignment layer and a second one kept as simple as possible without any alignment layer. The device with a rubbed anti-parallel planar alignment induce surface anchoring to the blue phase platelets hence the driving voltage tends to increase compared to the simple one.[110]

It has already been reported that the improved domain size in blue phase demonstrates a 15% increase in the response time and hence improves modulation ability. The retardance or the phase modulation ability has a linear relation to the device thickness. Consequently thicker devices can be attributed to a greater magnitude of phase modulation. The only trade-off is that the applied voltage would be higher compared to the thinner devices. [70] By carefully combining the above mentioned conditions and trade-off, over  $2\pi$  phase shift is possible to achieve. A  $20\mu\text{m}$  thick LCoS device without any surface alignment has been selected to observe phase modulation on a Young's slit interferometer, already calibrated by *R. Garsed*. [70]

### 6.12.1.2 Optical phase measurements:

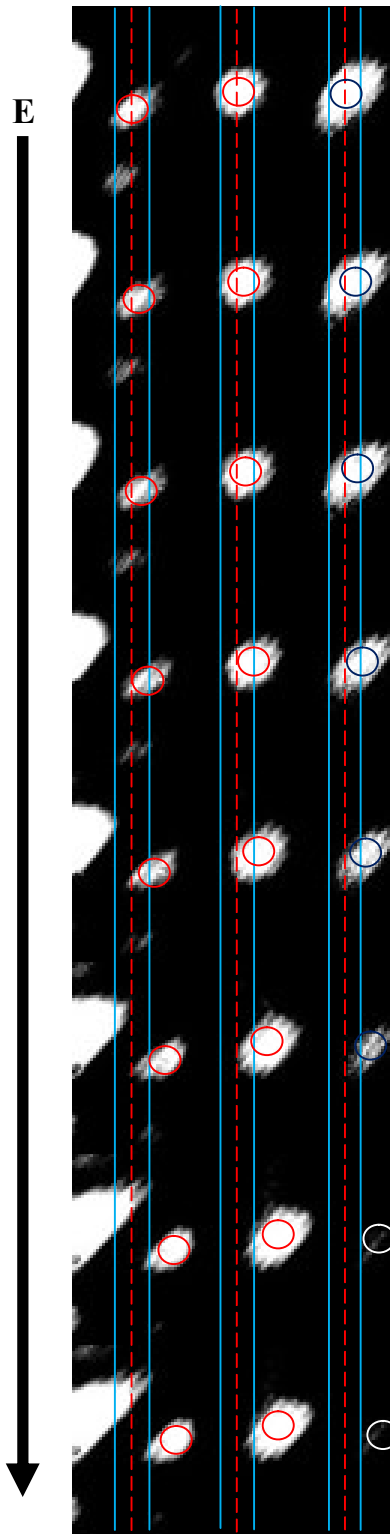
With the intention of measuring the magnitude of the phase modulation, an external field was applied to one pixel of the LCoS device behind one of the slits. This causes a change in the orientation of polymer stabilised blue phase platelets due to the existence of the dielectric component in the mixture. The light incident through this particular slit is then retarded compared to the un-driven pixel hence causing a shift in the position of maxima in the far field of the slits.

When no voltage was applied, the distance and positions between two maxima were measured and each image saved. Upon an applied voltage, again the image was saved and compared with the previous one to measure the change in maxima location. A similar procedure was adopted while consistently increasing the voltage till the saturation point or no

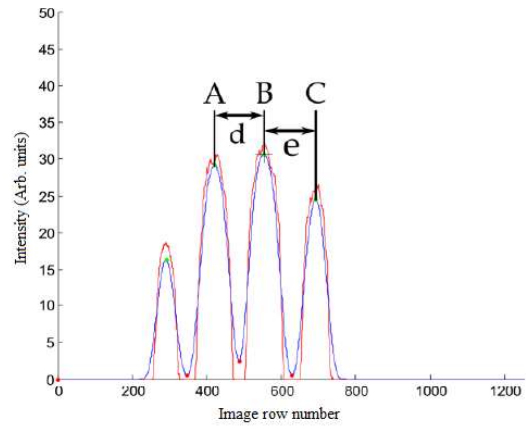
further change in maxima was achieved. The same process was followed with a regular decrease in the applied field to observe the shifting pattern in the replay field.

To obtain clear and discrete maxima, the CCD camera was operated manually so that it did not alter the exposure level. Images and voltage were saved before incrementing the voltage. A complete run with increasing and decreasing voltages for a number of steps and the captured images were saved. This process was repeated five times at 1 kHz and the spacing between maxima for each run was then averaged to reduce errors. For the initial image with no applied field, the spacing between two maxima was carefully measured and by comparing the images with incremental voltages it was possible to calculate the relative phase shift.

The reason for repeating the procedure was to achieve a better accuracy in the final result. Precaution was taken each time to track each maximum carefully on increasing the applied field. All five readings were made at the same position in the device to avoid any inaccuracy in the results. Figure 6.18 (a) shows the actual captured images of maxima in the replay field and the associated shift in maxima with respect to the increase in applied field and (b) is the illustration of the shift measurement.



(a)



(b)

If maxima shift to the right:

Movement of peak A relative to distance d.

Movement of peak B relative to distance e.

If maxima shift to the left:

Movement of peak C relative to distance e.

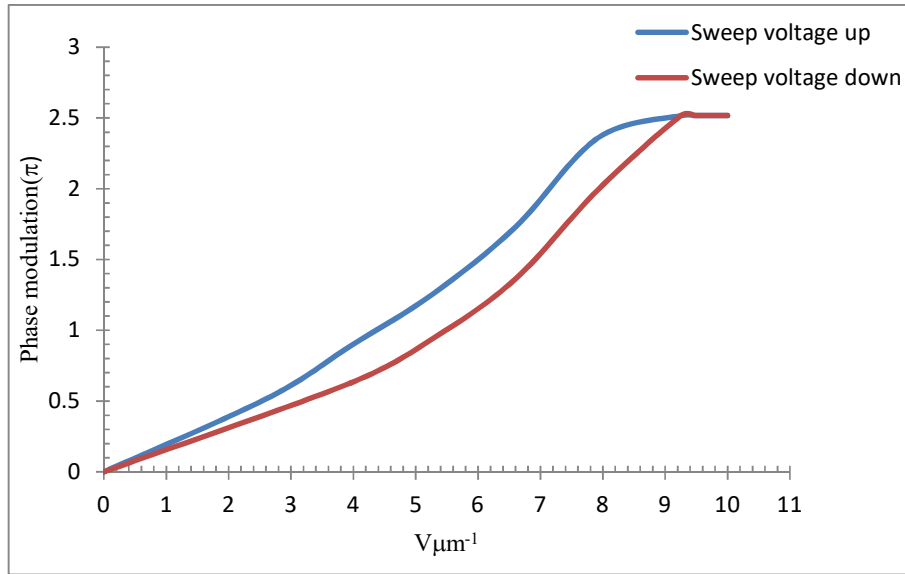
Movement of peak B relative to distance d.

**Figure 6.19** (a): Actual images of phase modulation in the replay field showing the maxima shift on increasing the voltage whereas, image (b) is the illustration for calculating the phase shift.

The separation of the two maxima was calibrated to be 200 camera pixels with  $\pm$  one pixel error which will incur an error of 0.03 radians in the phase modulation response. Phase modulation in radians can be calculated by following equation.

$$\text{Phase modulation (radians)} = \frac{\text{Number of pixels moved}}{\text{Number of pixels between two maxima}} \times 2\pi \quad \text{Equation 6.1}$$

All the measurements were taken at room temperature and without any polarisers to ensure polariser free phase modulation.



**Figure 6.20:** Phase modulation with respect to applied field.

Data obtained through this Young's slit interferometer by applying 0-10V  $\mu\text{m}^{-1}$  is presented in figure 6.19. A  $0.5\pi$  phase shift was achieved by applying  $2.6\text{V}\mu\text{m}^{-1}$  which is less than the sweep down voltage of  $3.45\mu\text{m}^{-1}$  to accomplish the same phase shift. A similar trend was observed in further results taken. There is an average  $1\text{V}\mu\text{m}^{-1}$  difference between the sweep up and sweep down voltages in acquiring the same phase shift. By applying  $9.25\text{V}\mu\text{m}^{-1}$  a  $2.5\pi$  phase shift was attained and further increment in the applied voltage did not make any further difference in the phase shift. These results show that a  $2.5\pi$  phase modulation is achieved by applying  $9.25\text{V}\mu\text{m}^{-1}$  which is far less compared to already published work at  $20\text{V}\mu\text{m}^{-1}$  for around  $10\mu\text{m}$  thick device. [70][110] Detailed results are summarised in the table 6.3.



Phase Shift ( $\pi$ )	Applied Field ( $V\mu\text{m}^{-1}$ )	
	Sweep up	Sweep down
0.5	2.60	3.45
1.0	4.45	5.65
1.5	6.00	7.00
2.0	7.20	7.95
2.5	9.25	9.25

**Table 6.4:** Change in phase shift with respect to the applied field per micrometer.

### Conclusion:

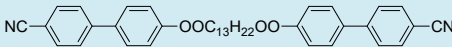
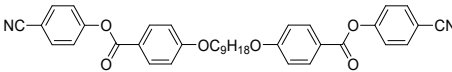
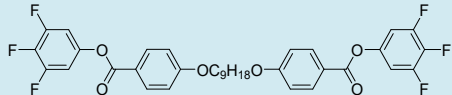
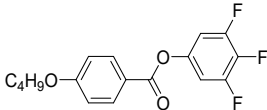
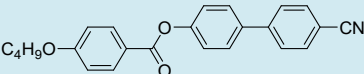
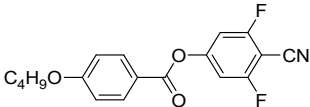
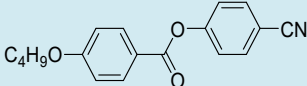
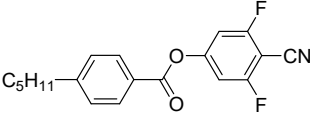
In this chapter an optimised formulation of wide temperature range blue phase mixture is presented. A new approach was adopted to devise a mixture by incorporating a flexo component in to the dielectric material to achieve the desired results. **Mix-2** gave a stable blue phase with an almost 3°C workable transition window compared to the earlier reported ones which have just a few degrees Kelvin. This mixture was easily polymer stabilised into an in-plane and a two pixel silicon device by using just a 10% wt. reactive mesogen mixture along with 0.1% wt. photoinitiator.

For the first time, switching of the BPI was observed clearly by applying an external field without any obvious changes in the polymer matrix at the low concentrations. To obtain diffraction patterns as a Kossel diagram, domain size was improved and Kossel pattern recorded. In order to observe the polymer network and orientation of the platelets, SEM micrographs were also recorded. Voltage transmission data is presented for three polarisation states along with the response times in an in-plane device.

Finally, the phase shift has been recorded by using a Young's slit interferometer in a two pixel blue phase liquid crystal on silicon (BPLCoS) device. A  $2.5\pi$  polariser free phase modulation at room temperature is achieved by just applying  $9.25V\mu\text{m}^{-1}$  which corresponds to the 185Vrms using twice thickness of silicon device (20 $\mu\text{m}$ ).

## **Chapter 7: Doping effects of novel mesogens**

This chapter highlights with the doping effects of synthesised mesogens when applied to **Mix-2** as it has been shown to be the most promising mixture. Synthetic routes of mesogenic dimers and monomers have already been discussed in chapter 4 and references are provided where necessary. Their structural as well as thermal characterisation data was also presented. The aim of this synthesis was to check their thermal and electro-optical effects when doped into the blue phase mixture **Mix-2**. Some of the compounds among dimers have shown the liquid crystalline transitions while all of the synthesised monomers have shown a single melting point. Their thermal transitions in pure state are summarised in table 7.1 below.

Compound code	Chemical structure	Thermal transition (°C)
3		K 130 N 160 I and I 160 N 110 K
17		K 165.5 N 181.5 I and I 182.5 N 154.5 K
18		85
27		71
28		K 124 N 285 I and I 283 N 121 K
29		76.8
30		115
31		28.5

**Table 7.1:** Thermal transition temperatures of newly synthesised dimers and monomers.

## 7.1 Doping of Mix-2 with synthesised compounds:

The **Mix-2** full characterisation by electro-optic study in the ULH state was presented in earlier chapters. **Mix-2** has been shown to furnish a stable, wide temperature range ( $\sim 3^{\circ}\text{C}$ ) blue phase. Polymer stabilisation of this blue phase has been done in an in-plane device and in an LCoS device to study the electro-optic effects. This robust polymer stabilised blue phase proved to be switchable at a very low applied voltage and provided a  $2.5\pi$  phase modulation.

A further study of **Mix-2** was carried out by doping this mixture with 10% of the synthesised monomers and dimers after their initial thermal characterisation. Mixture codes correspond to the numbers mentioned in the synthesis chapter (chapter 4) and in table 7.1. The doped mixture is coded by the parent mixture (which is Mix-2) and the code number of the synthesised compound. In total, 8 more mixtures have been formulated by doping into **Mix-2**.

Their transition temperatures were recorded and materials that had higher transition temperatures have raised the isotropic transition temperature of the new mixture. If a mixture exhibited blue phase while monitoring their thermal transitions, then their blue phase transition temperatures have been recorded as well. Compounds **18** and **30** were not liquid crystalline and showed a single melting point in their pure state. When doped into **Mix-2**, these compounds induced a smectic phase followed by a broad nematic transition. Table 7.2 summarises all the corresponding transitions of the doped **Mix-2** for all of the synthesised compounds.

It is worth noting, that by doping **Mix-2** with these synthesised mesogens, three of the compounds showed blue phase transitions in the new mixture well below that of the **Mix-2** blue phase transition. This could help to ease device fabrication; however it still needs further studies.

Mixture code	Doped thermal transitions of Mix-2(°C)	Blue phase appearance(°C)
Mix-2	-25 N 119 I	116.9-114
(Mix-2)+3	K 5 N 135 I	Not observed
(Mix-2)+17	K 40 N 125 I	Not observed
(Mix-2)+18	Sm 40 N 108 I	Not observed
(Mix-2)+27	-25 N 100 I	98-94
(Mix-2)+28	K -17 N 135 I	Not observed
(Mix-2)+29	K -18 N 106 I	Not observed
(Mix-2)+30	K 5 Sm 25 N 112 I	108-106
(Mix-2)+31	K -20 N 105 I	99.8-95.4

**Table 7.2:** Transition temperatures and blue phase transitions of **Mix-2** on 10% doping with newly synthesised materials.

## 7.2 Electro-optic Properties:

A precision component analyser (6440A Wayne Kerr) was used to determine the capacitance as a function of voltage (0-10V) at different temperatures. The temperature of the cell was controlled by using a hot-stage controller with a precision of  $\pm 0.1^{\circ}\text{C}$ . Details of the process have already been mentioned in chapter 5.

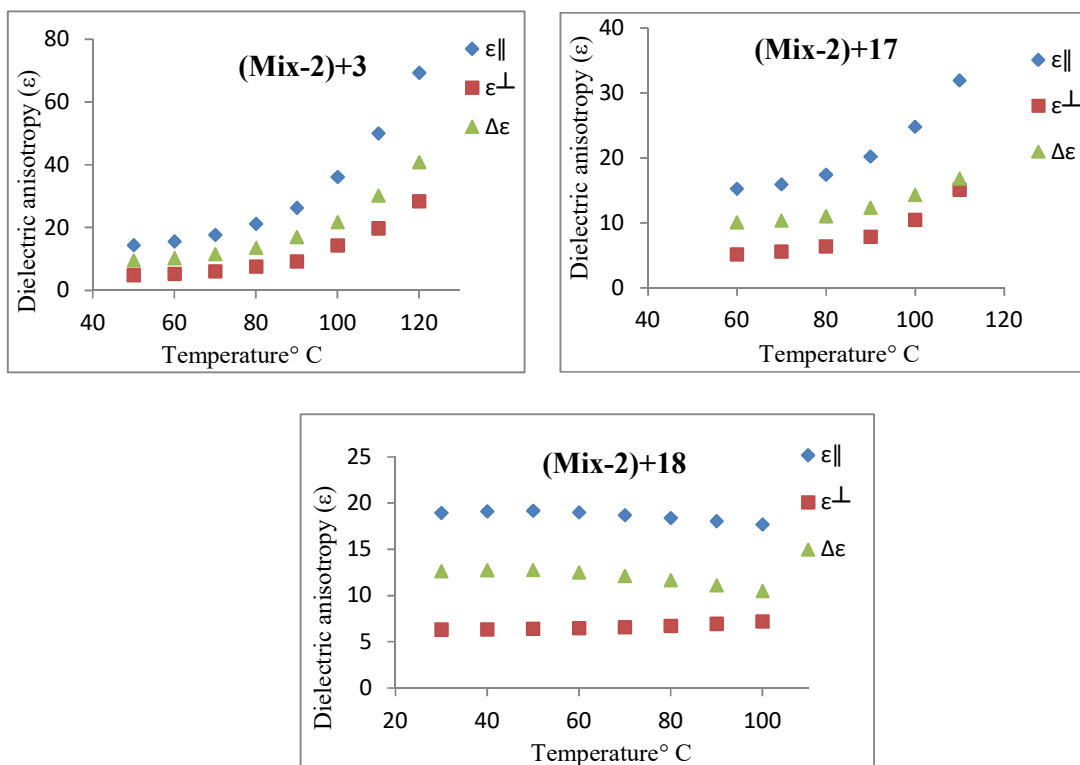
Formulated doped mixtures can be categorised into two classes based on the doped compound for a better insight into the nature and their effect on the electro-optic properties. The first class of mixtures corresponds to **Mix-2** doped with **dimers**. In this case **3**, **17** and **18** were the dimers doped into the **Mix-2**. The second set of mixtures deal with the **monomer** compounds **27-31**.

### 7.2.1 Mix-2 doped with dimers:

Compound **3** when doped into **Mix-2**, has induced similarly strange dielectric properties as shown in **Mix-6** and **Mix-7**. The ionic nature of compound **3** has already been ruled out by using a DC swap.

Compounds **17** and **18** have the same generic chemical structure except the difference in the terminal functional groups and it is worth mentioning that both compounds are symmetrical. **17** has a cyano group on both sides of the dimer while **18** contains three fluoro groups on each side. It is evident from the dielectric measurements that compound **17** has shown similar trends connected to the dielectric properties of **Mix-2** as compound **3**. This could be due to the presence of the polar cyano groups in these compounds.

Dimer **18** with three fluoro groups on each side, maintained the dielectric anisotropy between 12 and 10 from 30°C to 100°C. Figure 7.1 illustrates the detailed dielectric properties of **Mix-2** doped with mesogenic dimers.



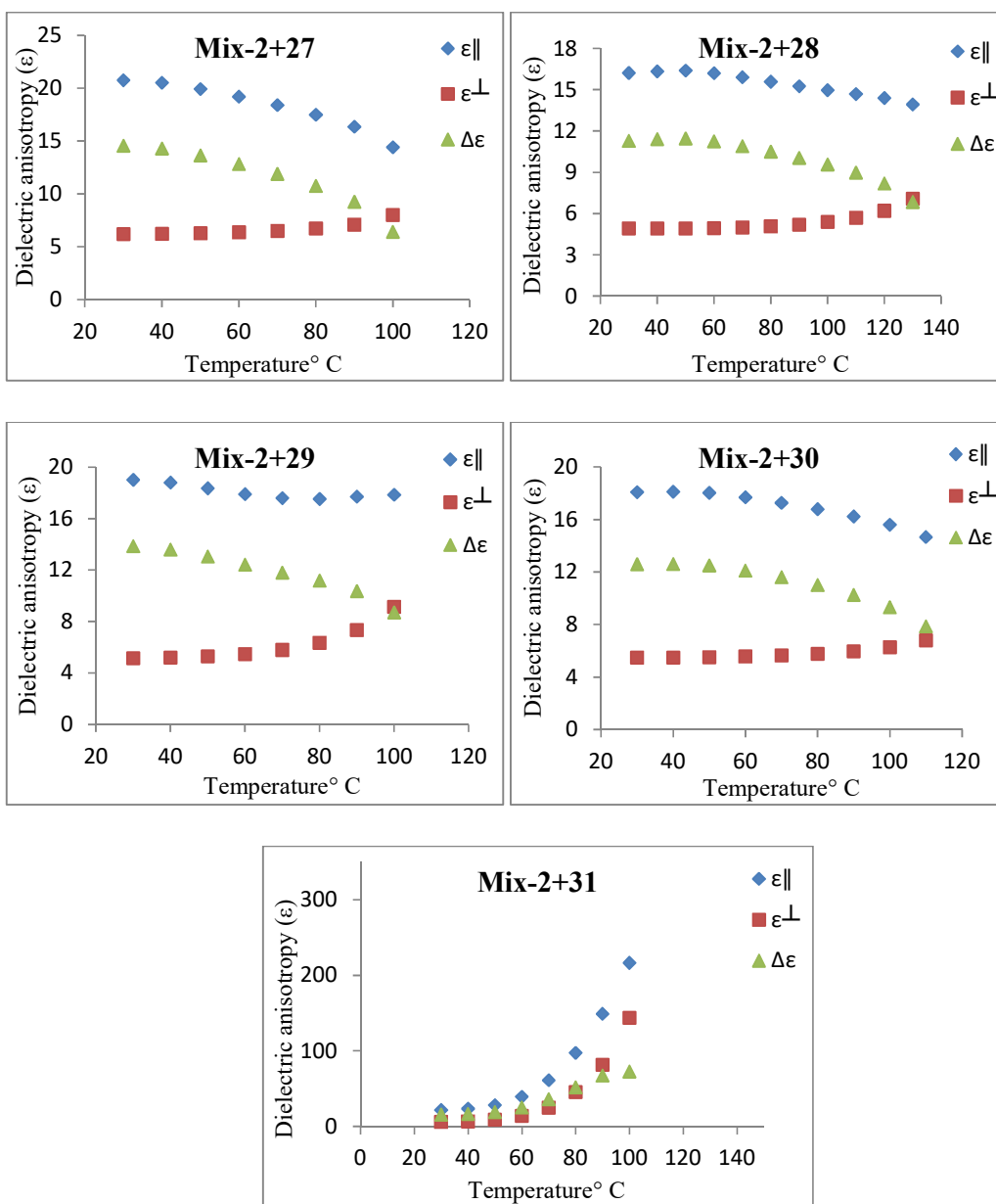
**Figure 7.1:** Dielectric measurements for **Mix-2** doped with synthesised mesogenic dimers.

It can be seen in figure 7.1 that at 60°C **Mix2+3**, **Mix-2+17** and **Mix-2+18** exhibit  $\Delta\epsilon$  values 10.3, 10.1 and 12.5 respectively. At 100°C the dielectric anisotropy was recorded at 21.8, 14.33 and 10.5 for **Mix2+3**, **Mix-2+17** and **Mix-2+18** respectively. The parallel permittivity and perpendicular permittivity increased for **Mix2+3** and **Mix-2+17** with respect to the increase in temperature and once again it is worth mentioning that compounds **3** and **17** have cyano substituents and hence furnished similar trends in their dielectric properties. However **Mix-2+18** exhibited a decrease in dielectric anisotropy ( $\Delta\epsilon$ ) from 12.6 to 10.5 with an increase in temperature

### 7.2.2 Mix-2 doped with monomers:

Monomers have unidirectional polarity and are responsive to the low threshold electric fields when compared to their equivalent mesogenic dimeric structure. To investigate the effect of these monomers on the dielectric properties of **Mix-2**, 10% wt. of each synthesised monomer was added into **Mix-2** to formulate five mixtures.

Monomers **27** to **30** showed the normal trend in their dielectric properties when doped into **Mix-2**. Further, there is no significant change in the parallel and perpendicular permittivity of these mixtures. However, **Mix-2+31** showed a significant increase in both parallel and perpendicular permittivity at 100°C. Overall dielectric anisotropy of this particular mixture has been measured from 30°C to 100°C and varies between 15 and 72. Again the ionic nature of this mixture has been ruled out by performing a DC swap. It is assumed that again this type of trend arises from the cyano group flanked by the two fluoro substituents in the chemical structure of monomer **31**. It does require further study to understand the nature of this monomer in **Mix-2**. The details of the dielectric measurements of **Mix-2** doped with monomers are given in the figure 7.2.



**Figure 7.2:** Dielectric measurements for Mix-2 doped with synthesised mesogenic monomers with respect to temperature.

It is evident from figure 7.2 that at 30°C **Mix-2+27**, **Mix-2+28**, **Mix-2+29** and **Mix-2+30** have dielectric anisotropy 14.57, 11.29, 13.86 and 12.6 respectively. Overall, dielectric anisotropy for each mixture has decreased on increasing temperature and is almost reduced to one half of the observed value at 30°C. However, **Mix-2+31** demonstrate a very interesting trend in its dielectric properties. There is almost a five times increase in its dielectric anisotropy and rises to 72.73 at 100°C when compared to 15.85 observed at 30°C. It could be the reason that parent mixture was doped with a high dielectric compound **31**. It seems that



substituent pattern of both dielectric dopant and base components (**Mix-2**) favour high polarisability and hence high dielectric permittivity. This peculiar result needs more detailed studies to fully understand the intrinsic properties of this particular mixture.

### 7.2.3 Flexoelectro-optic measurements:

Flexoelectro-optic measurements have been carried out using the same method adapted for the evaluation of **Mix-1** to **Mix-7**, using ULH configuration, as explained in chapter 5. All doped mixtures have been formulated keeping the amount of chiral dopant (7.5%wt) exactly same as it was in **Mix-2** to study the effect of the synthesised mesogenic compounds on **Mix-2**. All measurements have been done at the same frequency (1 kHz). The following are the outcomes for the flexoelectro-optic measurements for the doped mixtures.

#### **Mix-2+3:**

There were no difficulties in obtaining the ULH configuration for this mixture. However no change in the tilt angle was observed beyond 50°C and it was not possible to get a flexo response. Furthermore, compound **3** elevated the isotropic temperature to 135°C and the observed flexoelastic ratio increased two folds compared to the parent **Mix-2**. At higher temperature dielectric coupling dominated due to the reasonably high host BL006 but the best ULH was attained at 110°C.

#### **Mix-2+17:**

Compound **17** is a mesogenic dimer, when **Mix-2** was doped with this compound; the isotropic transition temperature elevated to 125°C. The very best flexo response in the ULH configuration was observed between 110°C and 60°C. The other main advantage of this mixture was to obtain a hassle free ULH mode within seconds after applying a moderate electric field. A slight improvement in the flexoelastic ratio was observed compared to **Mix-2**. However, there was no significant change as it was expected by the addition of a mesogenic dimer.

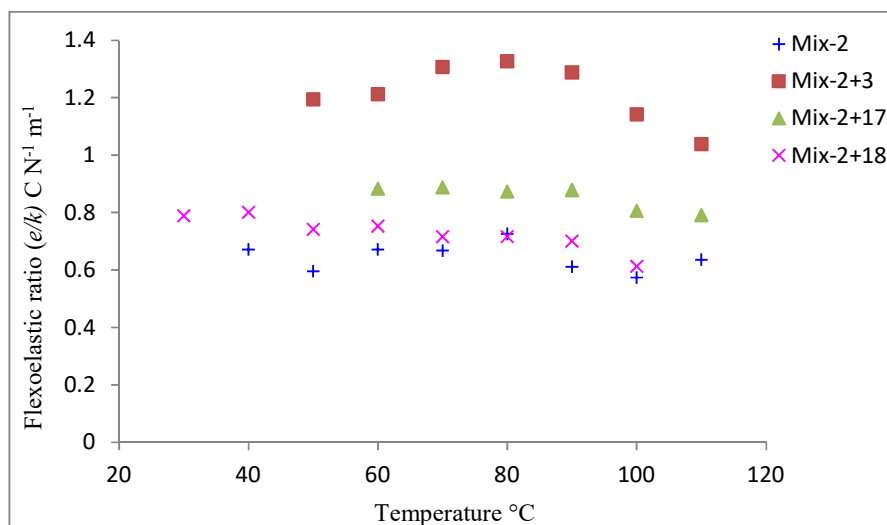
#### **Mix-2+18:**

Upon doping **Mix-2** with mesogenic dimer **18**, the mixture had no promising effect on the overall LC transition. However this mixture gave two texture transitions, a smectic liquid crystalline texture below 40°C and above this temperature it existed as a nematic liquid crystal. Due to this flexelastic ratios were measured between 40°C and 100°C and were

calculated from 0.77 to 0.62  $C N^{-1} m^{-1}$ . Again similar flexo trends were observed as per **Mix-2**.

Another observation made during this research project was that wherever a cyano group is present in the mesogenic material it always elevated transition temperature. While the presence of a fluoro group in the chemical structure facilitated lowering of the transition temperature which matches up existing literature studies. [74]

Figure 7.3 shows the flexoelastic ratio of Mix-2 on doping with mesogenic dimers with respect to temperature.



**Figure 7.3:** Flexoelastic ratio of Mix-2 doped with synthesised mesogenic dimers with respect to temperature.

**Mix-2+27:**

A flexo response can only be measured in the ULH configuration if the material exhibits a uniform arrangement of the ULH mode. It was possible to achieve such organisation of helices at 90°C for this particular mixture. Beyond this temperature, unwinding of the helices made it difficult to obtain a flexo response that follows the applied voltage. So overall there was a slight elevation in the flexoelastic ratio which stayed between 0.79 and 1.02  $C N^{-1} m^{-1}$  from 30°C to 90°C.

**Mix-2+28:**

This mixture showed isotropic point at 135°C and exhibited the uniform ULH at 120°C. Again there was no potential change in flexoelastic ratio compared to **Mix-2** and stayed between 0.48 and 0.68  $C N^{-1} m^{-1}$ . At high temperature and upon applying around

$5\text{V}\mu\text{m}^{-1}$ , unwinding of the helices was observed due to the dominance of dielectric coupling. However at  $30^\circ\text{C}$  the mixture was stable up to  $10\text{V}\mu\text{m}^{-1}$  and on further increase in voltage there was no change in the tilt angle.

#### **Mix-2+29:**

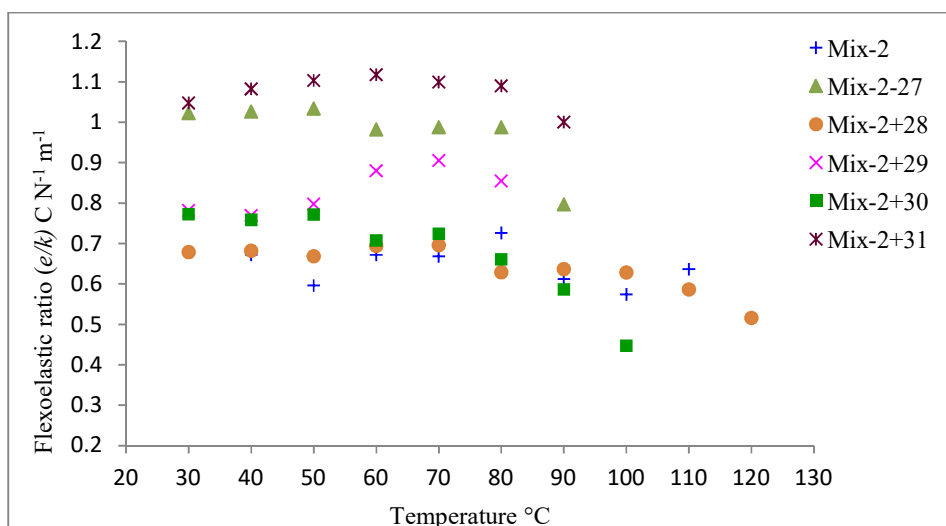
**Mix-2** doped with **29** revealed that the isotropic point of the mixture decreased to  $106^\circ\text{C}$  as compared to its parent mixture. It took a long time and effort to attain a reasonably uniform ULH configuration for this mixture and it was only possible at  $80^\circ\text{C}$ . The mixture showed unwinding of the helices and hence disorientation of the ULH configuration as well as affecting the flexo response at a higher fields. This mixture exhibited a moderate flexoelastic ratio between  $0.77$  and  $0.85\text{C N}^{-1}\text{m}^{-1}$  but achieving the uniform ULH mode was a truly difficult and painstaking task.

#### **Mix-2+30:**

Two phase transitions have been observed for this mixture while doing cover slip measurements for thermal transitions. This mixture exhibited a smectic transition below  $25^\circ\text{C}$  and stayed nematic below  $112^\circ$ , the isotropic point of this particular composition. However, it was not possible to get a steady ULH form further than  $100^\circ\text{C}$  due to the dominance of dielectric coupling. Its flexoelastic ratio was observed between  $0.44$  and  $0.77\text{C N}^{-1}\text{m}^{-1}$  and hence showed no potential change compared to the parent mixture.

#### **Mix-2+31:**

The flexoelastic ratio was measured between  $30^\circ\text{C}$  and  $90^\circ\text{C}$  as a consequence of the stability of ULH configuration of **Mix-2+31**. The observed isotropic point of this mixture was  $105^\circ\text{C}$  and was lower than **Mix-2** at  $119^\circ\text{C}$ . This particular mixture gave a peculiar dielectric response and has been discussed in the earlier section. It has not only shown an elevated dielectric response but has revealed enhanced flexo response. It was measured between to be  $1$  and  $1.11\text{C N}^{-1}\text{m}^{-1}$  which is almost twice that in comparison to its parent mixture (**Mix-2**). Detailed flexo responses have been summarised for **Mix-2** doped with monomers in the graph given in figure 7.4.



**Figure 7.4:** Flexo measurements for **Mix-2** doped with synthesised mesogenic monomers with respect to temperature.

#### 7.2.4 Response time of doped Mix-2:

It is well understood that the response time depends on the several factors as explained in the chapter 2 and 5. Rise and decay times for **Mix-2** doped with synthesised mesogenic compounds have been determined from an intensity change between 10% and 90%. Findings of the response time for each doped mixture are summarised below.

##### **Mix-2+3:**

The appearance of this mixture at room temperature was semi solid or gluey and hence was very viscous. At lower temperatures (50°C) the mixture exhibited faster response in its rise time (between 245 and 260µs) and decay time (between 132 and 185µs). However, at elevated temperature (110°C) the response was much slower and almost two folds compared to the observed ones at 50°C. Rise times have shown near linear trend with increments in applied electric field. However, the decay time has a linear response between 50°C and 60°C with respect to the field and above these temperatures there was a consistent drop in decay time. The chemical structure of compound **3** has two terminal cyano substituents one on either side and possesses a cyano-cyano dipole interaction due to the high polarisability of the cyano group. The details of the observed rise and decay time are presented as a graph in appendix 9.2.

**Mix-2+17:**

This mixture composition exhibited a much faster response in its rise and decay times between 30°C and 100°C at around 35-100µs. It also showed a linear response with only 20 µs difference between the readings, which was negligible. However, at higher temperature (110°C) there was an elevation in both rise and decay time to between 400-450 µs. Similar observations have been made with respect to the increment in the applied electric field. Furthermore, mesogenic dimer **17** has a cyano group at each terminal end quite similar to compound **3** and hence has dipole interactions among the cyano groups. These polar interactions may lead to the slower response in the applied field.

**Mix-2+18:**

**Mix-2** upon doping with compound **18** also showed a faster response in its rise and decay times at higher temperatures of around 119 and 154µs respectively. However at 30°C and 40°C this mixture showed a relatively slower response of around 200 and 220µs respectively. From 50°C to 100°C there is again barely 20µs difference between the readings. With the periodic increment in applied electric field, this mixture showed a linear trend in both rise and decay time. Compound **18** is chemically a sister compound of **17** and the only difference is in the substituent groups and has three terminal fluoro groups on either side instead of cyano ones. In this case though, the fluoro groups enhance the dielectric properties but it is less polarisable due to its smaller size compared to the bulky cyano groups. This might be the reason that this mixture possessed a faster response at higher temperatures.

**Mix-2+27:**

This mixture exhibits a faster rise and decay time from 90°C to 40°C and stayed at 134 to 158µs respectively. However, at 30°C response became slightly slower and was observed at around 200µs. The observed response time was independent of the applied field and kept on the same linear trend. Structurally compound **27** is a monomer and has increased the dielectric anisotropy which has stayed at 15 compared to **Mix-2** at 12. Again this compound contains three fluoro substituents on the terminal benzene ring and might be the reason for such a response due to the low polarisability of fluoro groups.

**Mix-2+28:**

Compound **28** has higher LC transition in its pure form (given in table 7.1) and elevated the isotropic point of the doped **Mix-2**. Between 120°C and 40°C, rise time was observed at 110 to 170µs with hardly 20µs difference among readings. However, at 30°C rise time was a bit high and was observed as 200µs. Overall a similar trend was observed in the decay time of this mixture. The observed response time of this particular mixture was independent of the applied voltage and remained unchanged with the increase in voltage. Compound **28** has a single cyano group at the biphenyl ring which may lead to a dipole interaction among the mixture molecules.

**Mix-2+29:**

This mixture showed similar response in its rise time and decay time as that exhibited by **Mix-2+28**. Both rise and decay times at low temperature were observed around at 190µs and at high temperatures from 80°C to 50°C, rise times were observed between 130µs and 170µs. However, at the same temperatures decay times were slightly faster and recorded between 130µs and 158µs. Again with increase in the applied voltage responses have shown almost a linear trend and were independent of applied field. Compound **29** has a cyano substituent on the terminal phenyl and is flanked by two fluoro groups. Fluoro group has a maximum electro negativity and low polarisability whereas; the bulky cyano group enhances the dipole interactions with other molecules.

**Mix-2+30:**

This mixture has been discussed in earlier sections of this chapter for its flexo and dielectric properties. It has shown response times quite similar to those mixtures doped with monomer containing terminal cyano functionality. Rise and decay times from 100°C to 40°C were observed between 115µs and 143µs. At 30°C rise time and decay times were observed at 174µs and 178µs respectively. A slight decrease (around 25µs) in rise time was only observed at 30°C with increase in applied voltage.

**Mix-2+31:**

**Mix-2+31** exhibited an extraordinary response in its dielectric properties and showed moderate flexoelectric response under the influence of applied voltage. Between 30°C and 50°C this mixture showed a faster response in its rise and decay time (150µs and 100µs

respectively) which is indicative of the dominating flexo coupling to facilitate a faster response. However, up to 90°C the observed response was much slower and increased two folds when compared to the observed response time at lower temperatures. Owing to the dominating dielectric coupling at elevated temperatures, this mixture takes longer to switch and relax back. With the increase in applied voltage, an almost linear trend was observed in rise time whereas the decay time showed a significant decrease at 90°C and 80°C. Compound **31** has a similar chemical structure to compound **29** except a C4 alkoxy group has been replaced by a C5 alkyl chain. There is no overall extended conjugation in monomer **31** due to this C5 alkyl chain and hence polarity has localised which could be the reason for the enhanced dielectric properties.

### 7.3 Blue phase appearance in the doped Mix-2:

So far three mixtures showed appearance of the blue phase; **Mix-2+27**, **Mix-2+30** and **Mix-2+ 31** conveniently at a faster cooling rate in addition to **Mix-2**. The transition temperatures for the appearance of blue phase were presented in the table 7.2. Further studies are required to explore the blue phase stabilisation for these mixtures. All of the doped mixtures can show a potential blue phase transition whilst controlling the temperature conditions, in particular the cooling rate from the isotropic point.

### Conclusions:

The doping effects in **Mix-2** with assorted monomers and dimers have been presented in this chapter.

Two dimers have ether ester hybrid system while one has a C11 carbon chain with ester linkage. All of the monomers have an ester linkage with different substitution patterns. These structural parameters have been utilised to characterise the formulated mixtures. Formulation of mixtures has been done on the same grounds as the original **Mix-2** to allow the comparison of physical and electro-optic properties. When **Mix-2** was doped with dimers, only **Mix-2+3** showed significant change in their dielectric properties. Whereas when **Mix-2** was doped with monomers, an extraordinary change in the dielectric properties was observed in **Mix-2+31** compared to the **Mix-2**. The rest of the mixtures had a similar trend in their dielectric anisotropy as per **Mix-2**. Flexo-elastic ratio was doubled for the **Mix-2+3** and was the maximum of all of the mixtures formulated by the doping of **Mix-2**. However, below 40°C the mixture does not follow the applied field and hence there had no observed flexo

response beyond this temperature. The second major change in the flexoelastic ratio was observed in the **Mix2+31** and was extended below 40°C.

A blue phase transition was observed in three of the eight formulated mixtures with the doping in **Mix-2**. **Mix2+27** and **Mix-2+31** have shown blue phase transitions below 100°C. Potential device fabrication using these mixtures may be easier and simplistic due to the existence of this blue phase transition below 100°C. However the third mixture, **Mix-2+30** exhibited blue phase transition above 100°C. All other mixtures may also show smaller blue phase transitions though this requires further studies.

According to the results in this chapter, it can be concluded that of all of the doped mixtures **Mix-2+31** showed the best potential properties beneficial for a switchable blue phase with a faster response time at a lower applied field.



## **Chapter 8: Conclusions and future plans**

## 8.1 Outcome of this dissertation:

This research work encompasses the formulation of blue phase materials which have ease of fabrication, low impact in voltage threshold and fast switching times. The implication of this highly ordered blue phase material is in the next generation of phase modulation devices and SLMs.

Initially, a mixture formulation was carried out using a mesogenic dimer and single component liquid crystal host 5CB to keep the composition simple. However, immiscibility of the mesogenic dimers in this host turned out to be a big issue and hence 5CB was disregarded. Another readily available commercial nematic host, E7, was tried but the outcome was similar to 5CB. Eventually, BL006 was selected, which is a well characterised commercial nematic liquid crystal (Merck) and found to be a good host to formulate homogeneous mixtures of the desired composition.

Mixtures were formulated using FFE9ECB and CBE11ECB as dopants in BL006 in the range of 10 to 80% wt. In the case of CBE11ECB as a dopant, only 10 and 20%wt mixtures were prepared because higher concentrations of this dopant led to crystallisation of the mixture at room temperature. Once homogenised mixtures were obtained, they were characterised with respect to their thermal transitions along with electro-optic performance including their dielectric and flexoelectric properties. The outcome of these results was an optimised mixture composition with wide temperature range, ample dielectric and moderate flexoelectric properties which was then selected to obtain a stable blue phase. **Mix-2** (20% FFE9ECB in BL006) emerged as the most suitable composition to study its blue phase transition combined with the possibility of a broad workable phase transition. Interestingly, the blue phase from this mixture was found to be very robust and resilient over a wide range temperature, even a sudden change in temperature showed no overall effect on its blue phase transition. Further, a growth of blue phase platelets more than 300  $\mu\text{m}$  in a 1x1 cm device was achieved under an hour which is quite unique on its own. Ordinarily, a blue phase appears soon after the isotropic point of its chiral mixture and usually is short lived for a few degrees Kelvin which often makes it difficult to characterise. In previous research work, [18] it was shown that the polymer templating method was convenient at obtaining blue phase from purely dielectric liquid crystals. However, there were few limitations associated with this method as it was a very time consuming, involving a wash-in-out process and rendering to get

initial stabilisation. The polymer matrix not only locks the blue phase geometry but it also ramps up the threshold applied voltage.

Therefore, for a detailed study at room temperature of a blue phase, it is quite important to acquire a stable blue phase at least over a degree Celsius which can be polymer stabilised to understand its electro-optic properties at room temperature. **Mix-2** has shown an ample blue phase transition of  $\sim 3^\circ\text{C}$  which made it easy to polymer stabilise. For the next step, polymer stabilised, different reactive mesogens were tried to achieve a suitable uniformity with an ease in the stabilisation process. Although, the addition of reactive mesogens into **Mix-2** further lowered the stable blue phase transition, it retained the  $\sim 3^\circ\text{C}$  of its blue phase transition which made it easier to polymer stabilise.

As literature study suggests, the compatible reactive mesogen concentration leads to a stable blue phase by making a fragile polymer network within the blue phase matrix, however, the right concentration of these reactive mesogen are quite critical. Lower concentration leads to instability in the blue phase system and it would not be able to withstand the applied field. These fragile polymer networks with lower concentrations of reactive mesogen get distorted upon an applied voltage and the blue phase reverted to the chiral nematic texture. Higher concentration of reactive mesogen rendered the blue phase unresponsive to the applied field and hence gave very high threshold voltages. For a fast and low threshold voltage switchable polymer stabilised blue phase using **Mix-2**, mixtures were tailored with minimum amounts of different reactive mesogens with the composition of three components; monomer, cross-linker and photo-initiator. Among the four sets mixed and tested, two polymer mixtures were successfully detailed in chapter 6.

The blue phase was stabilised in an in-plane device using **Mix-2** which showed full switching at  $4.2\text{V}\mu\text{m}^{-1}$  and was found to be very stable up to  $\sim 7\text{V}\mu\text{m}^{-1}$ . The voltage transmission data using an in-plane device is also presented in chapter 6 with respect to three defined polarisation states. The electro-optic data from this blue phase indicates polarisation independent switching with a low threshold applied field. This may have a positive impact on the display industry in terms of simplicity in both fabrication process and cost reduction.

After the success in the desired blue phase stabilisation, the next step was to observe its performance as a phase modulator using a Young's slits experiment as a basic interferometer. The phase modulation of light by liquid crystals has been characterised in the

past and the resulting device converts electrical signals to optical signals, often known as SLMs. These devices and their technological uses have already been discussed in chapter 2. In this present work, Young's slits silicon devices were fabricated as proposed in the literature [110] along with the PSBP of **Mix-2** as the switchable LC matrix. The experimental results from this interferometer were quite promising, with a  $2.5\pi$  phase shift observed at  $9.25 \text{ V}\mu\text{m}^{-1}$  in accordance with the postulated performance of the device in literature.

To try and push the performance faster and stable blue phase, in particular for phase modulation, some materials were also synthesised. Their chemical structures were considered to exploit the flexoelectro-optical properties on singly and in a commercial dielectric liquid crystal host. These synthesised materials were characterised by  $^1\text{H}$ NMR and  $^{13}\text{C}$ NMR for the confirmation of their chemical formula, and physical properties (phase transitions) which were characterised by using optical techniques and thermal transitions by DSC thermal scan.

To observe any improvement in physical and electro-optical properties of **Mix-2**, it was doped with 10% wt of the synthesised mesogenic materials to formulate 8 new mixtures. Physical properties and phase transitions of each mixture were recorded using an optical microscope. Furthermore, their dielectric, flexoelectro-optic properties and response times were observed as a function of temperature and applied electric field. **Mix-2+31** has shown promising results which are a good potential candidate for future research.

## 8.2 Future plans:

This research has very promising observations and could lead to a successful display device fabrication. However, there are some additional points of interest for future work.

- An approach towards further reduction in threshold of the applied field; **Mix-2** has shown switching of the PSBP under a desirable applied field range which was lower than the reported ones in literature. The formulated blue phase form of **Mix-2** has a switching threshold of  $\sim 1 \text{ V}\mu\text{m}^{-1}$ . However, after a successful polymer stabilisation with available reactive mesogens, the threshold voltage ramped up to  $\sim 7$  folds. It would be advantageous to investigate new reactive mesogens suitable for **Mix-2** to achieve a further decrease in the threshold applied field.

We have been informed by Merck that they have developed a new generation of reactive mesogen materials with the possibility of decreasing the loading concentrations and subsequently lowering the threshold voltage.

This study of compatible reactive mesogens would allow us to fabricate a high speed, full phase modulating, and polarisation independent SLM and display devices with the lowest threshold applied field.

- Synthesised chemical structures; a set of mesogens have been reported in chapter 3 along with their structural characterisation. Initial studies have revealed that these compounds were compatible with **Mix-2** and significantly increased the flexo-electric, dielectric and response times. Further work would be helpful to study their effects on blue phases and phase modulation.
- Phase modulation in reflection and transmission modes; for a device to be suitable for SLMs and displays, a comparative study of phase modulation in both reflection and transmission modes would be beneficial. So far, a complete phase modulation of light has been carried out only in the reflection mode. A new set of devices and electro-optic setup is required to envisage phase modulation in transmission mode. In addition, newly synthesised compounds and their designed mixtures would be of great interest to study the properties in their 3D self assembly for both reflection and transmission mode.
- Cross-talk in LCoS devices for phase modulation and an approach towards multi-pixel devices; Fabricated devices in this work have a cross-talk of electric field between the pixels and to the substrate. To overcome this, a new set of devices could be constructed using another non-conductive substrate, silicon carbide instead of silicon oxide. This would help in reducing noise or the cross-talk between the pixels to enhance the efficiency and stability of the device. The other possibility to reduce the cross-talk is to sandwich a thin layer of a non conductive coating between the substrate and the pixels *e.g* a single layer deposition of hydrogen boron nitride (h-BN) or transition metal dichalcogenides (TMDs). After successful investigation / study of above mentioned suggestions, it would be ideal to move on to a multi pixel device to explore this robust versatile 3D phase of liquid crystals.
- A comprehensive study of 3D- self assembly of mesogens by Kossel diffraction patterns; **Mix-2** has shown a resilient robust blue phase platelets of more

than 300  $\mu\text{m}$  in a 1x1 cm device under an hour which is quite unique. To investigate this in depth; the 3D- self assembly and packing interaction of this mixture of high dielectric with moderate flexo-electric properties requires comprehensive Kossel diffraction studies with respect to their thermal scan, applied fields and interactions with different wavelengths in particular RGB. The outcome of this study would be key to devising the next generation of 3D photonic devices. This is multidisciplinary study requires collaboration between engineers, chemists, physicists and mathematicians.

- Future devices: Another aspect of future plans would be to investigate interactions between the blue phase 3D lattice and 2D materials having an intrinsic domain structure like graphene, h-BN, and MoS etc. It would be ideal to observe the growth of blue phase – 3D photonic structures over a 2D surface. This study would envisage the replacement of traditional electrodes along with new understanding of the 3D photonic structures' surface anchoring, conductivity and alignment for next generation polarisation independent 3D photonics and their applications.

Due to time constraint the above mentioned points were rather difficult to visit. However, these could be a milestone for research scholars in this field or a possible research scope for my future work.

## **Bibliography:**

- [1] H. Kelker and E. Von -Schivizhoffen, "Use of liquid crystals in gas chromatography.," *Adv. Chromatogr. (New York, NY, United States)*, vol. 6, pp. 247–297, 1968.
- [2] A. Carrington and G. R. Luckhurst, "Electron paramagnetic resonance.," *Annu. Rev. Phys. Chem.*, vol. 19, pp. 31–58, 1968.
- [3] J. G. and T. G. Anderson, "Patent," 3,733,485, 1973.
- [4] P. H. Keyes, H. T. Weston, and W. B. Daniels, "Tricritical behavior in a liquid-crystal system.," *Phys. Rev. Lett.*, vol. 31, no. 10, pp. 628–630, 1973.
- [5] R. Parker, "Solid State RMS Recording Ammeter," *Power Apparatus and Systems, IEEE Transactions on*, vol. PAS-92, no. 1. pp. 104–107, 1973.
- [6] H. W. E. L. Adams J. E. Leder. L. B, "Patent," 3679290, 1972.
- [7] Stockman E.H, "Advances in Liquid Crystals," *Electronics*, vol. 42, p. 110, 1969.
- [8] O. S. Selawry, H. S. Selawry, and J. F. Holland, "The use of liquid cholesteric crystals for thermographic measurement of skin temperature in man.," *Mol. Cryst.*, vol. 1, no. 4, pp. 495–501, 1966.
- [9] E. M. Langman, W. Healy, and P. K. Dutt, "The influence of substituents on the stability of Schiff's bases. I. Hydrolysis of nitro-and methoxybenzylideneanilines.," *Q. J. Indian Chem. Soc.*, vol. 4, pp. 75–79, 1927.
- [10] L. A. Goodman, "Liquid crystal displays.," *J. Vac. Sci. Technol.*, vol. 10, no. 5, pp. 804–823, 1973.
- [11] "Electronic display market," *Business Communications Co. (BCC) Inc. in Norwalk, Conn.* [Online]. Available: <http://www.militaryaerospace.com/articles/print/volume-17/issue-6/departments/finish-line/electronic-display-market-will-reach-141-billion-by-2010.html>.
- [12] H. L. Ong, "Frame sequential color thin film transistor/liquid crystal displays: display characteristics and grayscale consideration.," *Japanese J. Appl. Physics, Part 1 Regul. Pap. Short Notes Rev. Pap.*, vol. 32, no. 9A, pp. 3879–3885, 1993.
- [13] J. S. Patel and R. B. Meyer, "Flexoelectric electrooptics of a cholesteric liquid crystal.," *Phys. Rev. Lett.*, vol. 58, no. 15, pp. 1538–1540, 1987.
- [14] B. Musgrave, P. Lehmann, and H. J. Coles, "A new series of chiral nematic bimesogens for the flexoelectrooptic effect.," *Liq. Cryst.*, vol. 26, no. 8, pp. 1235–1249, 1999.
- [15] C. Noot, M. J. Coles, B. Musgrave, S. P. Perkins, and H. J. Coles, "The flexoelectric behavior of a hypertwisted chiral nematic liquid crystal.," *Mol. Cryst. Liq. Cryst. Sci. Technol. Sect. A Mol. Cryst. Liq. Cryst.*, vol. 366, pp. 725–733, 2001.
- [16] H. J. Coles, B. Musgrave, M. J. Coles, and J. Willmott, "The effect of the molecular structure on flexoelectric coupling in the chiral nematic phase.," *J. Mater. Chem.*, vol. 11, no. 11, pp. 2709–2716, 2001.
- [17] H. Kikuchi, M. Yokota, Y. Hisakado, H. Yang, and T. Kajiyama, "Polymer-stabilized liquid crystal blue phases," *Nat. Mater.*, vol. 1, p. 64, Sep. 2002.
- [18] F. Castles *et al.*, "Blue-phase templated fabrication of three-dimensional nanostructures for photonic applications," *Nat Mater*, vol. 11, no. 7, pp. 599–603, Jul. 2012.
- [19] Hyman RM, "Polarization-independent phase modulation using a blue-phase liquid crystal over silicon device," University of Cambridge.
- [20] G. W. Gray, *Molecular structure and the properties of liquid crystals*. Academic Press, 1962.
- [21] G. Friedel, "The Mesomorphic States of Matter," *Ann. Phys. (Paris)*., vol. 18, pp. 162–174, 1922.

- [22] F. Reinitzer, "Beiträge zur Kenntniss des Cholesterins," *Monatshefte für Chemie und verwandte Teile anderer Wissenschaften*, vol. 9, no. 1, pp. 421–441, 1888.
- [23] O. Lehmann, "Extension of the existence range of liquid crystals by intermixtures. [machine translation].," *Ann. der Phys. (Weinheim, Ger.)*, vol. 21, no. 4, pp. 181–192, 1906.
- [24] "Liquid Crystal Group Hamburg." [Online]. Available: <http://liqcryst.chemie.uni-hamburg.de/>.
- [25] J. W. Goodby, "Mesogenic molecular crystalline materials.," *Curr. Opin. Solid State Mater. Sci.*, vol. 4, no. 4, pp. 361–368, 1999.
- [26] C. E. Fairhurst *et al.*, "Lyotropic Surfactant Liquid Crystals," in *Handbook of Liquid Crystals*, Wiley-VCH Verlag GmbH, 1998, pp. 341–392.
- [27] S. Friberg, L. Rydhag, and T. Doi, "Micellar and lyotropic liquid crystalline phases containing nonionic active substances.," *Adv. Chem. Ser.*, vol. 152, no. Lyotropic Liq. Cryst. Struct. Biomembr., Symp., 1974, pp. 28–42, 1976.
- [28] M. M. Qasim, "Synthesis and characterization of Troger's base liquid crystals," Macquarie University Sydney, 2008.
- [29] J. J. Brown, G. H. Wolken, *Liquid Crystals and Biological Structures*. Academic Press: New York, 1979.
- [30] S. Chandrasekhar, B. K. Sadashiva, and K. A. Suresh, "Liquid crystals of disc-like molecules.," *Pramana*, vol. 9, no. 5, pp. 471–480, 1977.
- [31] T. Seideman, "The liquid-crystalline blue phases.," *Reports Prog. Phys.*, vol. 53, no. 6, pp. 659–705, 1990.
- [32] Y. D.-K. and W. S-T, *Fundamentals of Liquid Crystal Devices*. John Wiley & Sons, Ltd, 2014.
- [33] H. Stegemeyer, T. Bluemel, K. Hiltrop, H. Onusseit, and F. Porsch, "Liquid crystalline blue phases: stability, structure, and electric-field effects.," *Wissenschaftliche Beitraege - Martin-Luther-Universitaet Halle-wittenb.*, no. 52, Zehn Arb. Fluss. Krist., pp. 64–95, 1986.
- [34] H. Kikuchi, "Liquid Crystalline Blue Phases," in *Liquid Crystalline Functional Assemblies and Their Supramolecular Structures SE - 75*, vol. 128, T. Kato, Ed. Springer Berlin Heidelberg, 2008, pp. 99–117.
- [35] J. E. B. Takashi Kato, *Liquid crystalline functional assemblies and their supramolecular structures*. Berlin : Springer, c2008.
- [36] L. Rao, J. Yan, S.-T. Wu, S. Yamamoto, and Y. Haseba, "A large Kerr constant polymer-stabilized blue phase liquid crystal," *Appl. Phys. Lett.*, vol. 98, no. 8, p. 81109, Feb. 2011.
- [37] M. S. Kim *et al.*, "A controllable viewing angle LCD with an optically isotropic liquid crystal," *J. Phys. D. Appl. Phys.*, vol. 43, no. 14, p. 145502, 2010.
- [38] Y. Hisakado, H. Kikuchi, T. Nagamura, and T. Kajiyama, "Large Electro-optic Kerr Effect in Polymer-Stabilized Liquid-Crystalline Blue Phases," *Adv. Mater.*, vol. 17, no. 1, pp. 96–98, Jan. 2005.
- [39] L. Rao, H.-C. Cheng, and S.-T. Wu, "Low Voltage Blue-Phase LCDs With Double-Penetrating Fringe Fields," *J. Disp. Technol.*, vol. 6, no. 8, pp. 287–289, 2010.
- [40] K.-M. Chen, S. Gauza, H. Xianyu, and S.-T. Wu, "Submillisecond Gray-Level Response Time of a Polymer-Stabilized Blue-Phase Liquid Crystal," *J. Disp. Technol.*, vol. 6, no. 2, pp. 49–51, 2010.
- [41] R. Steinstraesser and L. Pohl, "Chemistry and use of liquid crystals.," *Angew. Chemie*, vol. 85, no. 16, pp. 706–720, 1973.
- [42] P. Raynes, "LIQUID CRYSTALS — Second Edition, by S CHANDRASEKHAR, Cambridge University Press, (1992), ISBN 0-521-41747-3 (HB), ISBN 0-521-42741-X



- (PB),” *Liq. Cryst. Today*, vol. 3, no. 3, p. 7, Nov. 1993.
- [43] Peter J. Collings and Micheal Hird, *Introduction to Liquid Crystals: Chemistry and Physics*. CRC Press, 1997.
- [44] B. E. A. Saleh and M. C. Teich, “Electro-Optics,” in *Fundamentals of Photonics*, John Wiley & Sons, Inc., 1991, pp. 696–736.
- [45] D. J. Gardiner *et al.*, “Polymer stabilized chiral nematic liquid crystals for fast switching and high contrast electro-optic devices,” *Appl. Phys. Lett.*, vol. 98, no. 26, pp. 3–5, 2011.
- [46] H. Coles and S. Morris, “Flexoelectro-Optic Liquid Crystal Displays,” in *Handbook of Visual Display Technology SE - 100*, J. Chen, W. Cranton, and M. Fihn, Eds. Springer Berlin Heidelberg, 2012, pp. 1681–1694.
- [47] V. Fréedericksz and A. Repiewa, “Theoretisches und Experimentelles zur Frage nach der Natur der anisotropen Flüssigkeiten,” *Zeitschrift für Phys.*, vol. 42, no. 7, pp. 532–546, 1927.
- [48] R. B. Meyer, “Ferroelectric Liquid Crystals; A Review,” *Mol. Cryst. Liq. Cryst.*, vol. 40, no. 33, 1977.
- [49] P. Rudquist, “PhD Thesis,” Chalmers Technical University, Gothenburg, 1997.
- [50] R. B. Meyer, “Piezoelectric effects in liquid crystals.,” *Phys. Rev. Lett.*, vol. 22, no. 18, pp. 918–921, 1969.
- [51] I. Dozov and I. Penchev, “Structure of a hybrid aligned cholesteric liquid crystal cell,” *J. Phys. Fr.*, vol. 47, no. 3, pp. 373–377, 1986.
- [52] P. Rudquist, L. Komitov, and S. T. Lagerwall, “Linear electro-optic effect in a cholesteric liquid crystal,” *Phys. Rev. E*, vol. 50, no. 6, pp. 4735–4743, Dec. 1994.
- [53] J. S. Patel and S. Lee, “Fast linear electro-optic effect based on cholesteric liquid crystals,” *J. Appl. Phys.*, vol. 66, no. 4, pp. 1879–1881, Aug. 1989.
- [54] F. Ahmad, M. Jamil, and Y. J. Jeon, “New developments in the dye-doped polymer dispersed liquid crystals gratings: A review,” *Int. J. Polym. Anal. Charact.*, vol. 22, no. 8, pp. 659–668, Nov. 2017.
- [55] Steve Elston and Roy Sambles, *The optics of thermotropic liquid crystals*. Taylor & Francis, 1998.
- [56] O. Kabanova, E. (Alena Melnikova, I. Rushnova, and A. Tolstik, *Electrically Controlled Waveguide Liquid Crystal Elements*, vol. 40. 2014.
- [57] P. Yeh and C. Gu, *Optics of Liquid Crystal Displays*. Wiley, 2010.
- [58] I. C. Khoo, *Liquid Crystals*. Wiley, 2007.
- [59] J.-P. Uzan and B. Leclercq, “Fundamental constants: pillars of the edifice BT - The Natural Laws of the Universe: Understanding Fundamental Constants,” J.-P. Uzan and B. Leclercq, Eds. New York, NY: Praxis, 2008, pp. 21–35.
- [60] N. Collings, T. Davey, J. Christmas, D. Chu, and B. Crossland, “The Applications and Technology of Phase-Only Liquid Crystal on Silicon Devices,” *J. Disp. Technol.*, vol. 7, no. 3, pp. 112–119, 2011.
- [61] T. D. Wilkinson, C. D. Henderson, D. G. Leyva, and W. A. Crossland, “Phase modulation with the next generation of liquid crystal over silicon technology,” *J. Mater. Chem.*, vol. 16, no. 33, pp. 3359–3365, 2006.
- [62] M. R. Douglass, “Lifetime estimates and unique failure mechanisms of the Digital Micromirror Device (DMD),” in *1998 IEEE International Reliability Physics Symposium Proceedings. 36th Annual (Cat. No.98CH36173)*, 1998, pp. 9–16.
- [63] G. Lazarev, A. Hermerschmidt, S. Kruger, and S. Osten, “LCOS spatial light modulators: Trends and Applications,” *Opt. Imaging Metrol. Adv. Technol.*, pp. 1–29, 2012.
- [64] D. Dan, B. Yao, and M. Lei, “Structured illumination microscopy,” in *Optical*

- Nanoscopy and Novel Microscopy Techniques*, CRC Press, 2014, pp. 23–60.
- [65] Y. Sun, “Super resolution imaging with stochastic optical reconstruction microscopy (STORM) and photoactivated localization microscopy (PALM),” in *Optical Nanoscopy and Novel Microscopy Techniques*, CRC Press, 2014, pp. 61–84.
- [66] A. Hermerschmidt, G. Slm, and H. Photonics, “Flexible SLM technology finds many applications Polarization Control,” pp. 29–31.
- [67] J. L. Horner and C. K. Makekau, “Two-focal-length optical correlator,” *Appl. Opt.*, vol. 28, no. 24, pp. 5199–5201, 1989.
- [68] K. B. A. and G. D. G. Curtis J E, “Dynamic holographic optical tweezers,” *Opt. Commun*, vol. 207, pp. 169–75, 2002.
- [69] W. A. M, “Femtosecond pulse shaping using spatial light modulators,” *Rev. Sci. Instrum*, vol. 71, p. 1929, 2000.
- [70] R. Garsed, “Phase Modulation of Light using Liquid Crystal on Silicon Devices,” University of Cambridge, 2015.
- [71] R. Miller *et al.*, “Lattice Parameter Measurements from the Kossel Diagrams of the Cubic Liquid Crystal Blue Phases,” *J. Phys. II*, vol. 6, pp. 909–922, 1996.
- [72] R. Cano, “Bull. Soc. Fr.,” *Miner. Cristal.*, vol. 91, no. 20, 1968.
- [73] G. Gambirasio, “Measurement of cell thickness in infrared spectrophotometry,” *Appl. Opt.*, no. 6, pp. 477–80, 1967.
- [74] K. L. Atkinson *et al.*, “Increasing the flexoelectric ratio of liquid crystals using highly fluorinated ester-linked bimesogens,” *Phys. Chem. Chem. Phys.*, vol. 14, no. 47, pp. 16377–16385, 2012.
- [75] S. M. Morris, M. J. Clarke, A. E. Blatch, and H. J. Coles, “Structure-flexoelectric properties of bimesogenic liquid crystals,” *Phys. Rev. E - Stat. Nonlinear, Soft Matter Phys.*, 2007.
- [76] A. C. Griffin, S. R. Vaidya, R. S. L. Hung, and S. Gorman, “Effect of molecular structure on mesomorphic behavior. 17. Cyano terminated twin liquid crystals,” *Mol. Cryst. Liq. Crystals, Lett. Sect.*, vol. 1, no. 5, pp. 131–138, 1985.
- [77] G. W. Gray, M. Hird, D. Lacey, and K. J. Toyne, “The synthesis and transition temperatures of some fluoro-substituted 4-cyanophenyl and 4-cyanobiphenyl-4'-yl 4-pentyl- and 4-butoxybenzoates.,” *Mol. Cryst. Liq. Cryst.*, vol. 172, pp. 165–189, 1989.
- [78] G. Della Gatta, M. J. Richardson, and S. M. Sarge, “Commission on thermodynamics standards, calibration , and guidelines in microcalorimetry. (IUPAC Technical Report).,” *Union, Int. Pure, O F Chem. Appl. Div. Biophys. Chem. Thermodyn. Comm. Comm.*, vol. 78, no. 7, pp. 1455–1476, 2006.
- [79] F. Castles, “Highly Flexoelectric Liquid Crystals,” University of Cambridge, 2010.
- [80] NEMATEL, “Polymer dispersed liquid crystals (PDLC).” [Online]. Available: <https://www.nematel.de/>.
- [81] A. Buka and N. Éber, *Flexoelectricity in liquid crystals: Theory, experiments and applications*. 2012.
- [82] G. Carbone *et al.*, “Uniform lying helix alignment on periodic surface relief structure generated via laser scanning lithography,” *Mol. Cryst. Liq. Cryst.*, vol. 544, no. June, pp. 37–49, 2011.
- [83] and C. D. Coles, H. J., Coles, M. J., Perkins, S., Musgrave, B., “Bimesogenic Compounds and Flexoelectric Devices,” EP99119114, 1999.
- [84] J. S. Patel and R. B. Meyer, “Flexoelectric electro-optics of a cholesteric liquid crystal,” *Phys. Rev. Lett.*, vol. 58, no. 15, pp. 1538–1540, Apr. 1987.
- [85] F. L. Mackenzie, “Linear and H-Shaped Chiral Dimers for Applications in Photonic Liquid Crystals MSc by Research,” no. December, 2010.
- [86] H. J. Coles and M. N. Pivnenko, “Liquid crystal ‘blue phases’ with a wide temperature

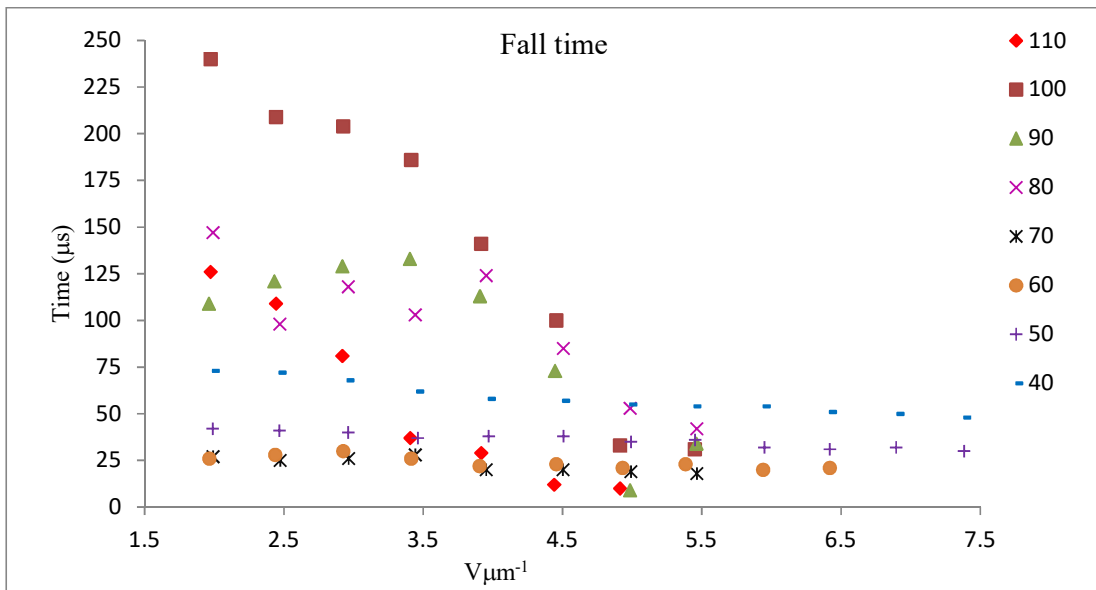
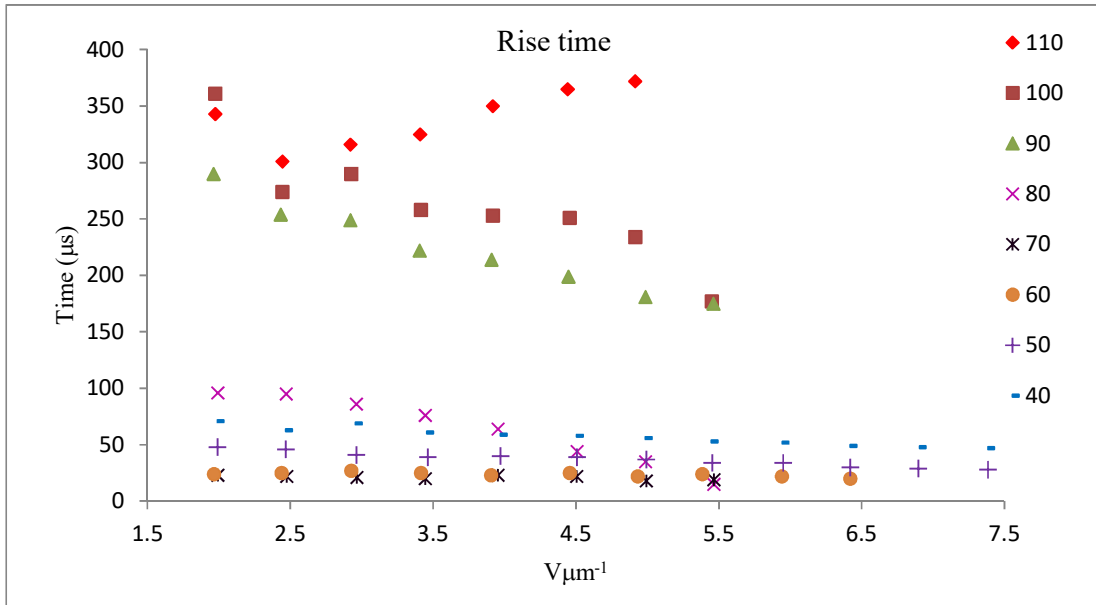
- range,” *Nature*, vol. 436, p. 997, Aug. 2005.
- [87] M. P. and J. H. H. Coles, “Blue phase,” US Patent US0115957, 2009.
- [88] K. L. Atkinson, S. M. Morris, F. Castles, M. M. Qasim, D. J. Gardiner, and H. J. Coles, “Flexoelectric and elastic coefficients of odd and even homologous bimesogens,” *Phys. Rev. E - Stat. Nonlinear, Soft Matter Phys.*, vol. 85, no. 1, pp. 1–4, 2012.
- [89] M. M. Sala-Tefelska *et al.*, “Influence of cylindrical geometry and alignment layers on the growth process and selective reflection of blue phase domains,” *Opt. Mater. (Amst.)*, vol. 75, no. November 2017, pp. 211–215, 2018.
- [90] Y. Chen and S.-T. Wu, “Recent advances on polymer-stabilized blue phase liquid crystal materials and devices,” *J. Appl. Polym. Sci.*, vol. 131, no. 13, p. n/a-n/a, Jul. 2014.
- [91] G. Nordendorf, A. Hoischen, J. Schmidtke, D. Wilkes, and H. S. Kitzerow, “Polymer-stabilized blue phases: Promising mesophases for a new generation of liquid crystal displays,” *Polym. Adv. Technol.*, vol. 25, no. 11, pp. 1195–1207, 2014.
- [92] W. Cao, A. Muñoz, P. Palffy-Muhoray, and B. Taheri, “Lasing in a three-dimensional photonic crystal of the liquid crystal blue phase II,” *Nat. Mater.*, vol. 1, p. 111, Sep. 2002.
- [93] Y.-H. Lin, H.-S. Chen, H.-C. Lin, Y.-S. Tsou, H.-K. Hsu, and W.-Y. Li, “Polarizer-free and fast response microlens arrays using polymer-stabilized blue phase liquid crystals,” *Appl. Phys. Lett.*, vol. 96, no. 11, p. 113505, 2010.
- [94] Y.-H. Chen, C.-T. Wang, C.-P. Yu, and T.-H. Lin, “Polarization independent Fabry-Pérot filter based on polymer-stabilized blue phase liquid crystals with fast response time,” *Opt. Express*, vol. 19, no. 25, p. 25441–25446, Dec. 2011.
- [95] Y.-H. Lin, H.-S. Chen, and T.-H. Chiang, “A reflective polarizer-free display using dye-doped polymer-stabilized blue-phase liquid crystals,” *J. Soc. Inf. Disp.*, vol. 20, no. 6, pp. 333–336, 2012.
- [96] G. Zhu *et al.*, “A fast response variable optical attenuator based on blue phase liquid crystal,” *Opt. Express*, vol. 21, no. 5, pp. 5332–7, 2013.
- [97] S.-J. Ge, W. Ji, G.-X. Cui, B.-Y. Wei, W. Hu, and Y.-Q. Lu, “Fast switchable optical vortex generator based on blue phase liquid crystal fork grating,” *Opt. Mater. Express*, vol. 4, no. 12, p. 2535, 2014.
- [98] Y. Yuan *et al.*, “Polymer-stabilized blue-phase liquid crystal grating cured with interfered visible light,” *Opt. Express*, vol. 23, no. 15, pp. 20007–20013, Jul. 2015.
- [99] L. R. a. Shin-TsonWu, “Emerging blue phase LCDs,” 2010.
- [100] T. Blümel and H. Stegemeyer, “Growth of three-dimensional liquid single crystals and morphological studies of cholesteric ‘blue phases,’” *J. Cryst. Growth*, vol. 66, no. 1, pp. 163–168, 1984.
- [101] M. Chen, Y.-H. Lin, H.-S. Chen, and H.-Y. Chen, “Electrically assisting crystal growth of blue phase liquid crystals,” *Opt. Mater. Express*, vol. 4, no. 5, pp. 953–959, 2014.
- [102] H.-S. Chen, Y.-H. Lin, C.-H. Wu, M. Chen, and H.-K. Hsu, “Hysteresis-free polymer-stabilized blue phase liquid crystals using thermal recycles,” *Opt. Mater. Express*, vol. 2, no. 8, pp. 1149–1155, 2012.
- [103] Y. Chen, F. Peng, T. Yamaguchi, X. Song, and S.-T. Wu, “High Performance Negative Dielectric Anisotropy Liquid Crystals for Display Applications,” *Crystals*, vol. 3, no. 3, 2013.
- [104] Y. Chen, J. Sun, H. Xianyu, S.-T. Wu, X. Liang, and H. Tang, “High Birefringence Fluoro-Terphenyls for Thin-Cell-Gap TFT-LCDs,” *J. Disp. Technol.*, vol. 7, no. 9, pp. 478–481, 2011.
- [105] M. Hird, “Fluorinated liquid crystals - properties and applications,” *Chem. Soc. Rev.*, vol. 36, no. 12, pp. 2070–2095, 2007.

- [106] G. W. Gray, M. Hird, and K. J. Toyne, "The Synthesis of Several Lateral Difluoro-substituted 4,4"-Dialkyl- and 4,4"-Alkoxyalkyl-Terphenyls and a Rationalisation of the Effect of Such Substitution on Mesophase Type and Transition Temperatures," *Mol. Cryst. Liq. Cryst.*, vol. 204, no. 1, pp. 43–64, Jul. 1991.
- [107] S.-T. Wu, C. S. Hsu, and J. M. Chen, "Room Temperature Difluoro-Tolane and Diphenyl-Diacetylene Liquid Crystals with Negative Dielectric Anisotropy," *Mol. Cryst. Liq. Cryst. Sci. Technol. Sect. A. Mol. Cryst. Liq. Cryst.*, vol. 304, no. 1, pp. 441–445, Sep. 1997.
- [108] G. T. and P. P. Cladis P. E., "No," *Phys. Rev. Lett.*, vol. 57, p. 2841, 1986.
- [109] X. Li *et al.*, "Mesoscale martensitic transformation in single crystals of topological defects," *Proc. Natl. Acad. Sci.*, vol. 114, no. 38, pp. 10011–10016, 2017.
- [110] E. Oton, E. Netter, T. Nakano, Y. D.-Katayama, and F. Inoue, "Monodomain Blue Phase Liquid Crystal Layers for Phase Modulation," *Sci. Rep.*, vol. 7, no. February, p. 44575, 2017.

# Addendum

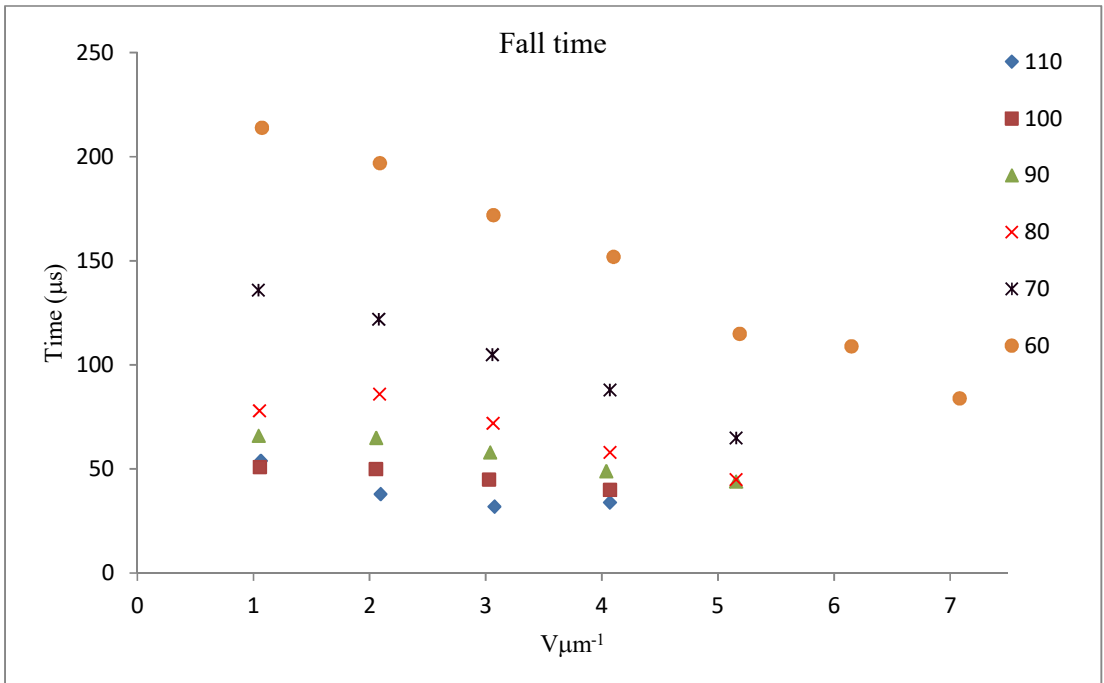
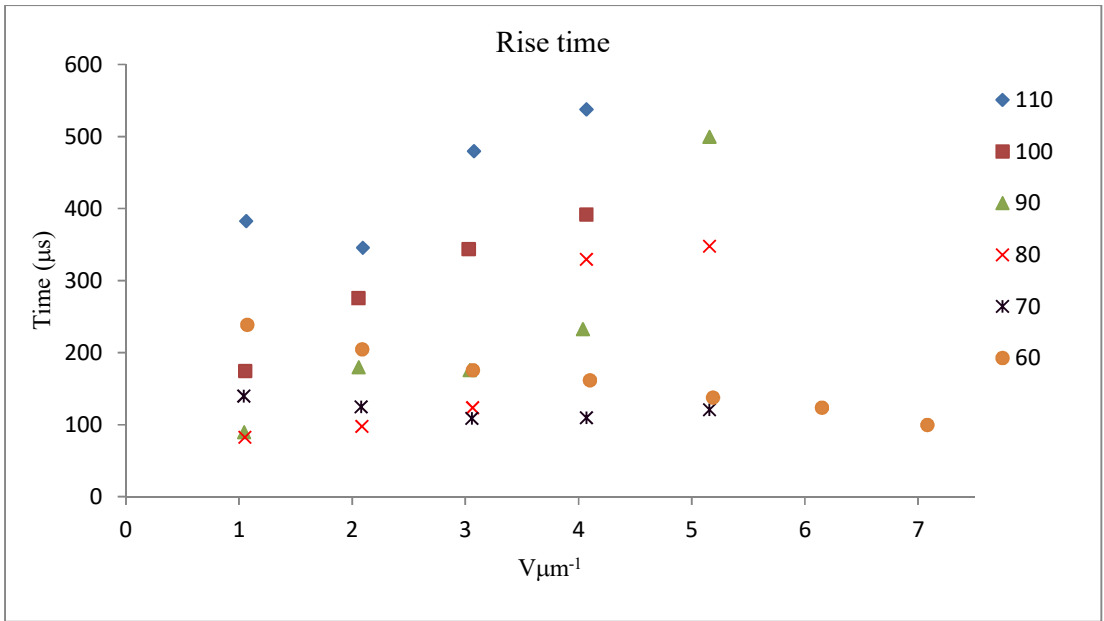
## 9.1 Selected response times:

Mix-2



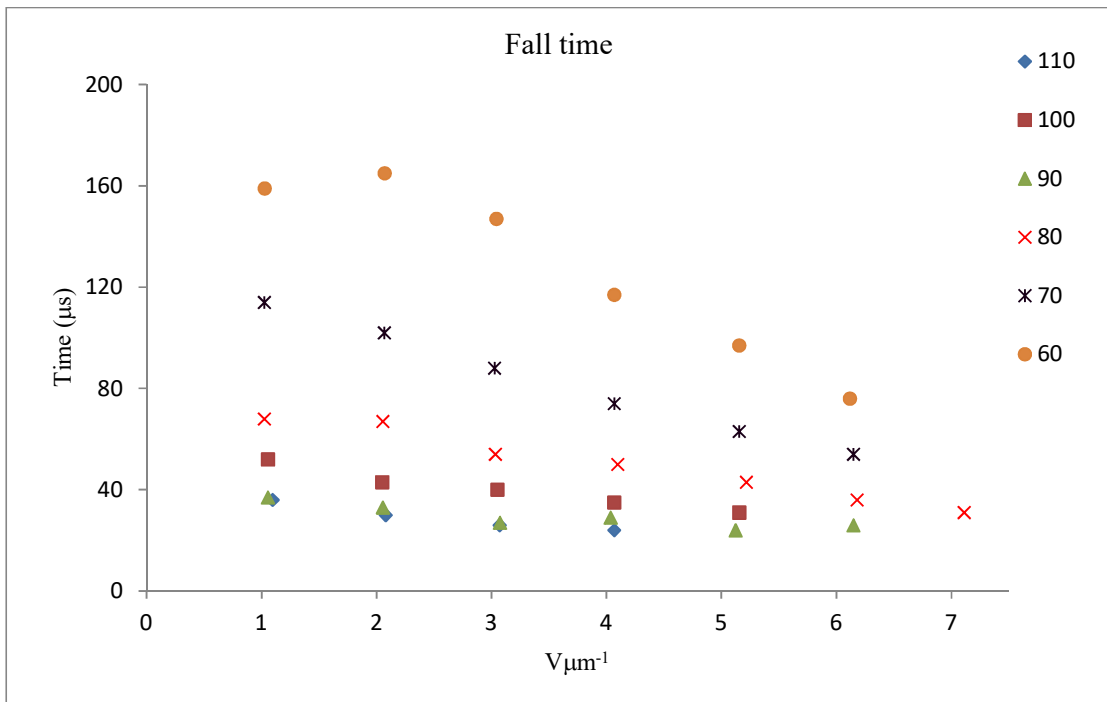
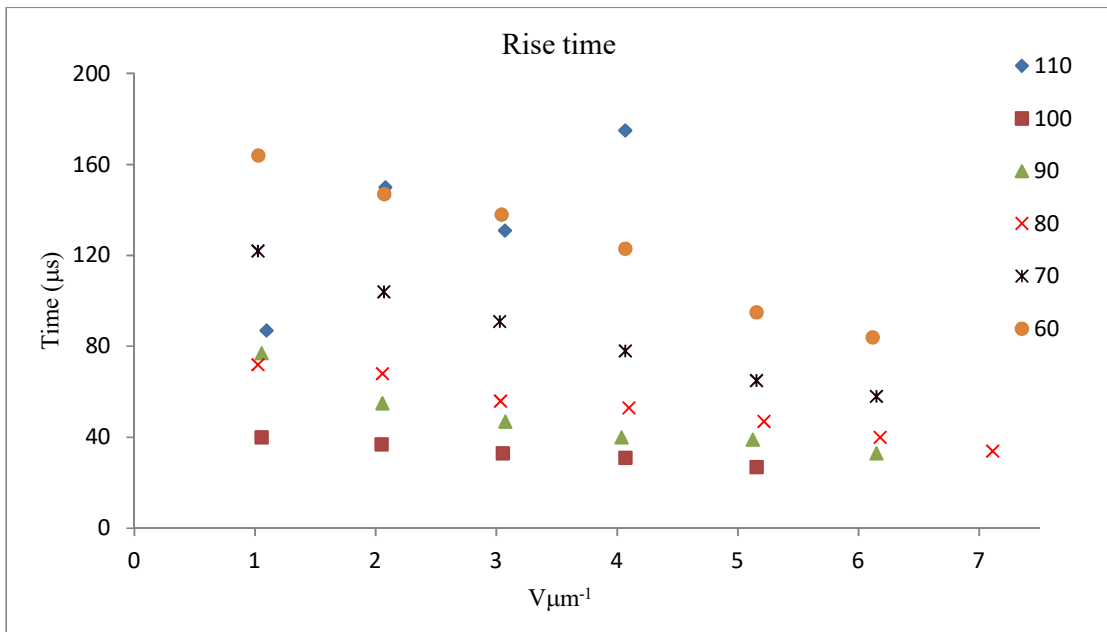
**Appendix Figure: 1** Rise and decay time of Mix-2 with respect to the applied voltage at different temperatures.

**Mix-3**



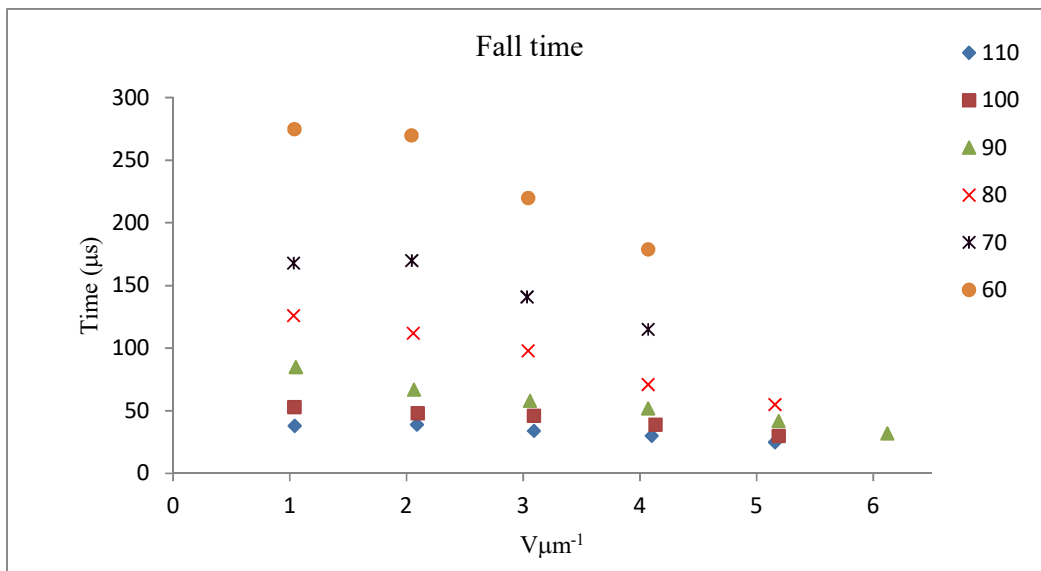
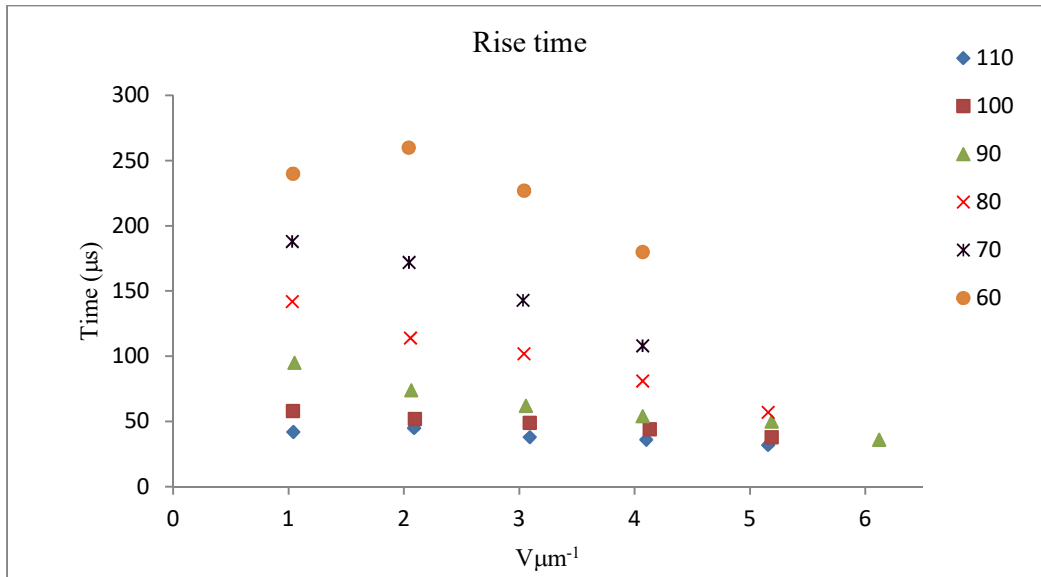
**Appendix Figure: 2** Rise and decay time of **Mix-3** with respect to the applied voltage at different temperatures.

**Mix-4**



**Appendix Figure: 3** Rise and decay time of **Mix-4** with respect to the applied voltage at different temperatures.

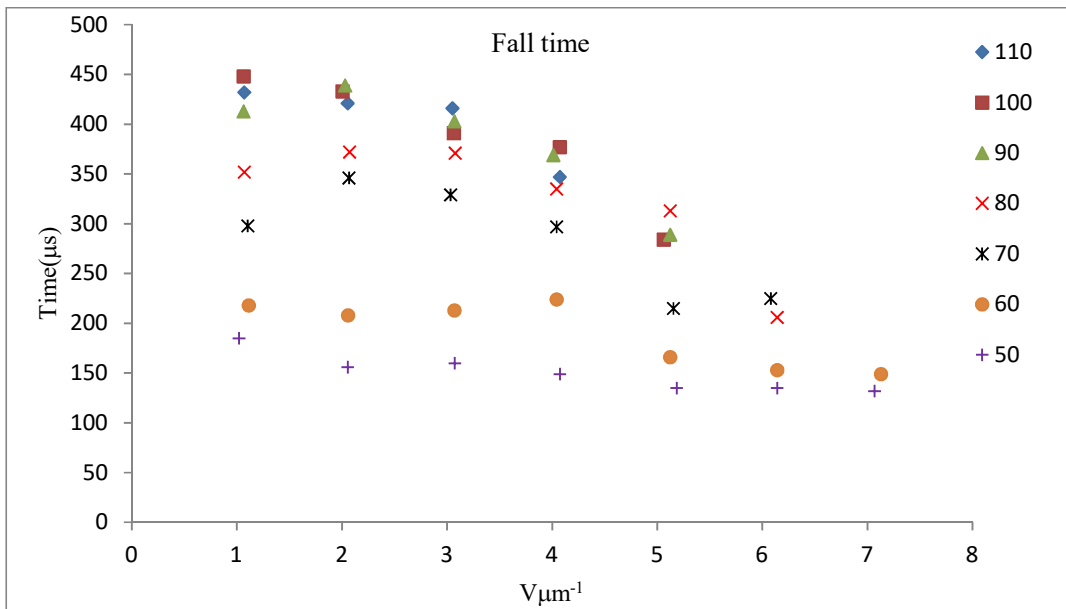
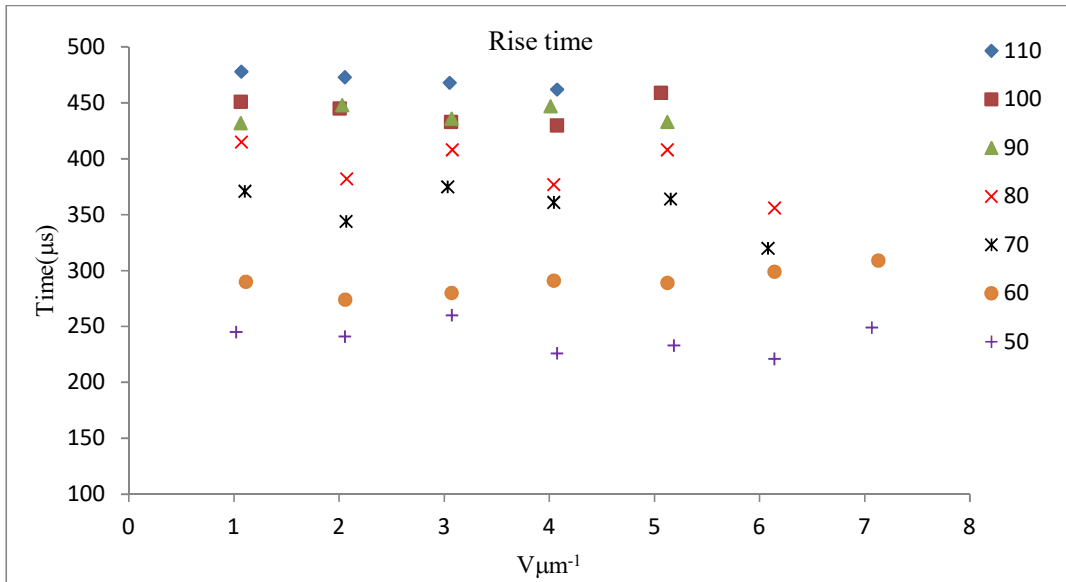
### Mix-5



**Appendix Figure: 4** Rise and decay time of **Mix-5** with respect to the applied voltage at different temperatures.

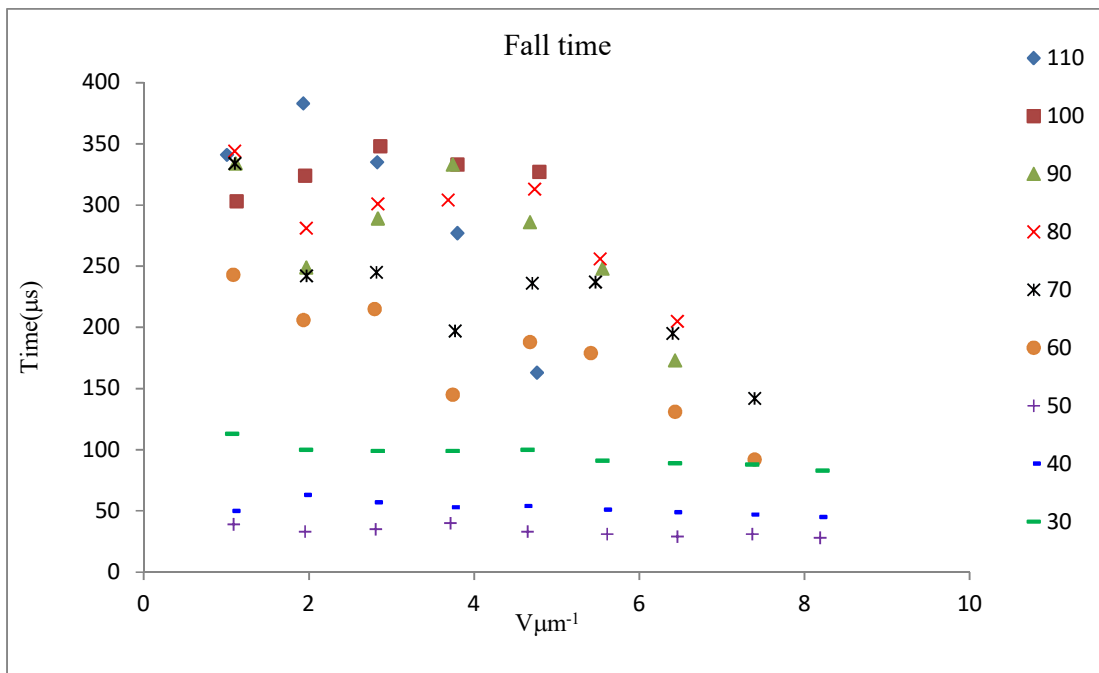
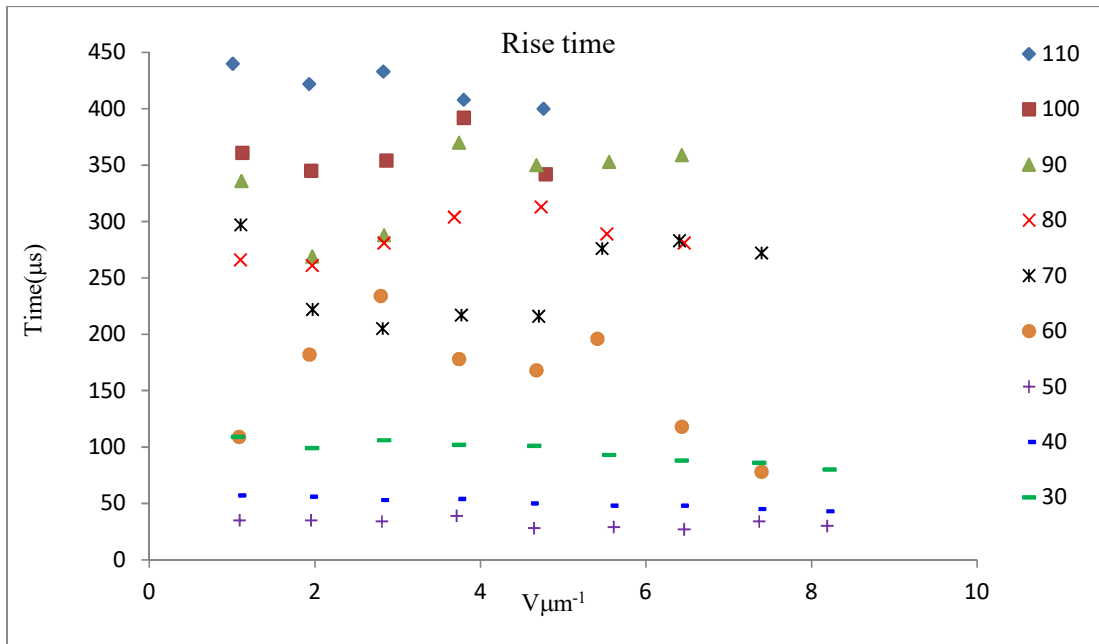


**9.2 Response times for Mix-2 doped with synthesised mesogens:  
Mix-2+3:**



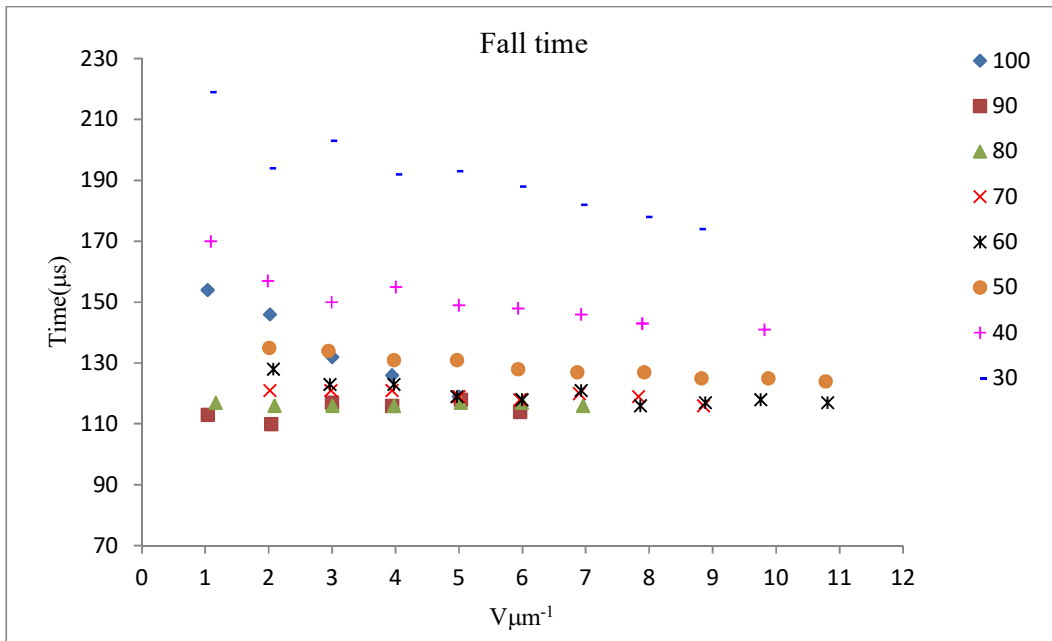
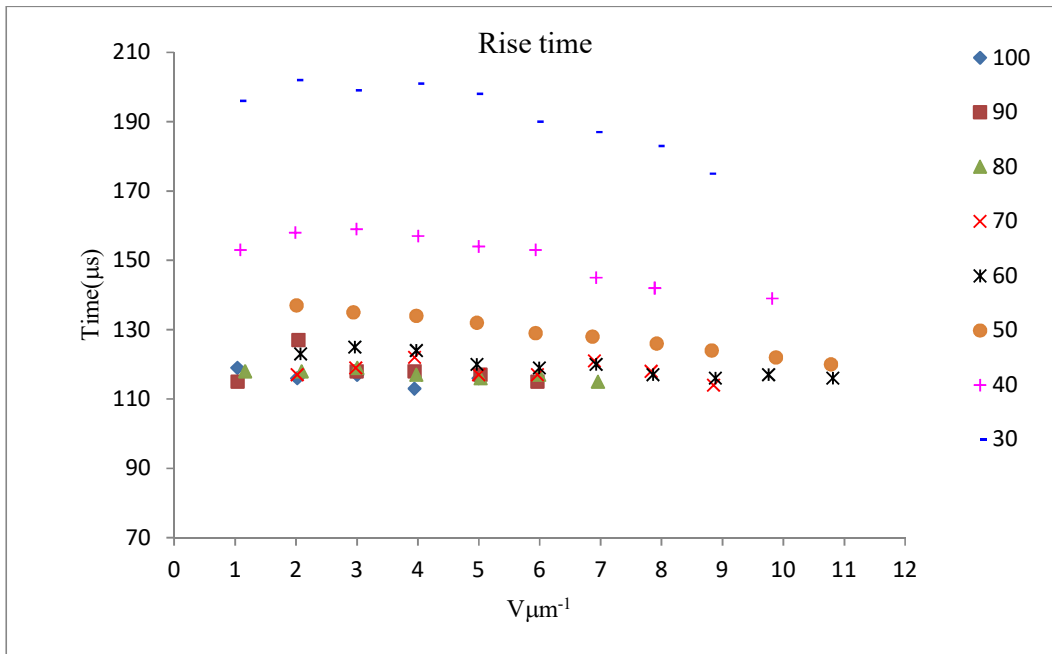
**Appendix Figure: 5** Rise and decay time of Mix-2+3 with respect to the applied voltage at different temperatures.

**Mix-2+17:**



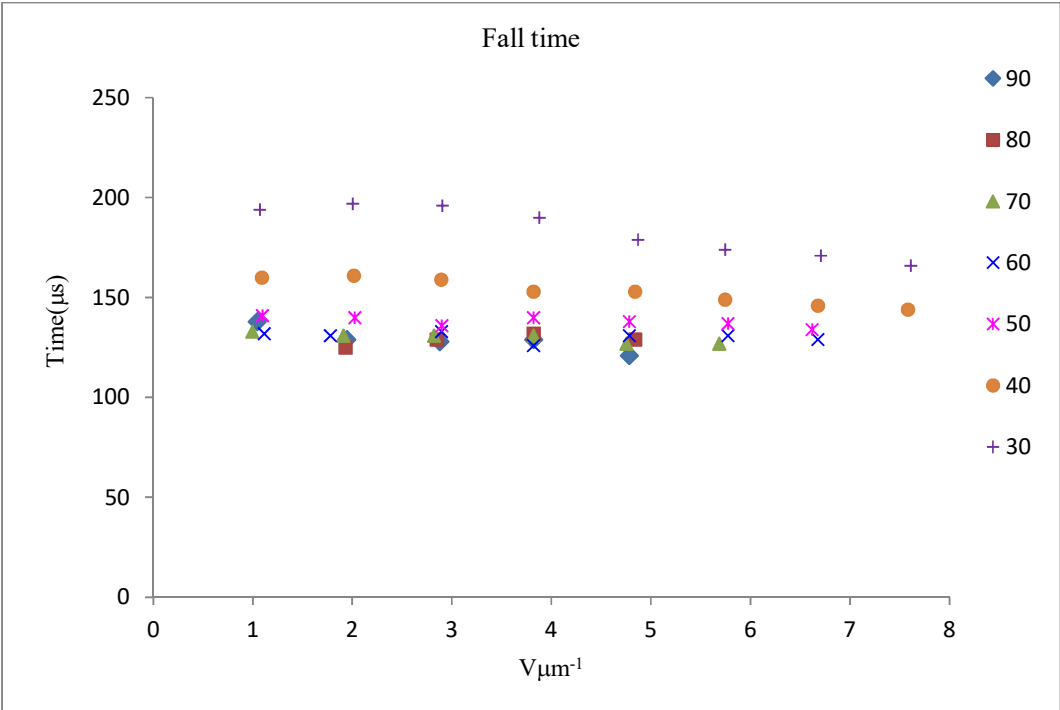
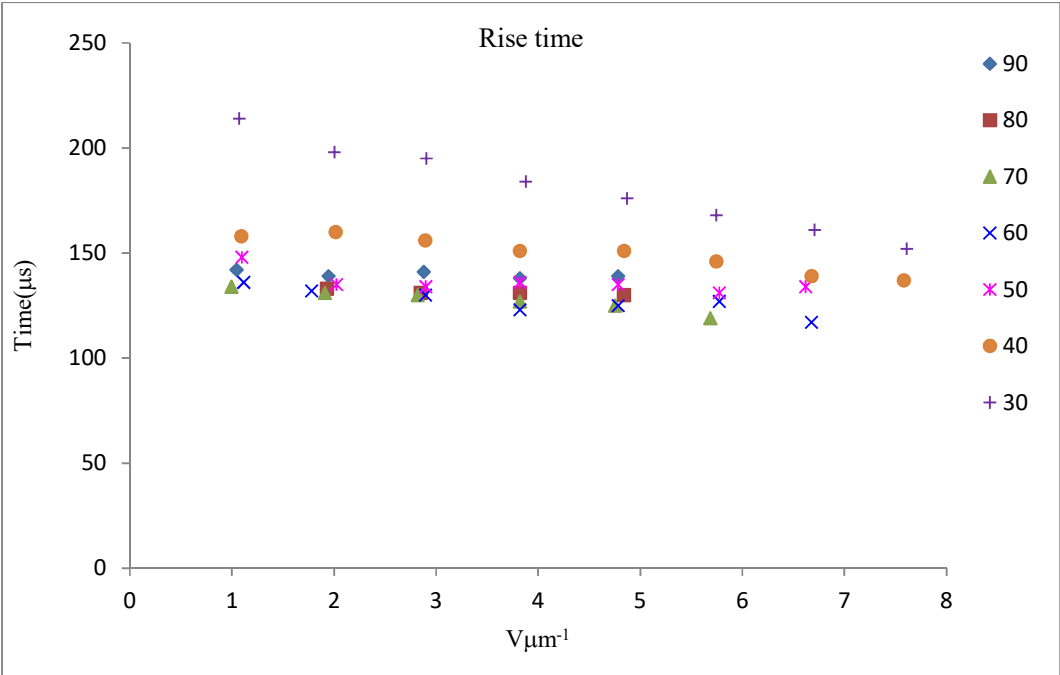
**Appendix Figure: 6** Rise and decay time of **Mix-2+17** with respect to the applied voltage at different temperatures.

**Mix-2+18:**



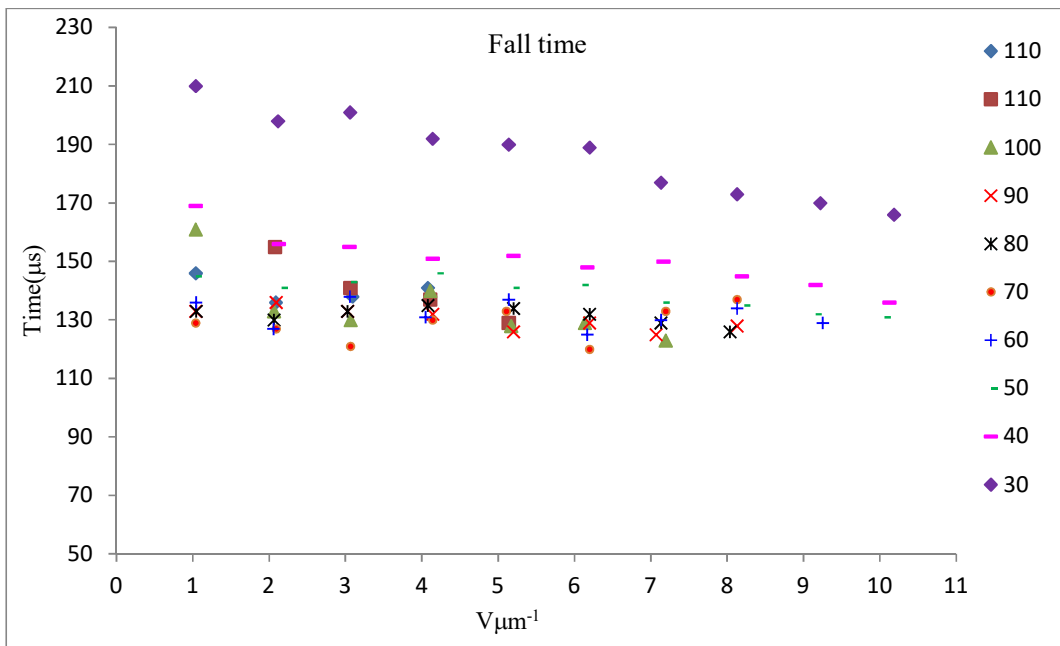
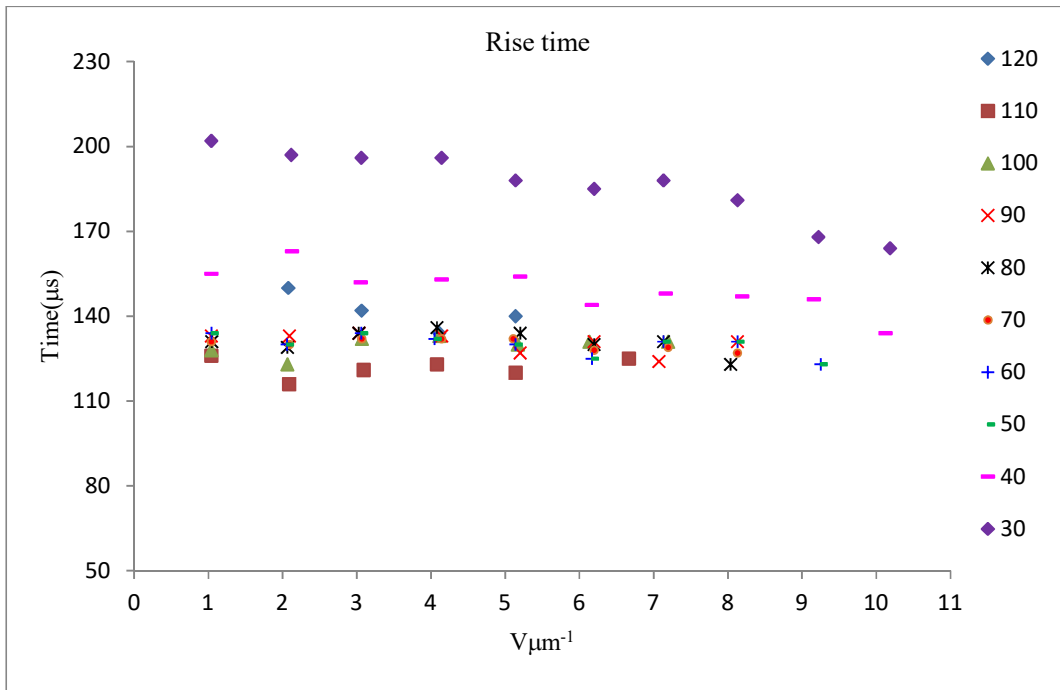
**Appendix Figure: 7** Rise and decay time of Mix-2+18 with respect to the applied voltage at different temperatures.

**Mix-2+27:**



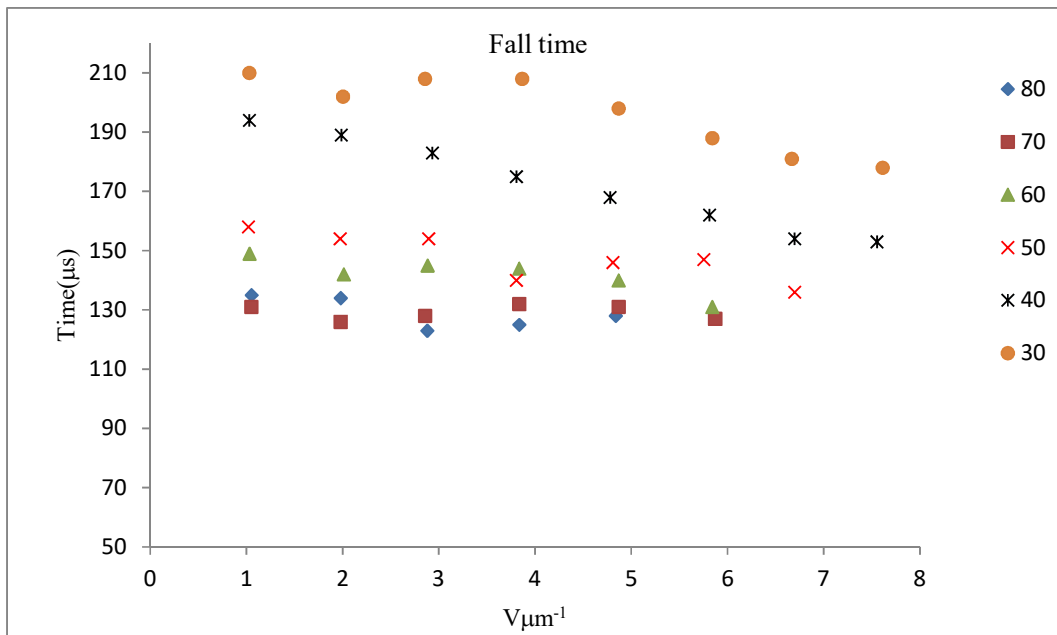
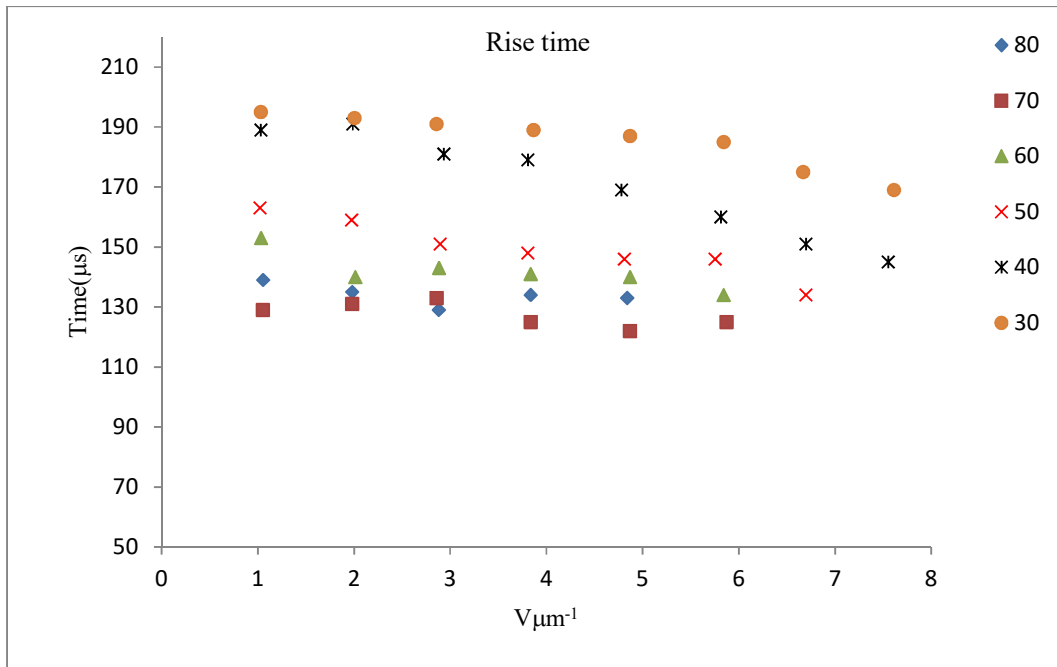
**Appendix Figure: 8** Rise and decay time of **Mix-2+27** with respect to the applied voltage at different temperatures.

**Mix-2+28:**



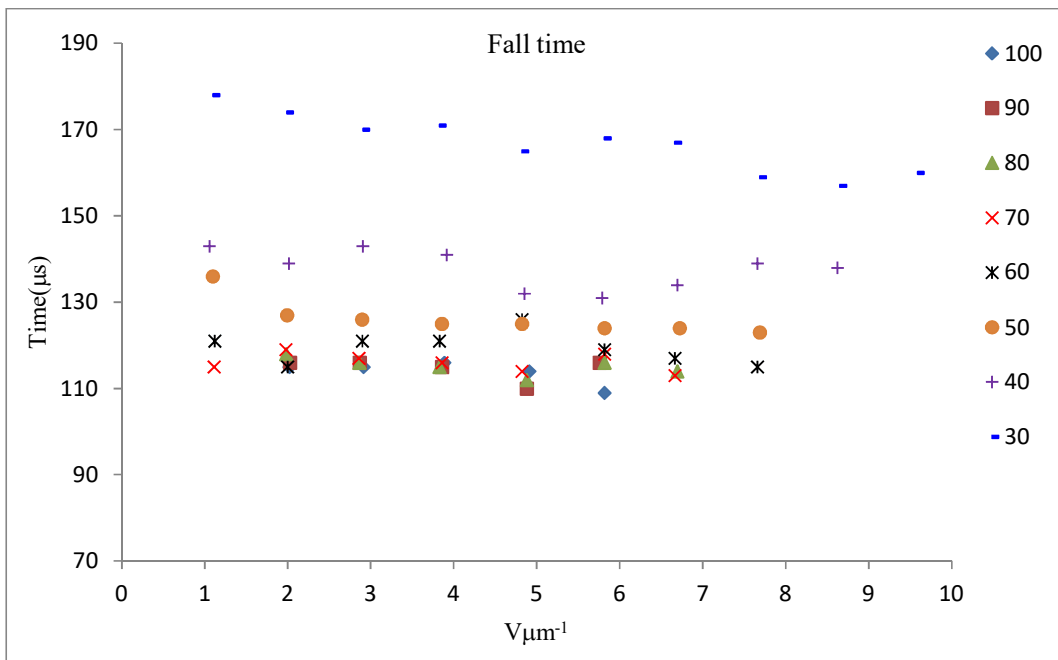
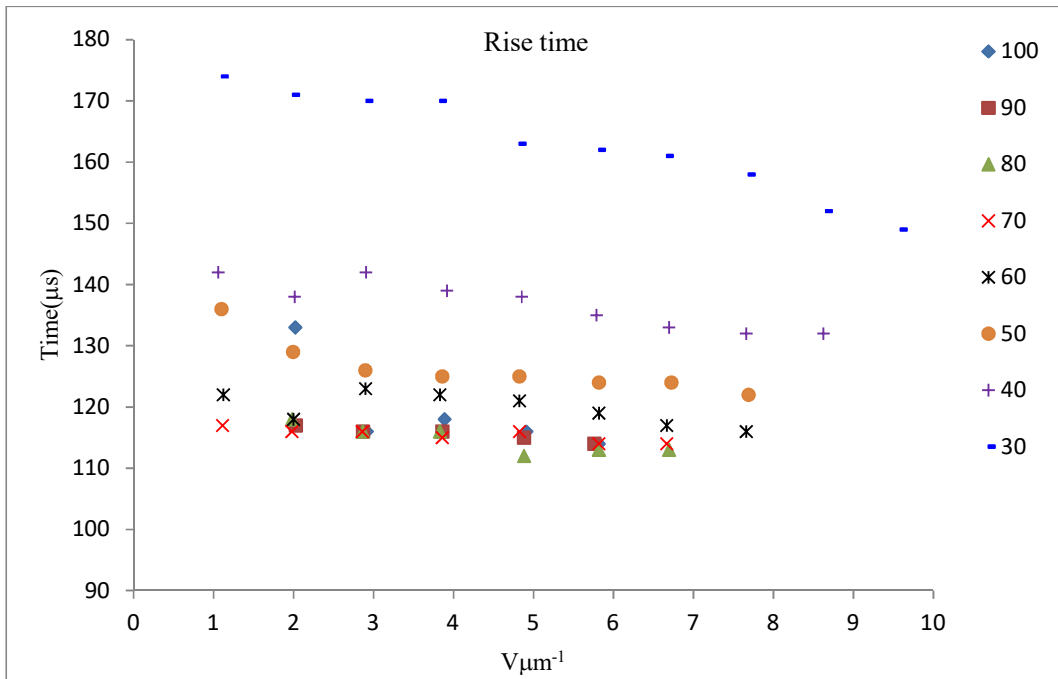
**Appendix Figure: 9** Rise and decay time of Mix-2+28 with respect to the applied voltage at different temperatures.

**Mix-2+29:**



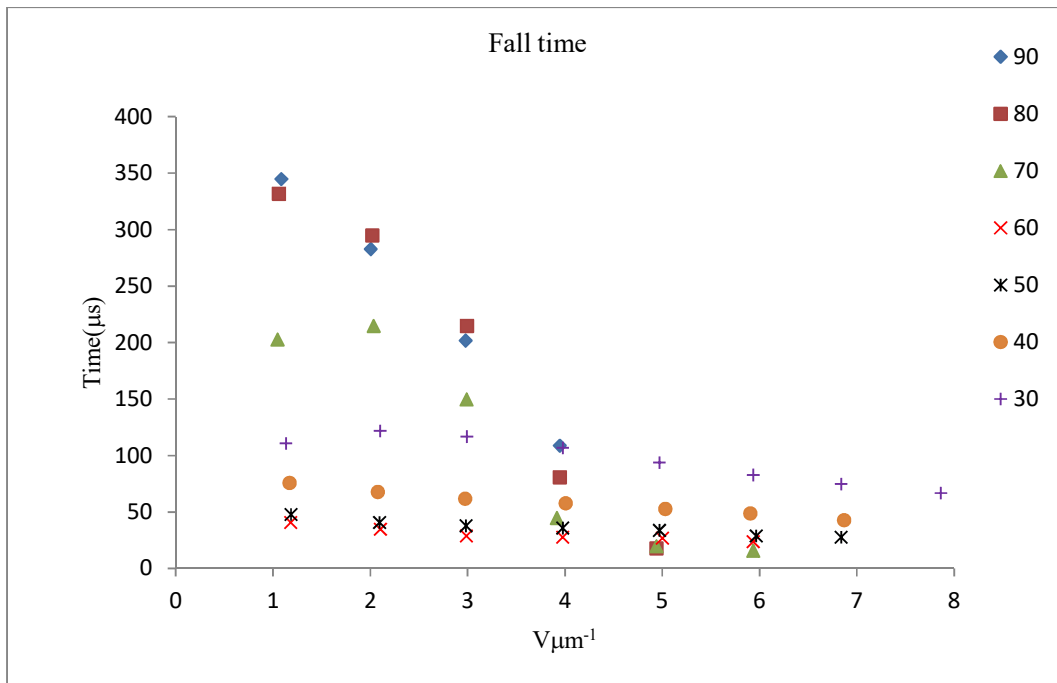
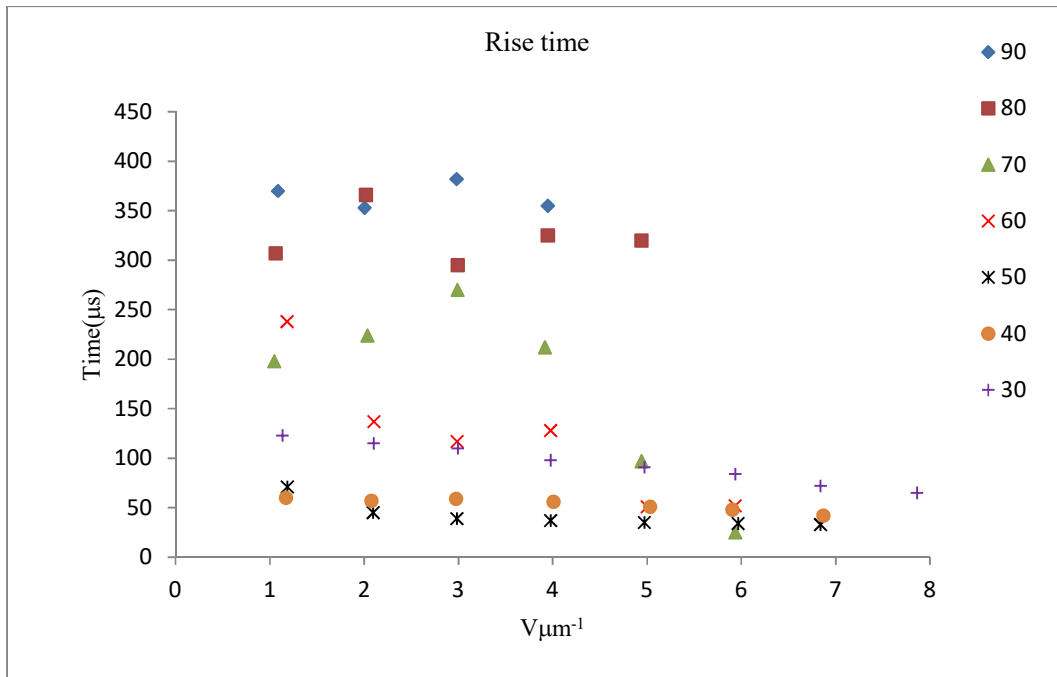
**Appendix Figure: 10** Rise and decay time of **Mix-2+29** with respect to the applied voltage at different temperatures.

**Mix-2+30:**



**Appendix Figure: 11** Rise and decay time of Mix-2+30 with respect to the applied voltage at different temperatures.

**Mix-2+31:**



**Appendix Figure: 12** Rise and decay time of **Mix-2+31** with respect to the applied voltage at different temperatures.